

การวิเคราะห์และจำลองการเปลี่ยนแปลงชั่วขณะในช่วงเริ่มต้นการทำงานของวงจรไหลเวียน
ตามธรรมชาติแบบสองสถานะ



นายสมชาย เป้าทอง

ศูนย์วิทยทรัพยากร จุฬาลงกรณ์มหาวิทยาลัย

วิทยานิพนธ์นี้เป็นส่วนหนึ่งของการศึกษาตามหลักสูตรปริญญาวิศวกรรมศาสตรดุษฎีบัณฑิต

สาขาวิชาวิศวกรรมนิวเคลียร์ ภาควิชานิวเคลียร์เทคโนโลยี

คณะวิศวกรรมศาสตร์ จุฬาลงกรณ์มหาวิทยาลัย

ปีการศึกษา 2553

ลิขสิทธิ์ของจุฬาลงกรณ์มหาวิทยาลัย

ANALYSIS AND SIMULATION OF STARTUP TRANSIENT IN TWO-PHASE NATURAL
CIRCULATION LOOP



Mr. Somchai Baotong

ศูนย์วิทยทรัพยากร
จุฬาลงกรณ์มหาวิทยาลัย

A Dissertation Submitted in Partial Fulfillment of the Requirements
for the Degree of Doctor of Engineering Program in Nuclear Engineering

Department of Nuclear Technology

Faculty of Engineering

Chulalongkorn University

Academic Year 2010


Copyright of Chulalongkorn University

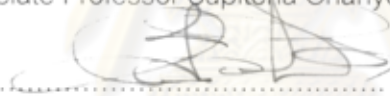
Thesis Title ANALYSIS AND SIMULATION OF STARTUP TRANSIENT IN
TWO-PHASE NATURAL CIRCULATION LOOP
By Mr. Somchai Baotong
Field of Study Nuclear Engineering
Thesis Advisor Associate Professor Sunchai Nilsuwankosit, Ph.D.
Thesis Co-advisor Phongphaeth Pengvanich, Ph.D.


Accepted by the Faculty of Engineering, Chulalongkorn University in Partial
Fulfillment of the Requirements for the Doctoral Degree


..... Dean of the Faculty of Engineering
(Associate Professor Boonsom Lerdhirunwong, Dr. Ing.)

THESIS COMMITTEE

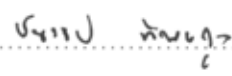
..... Chairman
(Associate Professor Supitcha Chanyotha, Ph.D.)

..... Thesis Advisor
(Associate Professor Sunchai Nilsuwankosit, Ph.D.)

..... Thesis Co-advisor
(Phongphaeth Pengvanich, Ph.D.)

..... Examiner
(Associate Professor Somyot Srisatit)

..... Examiner
(Assistant Professor Doonyapong Wongsawaeng, Ph.D.)

..... External Examiner
(Chanatip Tippayakul, Ph.D.)

สมชาย เบ้าทอง : การวิเคราะห์และจำลองการเปลี่ยนแปลงชั่วขณะในช่วงเริ่มต้นการทำงาน
 ของวงจรการไหลเวียนตามธรรมชาติแบบสองสถานะ. (ANALYSIS AND SIMULATION OF
 STARTUP TRANSIENT IN TWO-PHASE NATURAL CIRCULATION LOOP) อ. ที่ปรึกษาวิทยานิพนธ์หลัก : รศ.ดร. สัญชัย นิลสุวรรณ
 โฆษิต, อ. ที่ปรึกษาวิทยานิพนธ์ร่วม : อ.ดร.พงษ์แพทย์ เพ่งวาณิชย์, 89 หน้า.

จุดประสงค์หลักของงานวิจัยนี้คือการวิเคราะห์และจำลองการเปลี่ยนแปลงชั่วขณะ
 ในช่วงเริ่มต้นการทำงานของวงจรการไหลเวียนตามธรรมชาติแบบสองสถานะ การจำลองการ
 ไหลแบบสองสถานะกระทำโดยใช้วงจรการไหลเวียนรูปสี่เหลี่ยมลักษณะต่างๆกันที่สร้างขึ้น
 จากนั้นนำผลการจำลองที่ได้มาทำการวิเคราะห์ความถี่การแกว่งของอุณหภูมิและความดัน
 ด้วยการแปลงฟูริเยร์อย่างรวดเร็ว พร้อมกันนั้นก็ได้อัดแปลงโปรแกรมคอมพิวเตอร์ "เทกซ์" เพื่อ
 ใช้วิเคราะห์ลักษณะการไหลในเชิงคำนวณเพื่อเปรียบเทียบ

จากผลการจำลองพบว่า การเปิดหรือปิดระบบทำความเย็นไม่มีผลต่อผลต่างอุณหภูมิ
 ของน้ำที่ไหลเข้าและออกในส่วนให้ความร้อนอย่างมีนัยสำคัญ การแกว่งของอุณหภูมิเป็นผล
 จากการไหลแบบสองสถานะในท่อแนวนอนเป็นหลัก และในกรณีที่มีการขยายขนาดของช่อง
 ท่อการไหลอย่างทันทีหลังส่วนให้ความร้อน การแกว่งของอุณหภูมิจะเป็นผลจากการไหล
 แบบไม่เสถียรที่เรียกว่า Geysering และ Flashing ในการวิเคราะห์ความถี่การแกว่งของ
 อุณหภูมิที่ตำแหน่งทางออกจากตัวควบคุมไอน้ำพบว่า มีค่าแปรผันตรงกับปริมาณความร้อน
 ที่ให้ในส่วนให้ความร้อน ผลการคำนวณมีความสอดคล้องกับผลการทดลอง อย่างไรก็ตาม
 โปรแกรมยังมีข้อจำกัดในการวิเคราะห์และยังคงต้องได้รับการปรับปรุง

ภาควิชา..... วิศวกรรมเทคโนโลยี
 สาขาวิชา..... วิศวกรรมนิวเคลียร์
 ปีการศึกษา 2553.....

ลายมือชื่อนิสิต สมชาย เบ้าทอง
 ลายมือชื่อ อ.ที่ปรึกษาวิทยานิพนธ์หลัก
 ลายมือชื่อ อ.ที่ปรึกษาวิทยานิพนธ์ร่วม Ph.P.

4971832421 : MAJOR NUCLEAR ENGINEERING

KEYWORDS : TWO-PHASE FLOW / NATURAL CIRCULATION LOOP / TEXAS V /
TEMPERATURE OSCILLATION / FAST FOURIER TRANSFORM

SOMCHAI BAOTONG : ANALYSIS AND SIMULATION OF STARTUP
TRANSIENT IN TWO-PHASE NATURAL CIRCULATION LOOP. ADVISOR :
ASSOC. PROF. SUNCHAI NILSUWANKOSIT, Ph.D., CO-ADVISOR :
PHONGPHAETH PENGVANICH, Ph.D., 89 pp.

The main objective of this research is to analyze and simulate the startup transient in two-phase natural circulation loop. Two rectangular loops have been designed and constructed to simulate a two-phase flow under two different configurations. Fast Fourier Transform (FFT) is used to analyze the oscillation of unstable temperature and differential pressure. A computer program, TEXAS, has been modified to simulate the two-phase flow in the rectangular natural circulation loop and compared with the experimental data.

The same water temperature difference across the heater was measured both when the cooling system was turned on and turned off. The temperature oscillation was observed in both loops under unstable boiling condition. The temperature oscillation was due to two factors. The first factor was the presence of the horizontal tube. The second was the flow instabilities, known as geysering and flashing-induced density wave oscillation, which occurred when water flowed from small channel to large channel in the heated section. The frequency of the temperature oscillation at the condenser outlet increased when the heat flux increased. The results from the computer simulation agreed with the experimental results. However, the simulation had some limitation, and still required further modification.

Department : Nuclear Technology

Field of Study : Nuclear Engineering

Academic Year : 2010

Student's Signature 

Advisor's Signature 

Co-advisor's Signature 

Acknowledgments

I would like to thank my advisor, Associate Professor Dr. Sunchai Nilsuwankosit, and my co-advisor, Dr. Phongphaeth Pengvanich, for their guidance and assistance in the completion of this work.

Thanks to Assistant Professor Suvit Punnachaiya for his advice and recommendation. I also would like to thank Decho Thong-Aram for training and introducing me to the world of microcontroller. Thanks to Kamontip Ploykrachang and Piyathap Chobthumkit for their assistance in the lab. Thanks also to my leader, Dr. Visit Thaveeprungsriporn, for his guidance on how to succeed in PhD.

Thanks to my father Plueang and my mother Sanit for their encouragement and support. Thanks also to Prapas Kunnam and Monnapas Morakotjinda for their support and belief in me. I also thank Rungtiwa Chantarasakha for understanding and love during the time of study.

This work was supported by the Thailand Research Fund under the Royal Golden Jubilee Ph.D. program grant number PHD/0216/2548.



ศูนย์วิทยทรัพยากร
จุฬาลงกรณ์มหาวิทยาลัย

Contents

	Page
Abstract (Thai).....	iv
Abstract (English).....	v
Acknowledgements.....	vi
Contents.....	vii
List of tables.....	ix
List of figures.....	x
Chapter	
I INTRODUCTION.....	1
1.1 Background on problems of interest.....	1
1.2 Thesis objective.....	5
1.3 Scope of work.....	5
II TWO-PHASE FLOW.....	6
2.1 Flow patterns in vertical tubes	6
2.2 The different heat transfer regions in two-phase flow.....	8
2.3 One-Dimensional Two-fluid Model	10
III TEXAS CODE.....	17
3.1 Brief description of TEXAS code.....	17
3.2 Conservation Equations.....	19
3.2.1 Mass Equations.....	20
3.2.2 Momentum Equation.....	20
3.3.3 Energy Equations.....	21
3.3 Phase Change Model.....	23
3.4 Switch Void Fraction (SVF) in Pressure Iteration.....	24
3.5 Modification of TEXAS code.....	26
IV EXPERIMENTAL APPARATUS AND PROCEDURE.....	28
4.1 Experimental apparatus for the NCL#1.....	28
4.2 Experimental procedure for the NCL#1.....	29

Chapter	Page
4.3 Experimental apparatus for the NCL#2.....	31
4.4 Experimental procedure for the NCL#1.....	34
4.5 Fast Fourier Transform method.....	35
V RESULTS AND DISCUSSION.....	36
5.1 The results of the NCL#1.....	36
5.1.1 Effect of cooling system on single-phase natural circulation..	36
5.1.2 The temperature oscillation.....	39
5.2 The results of the NCL#2.....	44
5.2.1 Geysering induced by condensation.....	45
5.2.2 Flashing-induced density wave oscillation.....	47
5.2.3 Spectrum analysis with FFT.....	48
5.3 The results from computer simulation.....	53
5.4 Comparison of numerical and experimental results.....	59
VI CONCLUSION AND SUGGESTION.....	60
6.1 Conclusions.....	60
6.2 Suggestions.....	62
References.....	64
Appendices.....	67
Appendix A.1 Temperature profiles for the NCL#2.....	68
Appendix A.2 Differential pressure across the heater for the NCL#2.....	71
Appendix B.1 MATLAB code for FFT.....	74
Appendix B.2 FFT profiles of temperature at the heater outlet for the NCL#2.....	77
Appendix B.3 FFT profiles of temperature at the condenser outlet for the NCL#2.....	80
Appendix B.2 FFT profiles of differential pressure across the heater for the NCL#2.....	83
Appendix C Input file for the computer simulation.....	86

Biography.....	Page 89
----------------	---------



ศูนย์วิทยทรัพยากร
จุฬาลงกรณ์มหาวิทยาลัย

List of Tables

	Page
Table 5.1 Initial conditions for computer simulation.....	53



ศูนย์วิทยทรัพยากร
จุฬาลงกรณ์มหาวิทยาลัย

List of Figures

	Page
Fig. 2.1 Two-phase flow patterns in vertical upflow	6
Fig. 2.2 Wall and liquid temperatures, flow pattern and the associated heat transfer regions, heated tube.....	9
Fig. 2.3 The phasic heat transfer rate at the interface.....	15
Fig. 3.1 Conceptual picture of current TEXAS mixing model.....	19
Fig. 3.2 The TEXAS program.....	27
Fig. 3.3 The modification of TEXAS program.....	27
Fig. 4.1 Schematic diagram of the NCL#1.....	29
Fig. 4.2 The picture of NCL#1.....	30
Fig. 4.3 Schematic diagram of the NCL#2.....	32
Fig. 4.4 The picture of NCL#2.....	33
Fig. 4.5 Block diagram of the data recorder.....	34
Fig. 4.6 Block diagram of the power controller.....	34
Fig. 5.1 The water temperature at 473 W heating powers when the cooling system was turned off.....	36
Fig. 5.2 The water temperature at 473 W heating powers when the cooling system was turned on.....	37
Fig. 5.3 The maximum temperature at the outlet heater for the different heating power levels.....	38
Fig. 5.4 Effect of heating power on the temperature difference across the heater.....	38
Fig. 5.5 Effect of heating power on the mass flow rates.....	39
Fig. 5.6 The water temperature at the heater inlet and outlet of 575 W heating powers.....	40
Fig. 5.7 The amplitude of initial fluctuation of the water temperature at the heater outlet.....	41

	Page
Fig. 5.8 The process of the water temperature oscillation after the water boiling.....	42
Fig. 5.9 FFT profile of the temperature oscillation at 550 W heating powers.....	43
Fig. 5.10 FFT profile of the temperature oscillation at 630 W heating powers.....	43
Fig. 5.11 The temperature profiles at various heat flux levels (a) 6.0 kW/m ² , (b) 8.0 kW/m ² , (c) 12.5 kW/m ² , and (d) 18.0 kW/m ²	44
Fig. 5.12 The differential pressure across the heater at various heat flux levels (a) 6.0 kW/m ² , (b) 8.0 kW/m ² , (c) 12.5 kW/m ² , and (d) 18.0 kW/m ²	45
Fig. 5.13 Proposed model of geysering in parallel boiling channels.....	46
Fig. 5.14 Recorded bubble images at the heater outlet.....	46
Fig. 5.15 Process of flashing-induced density wave oscillation.....	47
Fig. 5.16 Recorded bubble images at the riser middle.....	48
Fig. 5.17 FFT profiles of the temperature oscillation at the heater outlet and the condenser outlet for 8.0 kW/m ² heat flux.....	49
Fig. 5.18 FFT profiles of the temperature oscillation at the heater outlet and the condenser outlet for 12.5 kW/m ² heat flux.....	49
Fig. 5.19 FFT profiles of the temperature oscillation at the heater outlet and the condenser outlet for 18.0 kW/m ² heat flux.....	50
Fig. 5.20 FFT profiles of the differential pressure across the heater at 8.0 kW/m ² heat flux.....	51
Fig. 5.21 FFT profiles of the differential pressure across the heater at 12.5 kW/m ² heat flux.....	51
Fig. 5.22 FFT profiles of the differential pressure across the heater at 18.0 kW/m ² heat flux.....	52
Fig. 5.23 A computer model for (a) the NCL#1 and (b) the NCL#2.....	53
Fig. 5.24 Temperature profiles at 400 W heating powers.....	54
Fig. 5.25 Liquid velocity at 400 W heating powers.....	54

	Page
Fig. 5.26 Pressure at 400 W heating powers.....	55
Fig. 5.27 The water temperature at various heating power levels.....	55
Fig. 5.28 The relationship between the water temperature and the water density.....	56
Fig. 5.29 Temperature profiles at 575 W heating powers.....	56
Fig. 5.30 Differential pressure across the heater at 575 W heating powers.....	57
Fig. 5.31 Void fraction at the heater outlet at 575 W heating powers.....	57
Fig. 5.32 Temperature profiles at 12.5 kW/m ² heat fluxes.....	58
Fig. 5.33 Liquid velocity at 12.5 kW/m ² heat fluxes.....	58
Fig. 5.34 Differential pressure across the heater at 12.5 kW/m ² heat fluxes.....	58
Fig. 5.35 Comparison of numerical and experimental results for the maximum water temperature.....	59
Fig. 5.36 Comparison of numerical and experimental results for the temperature difference across the heater.....	59
Fig. 5.37 Comparison of numerical and experimental results for the amplitude of initial fluctuation.....	60
Fig. A1.1 Temperature profiles at 6.0 kW/m ² heat flux.....	68
Fig. A1.2 Temperature profiles at 8.0 kW/m ² heat flux.....	68
Fig. A1.3 Temperature profiles at 10.5 kW/m ² heat flux.....	69
Fig. A1.4 Temperature profiles at 12.5 kW/m ² heat flux.....	69
Fig. A1.5 Temperature profiles at 15.0 kW/m ² heat flux.....	70
Fig. A1.6 Temperature profiles at 18.0 kW/m ² heat flux.....	70
Fig. A2.1 Differential pressure across the heater at 6.0 kW/m ² heat flux.....	71
Fig. A2.2 Differential pressure across the heater at 8.0 kW/m ² heat flux.....	71
Fig. A2.3 Differential pressure across the heater at 10.5 kW/m ² heat flux.....	72
Fig. A2.4 Differential pressure across the heater at 12.5 kW/m ² heat flux.....	72
Fig. A2.5 Differential pressure across the heater at 15.0 kW/m ² heat flux.....	73
Fig. A2.6 Differential pressure across the heater at 18.0 kW/m ² heat flux.....	73

	Page
Fig. B2.1 FFT profile of temperature at the heater outlet at 8.0 kW/m ² heat flux...	77
Fig. B2.2 FFT profile of temperature at the heater outlet at 10.5 kW/m ² heat flux.	77
Fig. B2.3 FFT profile of temperature at the heater outlet at 12.5 kW/m ² heat flux.	78
Fig. B2.4 FFT profile of temperature at the heater outlet at 15.0 kW/m ² heat flux.	78
Fig. B2.5 FFT profile of temperature at the heater outlet at 18.0 kW/m ² heat flux.	79
Fig. B3.1 FFT profile of temperature at the condenser outlet at 8.0 kW/m ² heat flux.....	80
Fig. B3.2 FFT profile of temperature at the condenser outlet at 10.5 kW/m ² heat flux.....	80
Fig. B3.3 FFT profile of temperature at the condenser outlet at 12.5 kW/m ² heat flux.....	81
Fig. B3.4 FFT profile of temperature at the condenser outlet at 15.0 kW/m ² heat flux.....	81
Fig. B3.5 FFT profile of temperature at the condenser outlet at 18.0 kW/m ² heat flux.....	82
Fig. B4.1 FFT profile of differential pressure across the heater at 8.0 kW/m ² heat flux.....	83
Fig. B4.2 FFT profile of differential pressure across the heater at 10.5 kW/m ² heat flux.....	83
Fig. B4.3 FFT profile of differential pressure across the heater at 12.5 kW/m ² heat flux.....	84
Fig. B4.4 FFT profile of differential pressure across the heater at 15.0 kW/m ² heat flux.....	84
Fig. B4.5 FFT profile of differential pressure across the heater at 18.0 kW/m ² heat flux.....	85
Fig. C.1 Computer program.....	88

CHAPTER I

INTRODUCTION

1.1 Background on problems of interest

Two-phase natural circulation systems have found their places in many of the modern nuclear reactor designs and industrial processes because they commonly possess three important features: passive, economical, and simple. The systems' passive nature allows less usage of valves and pumps for flow regulation. The production cost can therefore be reduced, and maintenances are generally simpler in comparison to the conventional active systems. In addition, the risk of failures associated with the usages of valves and pumps also decrease. There is a caveat, however. Various types of instabilities can occur in the flow, preventing the two-phase natural circulation systems from being effectively implemented. The sources of the instabilities can vary depending upon the systems' geometries and their operating conditions. Nevertheless, they can cause problem to the system operation and control, and may reduce the thermal margin [1].

Oscillations of flow rate and system pressure are undesirable, as they can cause mechanical vibrations, problems of system control and in extreme circumstances, disturb the heat transfer characteristics so that the heat transfer surface may burn-out. In a recirculating plant, where burn-out must be avoided, flow oscillations could lead to transient burn-out. Under certain circumstances, large flow oscillations can lead to tube failures due to increased wall temperature. Another cause of failure would be due to thermal fatigue resulting from continual cycling of the wall temperature; the thermal stresses set up in the wall and the cladding material in nuclear reactor fuel elements can cause mechanical breakdown, leading to more serious accidents, such as release of radioactive materials. It is clear from these examples that the flow instabilities must be avoided, and every effort needs to be made to ensure that any two-phase system has an adequate margin against them [2].

There are several reviews of flow instabilities in boiling system [2,3,4,5,6,7]. These reviews indicate that different models of two-phase flow have been

employed for modeling thermal hydraulics. In most of the studies of two-phase flow instabilities, the homogenous equilibrium model is widely used. This model treats the two-phase flow as the flow of single phase compressible fluid. The velocity of both phases is assumed to be equal, and the temperature is taken to be the saturated temperature. These assumptions are valid for rapid interfacial rates of heat and momentum transfer. Therefore, the model can be expected to be most applicable for those two-phase regimes where the phases are well-mixed, such as bubbly, churn, or drop flow regimes. The drift-flux model, which has gained much acclaim in the last decade, takes the relative velocity between the phases into account, while assuming thermodynamic equilibrium. It is presumably most valid for cases in which the drift velocity is significant compared with the volumetric flux. This limits its usefulness to the bubbly, slug and churn flow patterns. In the most general formulation of the two-phase flow problem, the conservation equations are written separately for each of the phases which is called two-fluid model. Although this model is the most satisfactory in theory, it is complicated to use in problems of practical importance because of the seven constitutive laws that are required, viz. four at the wall (friction and heat transfer for the two phases) and three at the interface of the phases (mass, momentum and energy transfer). However, it is the only model available for accurate modeling of the two-phase phenomena where the two phases are weakly coupled. Examples of these are sudden mixing of two phases, transient flooding and flow reversal, transient countercurrent flow and two-phase flow with sudden acceleration. Therefore two-fluid modeling is open for future research.

Natural circulation systems may undergo thermal hydraulic instabilities under low pressure condition, which occur during start-up. At low pressure, a natural circulation loop typically has three operating ranges: single-phase stable region, two-phase unstable region and two-phase stable region. Numerous investigations, both theoretical and experimental have been conducted to understand the stability at low pressure startup in two-phase natural circulation loop. Aritomi et al. [8] and Chiang et al. [9] pointed out three types of the instabilities, namely geysering, natural circulation oscillations and density wave oscillations, which could occur in the boiling natural

circulation loop. Kuran et al. [10] and Furuya et al. [11] conducted several experiments to investigate instabilities that may occur at low-pressure and low-flow conditions during the startup of boiling natural circulation loop. The experimental results showed the signature of condensation-induced oscillations during the single-phase to two-phase natural circulation transition. A large number of thermal hydraulic codes and models exist, which have been developed to deal with the stability issues, ranging from sophisticated system analysis codes that can simulate plant behavior, to simple models such as a single channel homogeneous equilibrium model to study basic physical phenomena.

In 1999, Paniagua et al. [12] developed a thermal hydraulics computer code for simulate the geysering instability in a natural circulation system starting from subcooled conditions and to assess the impact of the system pressure and channel inlet subcooling on the inception of instability. The formulation of thermal hydraulics is inherently general and accounts for both single-phase liquid flow and nonhomogeneous, nonequilibrium two-phase flow. The computer code is based on momentum integral method where the current practice of basing fluid properties on the system averaged pressure has been relaxed and the local properties are based on local pressures estimated using the shape of steady-state pressure distribution, thereby, improving the predictions while preserving the computation speed, one of the important strength of the integral methods. This is an important modeling feature since the local vapor generation rate depends on local saturation temperature. The methodology has been validated with the experiments conducted to investigate the instabilities in a low pressure natural circulation loop at low powers and high inlet subcoolings. The numerical simulations predicted periodic channel flow reversal, which is one of the feature of condensation-induced geysering. Basing local properties on local pressures instead of system average pressure led to decrease in the discrepancy in the prediction of the positive side amplitude from 40% to 6% and in the frequency from -15% to 5%. In addition, it was observed that the start-up instability can be avoided by increasing system pressure or by decreasing channel inlet subcooling. This study showed that the integral method

coupled with local pressure variation for the vapor generation model is suitable to predict startup or geysering transients.

In 2002, Chaiwat Muncharoen [13] studied effect of heat flux, pressure and subcooling on instabilities of two-phase natural circulation in parallel channels system. The heat flux was increased from 50 to 550 kW/m². The system pressure was varied from 0.1-0.7 MPaA and the inlet subcooling was fixed to 5, 10 and 15 K. The numerical code was developed by using two-fluid model for predict stability in two-phase natural circulation. The semi-implicit scheme was utilized for finite difference equations. Newton block gauss seidel method was employed to solve the system equations for unknown variable. The experimental results indicate that the increase in system pressure and subcooling stabilize the system. In addition, the two-fluid model can give the good results and are in good agreement with experimental results.

In 2006, Nayak et al. [14] presented a numerical study of boiling flow instability of a reactor thermosyphon system. The numerical model solves the conservation equations of mass, momentum and energy applicable to a two-fluid and three-field steam-water system using a finite difference technique. The main conclusions of this study are 1) conventional homogeneous two-phase flow models with empirical relations for void fraction and two-phase friction factor multiplier overestimate the natural circulation flow of the reactor, 2) the two-fluid model predicts the natural circulation flow closest to the measured value of the reactor and 3) an increase in power or a decrease in subcooling has a destabilizing effect on the natural circulation.

Several scale test facilities [10,11] have been built to investigate flow instabilities. The results obtained from these facilities were more accurate and could be used in predicting flow behavior of typical natural circulation system implemented in boiling water reactor (BWR). However, the construction cost was expensive due to its complexity and large size. Alternately, rectangular natural circulation loop [9,12,15,16,17] can also be used for the study. It has advantage over scale test facilities because of its simplicity, low cost, and adaptability for various configurations of heating and cooling sections.

One of the main interests in flow instability is the temperature oscillation. Such oscillation in the worst scenario can seriously damage the heater and the flow loop. In a normal circumstance, such oscillation can interrupt the heat transfer process, and thus reduces the process efficiency. A number of observations in the oscillation of temperature under the flow instability have been reported and the data are analyzed. For example, Khodabandeh [18] used fluctuation value, defined as the maximum deviation from the average value, to analyze the wall temperature oscillation. Of particular interest was the usage of Fast Fourier Transform (FFT) method to analyze the oscillation curve of mass flow in the twin-channel system instability under ocean conditions by Yun [19]. Kosar [20] also reported that FFT method can also be used to analyze the oscillation of pressure signals during the unstable boiling condition.

1.2 Thesis objective

1. To modify and apply a computer program for simulating the two-phase flow to simulate the transient in a natural circulation loop.
2. To develop the two-phase natural circulation loop for measuring mass flow rate, pressure drop, inlet subcooling and heating power in order to benchmark the modified computer program.
3. To simulate and analyze the startup transient for the two-phase natural circulation loop under different configurations.

1.3 Scope of work

1. Design and construct a two-phase rectangular natural circulation loop.
2. The effect of initial conditions such as water temperature and heating power on the two-phase rectangular natural circulation loop will be investigated.
3. Modify and apply an existed one-dimensional two-fluid numerical code, TEXAS (Thermal EXplosion Analysis Simulation), to simulate the transient.
4. The results from computer program will be compared with the experimental data and analyzed.
5. Simulate and analyze the startup transient for the two-phase natural circulation loop under different configurations.

CHAPTER II

TWO-PHASE FLOW

In this chapter, flow patterns inside tube will be described for vertical upward flows. Next, the different heat transfer regions in two-phase flow will be presented. Finally, the balance equations for two-phase flow will be discussed.

2.1 Flow patterns in vertical tubes [21]

For co-current upflow of gas and liquid in a vertical tube, the liquid and gas phases distribute themselves into several recognizable flow structures. These are referred to as flow patterns and they are depicted in Fig. 2.1 and can be described as follows:

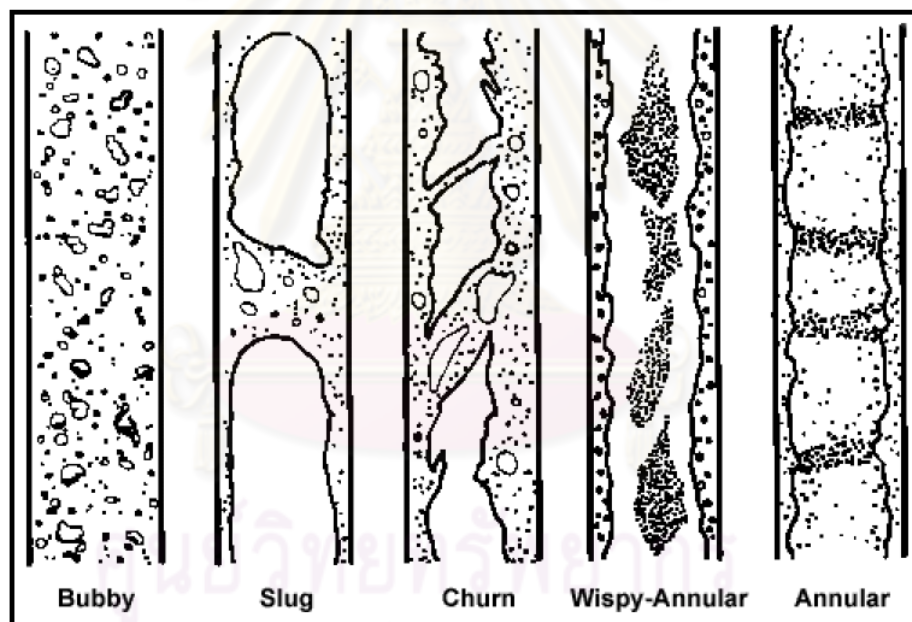


Fig. 2.1 Two-phase flow patterns in vertical upflow [21].

- **Bubbly flow.** Numerous bubbles are observable as the gas is dispersed in the form of discrete bubbles in the continuous liquid phase. The bubbles may vary widely in size and shape but they are typically nearly spherical and are much smaller than the diameter of the tube itself.

- **Slug flow.** With increasing gas void fraction, the proximity of the bubbles is very close such that bubbles collide and coalesce to form larger bubbles, which are similar in dimension to the tube diameter. These bubbles have a characteristic shape similar to a bullet with a hemispherical nose with a blunt tail end. They are commonly referred to as Taylor bubbles after the instability of that name. Taylor bubbles are separated from one another by slugs of liquid, which may include small bubbles. Taylor bubbles are surrounded by a thin liquid film between them and the tube wall, which may flow downward due to the force of gravity, even though the net flow of fluid is upward.

- **Churn flow.** Increasing the velocity of the flow, the structure of the flow becomes unstable with the fluid traveling up and down in an oscillatory fashion but with a net upward flow. The instability is the result of relative parity of the gravity and shear forces acting in opposing directions on the thin film of liquid of Taylor bubbles. This flow pattern is in fact an intermediate regime between the slug flow and annular flow regimes. In small diameter tubes, churn flow may not develop at all and the flow passes directly from slug flow to annular flow. Churn flow is typically a flow regime to be avoided in two-phase transfer lines, such as those from a reboiler back to a distillation column or in refrigerant piping networks, because the mass of the slugs may have a destructive consequence on the piping system.

- **Annular flow.** Once the interfacial shear of the high velocity gas on the liquid film becomes dominant over gravity, the liquid is expelled from the center of the tube and flows as a thin film on the wall (forming an annular ring of liquid) while the gas flows as a continuous phase up the center of the tube. The interface is disturbed by high frequency waves and ripples. In addition, liquid may be entrained in the gas core as small droplets, so much so that the fraction of liquid entrained may become similar to that in the film. This flow regime is particularly stable and is the desired flow pattern for two-phase pipe flows.

- **Wispy annular flow.** When the flow rate is further increased, the entrained droplets may form transient coherent structures as clouds or wisps of liquid in the central vapor core.

- **Mist flow.** At very high gas flow rates, the annular film is thinned by the shear of the gas core on the interface until it becomes unstable and is destroyed, such that all the liquid is entrained as droplets in the continuous gas phase, analogous to the inverse of the bubbly flow regime. Impinging liquid droplets intermittently wet the tube wall locally. The droplets in the mist are often too small to be seen without special lighting and/or magnification.

2.2 The different heat transfer regions in two-phase flow [22]

We shall now consider subcooled liquid fed into the bottom of a vertical evaporator tube, which is uniformly heated along its entire length. The heat flux \dot{q} is assumed to be low and the tube should be long enough such that the liquid can be completely evaporated. Fig. 2.2 shows, on the left, alongside the various heat exchange regions that have already been explained, the profiles of the liquid and wall temperatures.

As long as the wall temperature stays below that required for the formation of vapor bubbles, heat will be transferred by single-phase, forced flow. If the wall is adequately superheated, vapor bubbles can form even though the core liquid is still subcooled. This is a region of subcooled boiling. In this area, the wall temperature is virtually constant and lies a few Kelvin above the saturation temperature. The transition to nucleate boiling is, by definition, at the point where the liquid reaches the saturation temperature at its centre, and with that the thermodynamic quality is $x_{th}^* = 0$. In reality, as Fig. 2.2 indicates, the liquid at the core is still subcooled due to the radial temperature profile, whilst at the same time vapor bubbles form at the wall, so that the mean enthalpy is the same as that of the saturated liquid.

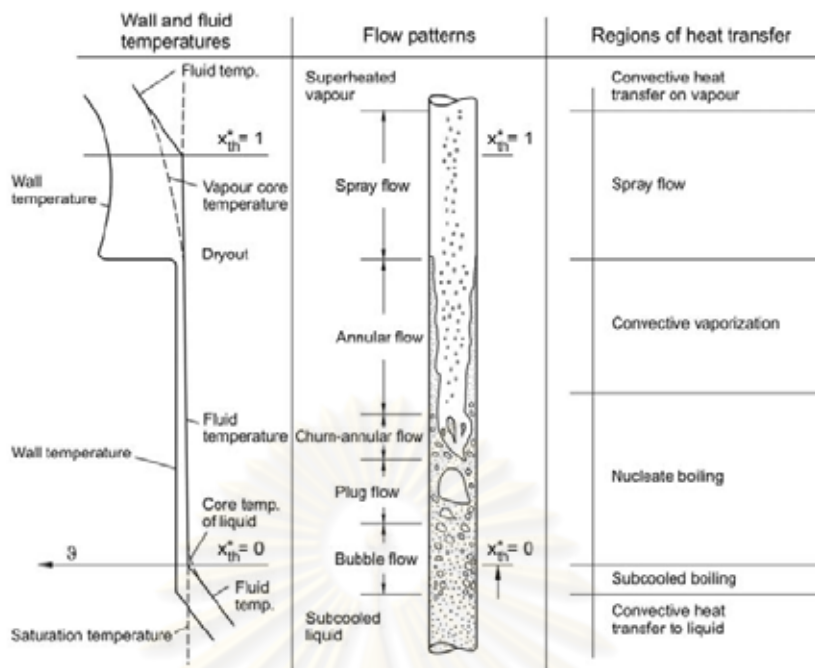


Fig. 2.2 Wall and liquid temperatures, flow pattern and the associated heat transfer regions, heated tube [22].

In the nucleate boiling region heat transfer is chiefly determined by the formation of vapor bubbles and only to a small extent by convection. This region encompasses the bubble, plug, churn and a part of the annular flow regimes. The vapor content constantly increases downstream, and at sufficiently high vapor content the churn flow converts into an annular flow, with a liquid film at the wall and vapor, with liquid droplets, in the core. The entire nucleate boiling region is characterized by the formation of vapor bubbles at the wall. However in annular flow, the liquid film downstream is so thin and its resistance to heat transfer is so low, that the liquid close to the wall is no longer sufficiently superheated, and the formation of bubbles at the wall is suppressed. Heat is conducted principally by the liquid that is evaporating at its surface. Heat is transferred by “convective evaporation”.

As soon as the liquid film at the wall is completely evaporated, the temperature of a wall being heated with constant heat flux rises. This transition is known as dryout. The spray flow region is entered, followed by a region where all the liquid droplets being carried along by the vapor are completely evaporated, in which heat is transferred by convection to the vapor.

2.3 One-Dimensional Two-fluid Model [23]

The two-fluid model treats each phase separately in terms of two sets of conservation equations that govern the balance of mass, momentum and energy with proper averaging methods. Some simplifying assumptions are adopted to reach their most commonly used form. These simplifying assumption are discussed below.

1. The average of products is approximated by the products of averages.

It is quite clear that $\langle ab \rangle \neq \langle a \rangle \langle b \rangle$, since the two variables may have non-uniform distributions on the cross sections; assuming $\langle ab \rangle \approx \langle a \rangle \langle b \rangle$ is a useful but rough approximation; however, to make it better, we should know the local distributions of a and b , just the information we have lost in space averaging. We will also suppress the explicit indication of space averages by $\langle \circ \rangle$.

2. The two phasic pressures are assumed to be equal.

This assumption appears a reasonable one, considering that in 1D duct generally the difference between phasic pressures is very small. However, the assumption $p_l = p_v = p$ is less trivial that it seems; in fact:

- Such a choice implies that pressure perturbations are transferred instantaneously from one phase to the other, which is obviously not true;

- If we would also assume that the interfacial pressure is equal to the common value p this would lead to the impossibility to simulate the transport of void fraction, e.g., in the case of stratified flow, where superficial waves propagate due to pressure difference in the two phases; to overcome this problem, pressure at the interface is sometimes assumed different from the common value of phasic pressures;

- Assuming $p_l = p_v = p$ has also consequence on the mathematical character of balance equations that, also because of that, tend to lose the hyperbolic well-posed character it would be desirable, showing in some cases a partially-elliptic behavior; we will come back on this aspect later on.

3. The interface is assumed as an immaterial surface.

The jump conditions are written assuming that then interface cannot accumulate mass or momentum or energy. This appears obvious, but there are detailed

aspects related to surface tension that should be considered. We will neglect them in the present treatment.

4. Axial diffusion terms are neglected.

Also this choice might appear obvious, since conductivity and viscosity of water (largely the most important fluid in our applications) are small enough that even a little velocity in the fluid will make advection transport so overwhelming with respect to diffusion transport to immediately justify this assumption. However, this choice eliminates any axial diffusion, changing the mathematical character of the equations. Anyway, numerical discretization will make spurious axial diffusion terms, even much larger than the physical ones, to appear again: nothing to be really desired...

5. Phasic velocities and pressures at the interface are assumed equal.

For the continuity of the velocity field through the interface, it is:

$$w_{z,li} = w_{z,vi} = w_{z,i}$$

On the other hand, assuming

$$\langle p_l \rangle_i = \langle p_v \rangle_i = p_i$$

Requires neglecting the effect of surface tension on stresses at the interface, something we normally do not really need to account for.

With these assumptions we have:

MASS BALANCE EQUATIONS:

$$\frac{\partial}{\partial t} A \alpha_k \rho_k + \frac{\partial}{\partial z} A \alpha_k \rho_k w_k = A \Gamma_k \quad (k = l, v)$$

(rate of change + advection = mass transfer rate)

In this equation, the only constitutive term is the mass transfer rate, Γ_k .

The related jump condition is $\Gamma_v = -\Gamma_l$

MOMENTUM BALANCE EQUATIONS:

$$\begin{aligned} & \frac{\partial}{\partial t} A\alpha_k \rho_k w_k + \frac{\partial}{\partial z} A\alpha_k \rho_k w_k^2 + A\alpha_k \frac{\partial p}{\partial z} \\ & + (p - p_i) \frac{\partial}{\partial z} A\alpha_k = A\alpha_k \rho_k g_z + A\Gamma_k w_i - AF'_{k,vm} \quad (k = l, v) \\ & - AF_{k,i} - AF_{k,w} + C_{w,k} (p_w - p_i) \frac{\partial A}{\partial z} \end{aligned}$$

(rate of change + advection + phasic pressure gradient

+ interfacial pressure term = body force + mass transfer term - virtual mass term

- interfacial friction - wall friction + wall pressure term)

In this equation, constitutive laws are required for specifying:

- The mass transfer rate $\Gamma_k = \left[\frac{kg}{m^3 s} \right]$: this is related to heat transfer at the

interface as discussed below;

- The interfacial velocity $w_i = \left[\frac{m}{s} \right]$: it is generally assumed

$w_i = \lambda w_v + (1 - \lambda) w_l$ ($0 \leq \lambda \leq 1$);

- The virtual mass term $F'_{k,vm} = \left[\frac{force}{volume} \right] = \left[\frac{kg}{m^2 s^2} \right]$: it is due to the local

variation of interfacial pressure due to accelerating phases (the $\Delta p'_{ki}$ term) and it

appears as a “virtual” (or “added”) mass sticking to one phase when it accelerates with

respect to the other in space or time; the classical formulation adopted to account for it

is:

$$F'_{k,vm} = \pm C_{vm} \alpha_l \alpha_v \rho_m \left[\frac{D_v w_v}{Dt} - \frac{D_l w_l}{Dt} \right] \quad (+ \text{ for vapor, } - \text{ for liquid})$$

where C_{vm} is a flow regime dependent virtual mass coefficient (e.g.,

taking the values 0.5 and 0 respectively for bubbly flow and stratified flow), ρ_m is a

mixture density and the Lagrangian derivatives appearing above are defined as:

$$\frac{D_k \circ}{Dt} = \frac{\partial \circ}{\partial t} + w_k \frac{\partial \circ}{\partial z}$$

- The interfacial friction term $F_{k,i} = \left[\frac{force}{volume} \right] = \left[\frac{kg}{m^2 s^2} \right]$: this generally

depends on the square of the relative velocity $w_r = w_v - w_l$ and it is strongly flow regime

dependent, also through the interfacial area per unit volume a_i ;

- The wall friction term $F_{k,w} = \left[\frac{\text{force}}{\text{volume}} \right] = \left[\frac{\text{kg}}{\text{m}^2 \text{s}^2} \right]$: it generally depends on the square of the phasic velocity w_k and is also flow regime dependent, also according to the fraction of the k-th phase assumed to be present at the wall;

- The pressure at the interface p_i : this term is of basic importance for two reasons:

1. Its neglect may give rise to an ill-posed problem;

2. As said, it is important to simulate gravity waves in stratified horizontal flow

- The pressure at the wall p_w : it may be assumed equal or different from the value of the common phasic pressure p , also depending on the flow regime;

- The fraction of presence of the k-th phase at the wall, $C_{w,k}$ also flow regime dependent; it must be $C_{w,l} + C_{w,v} = 1$. The jump condition in this case is, obviously enough, $F_{l,i} = -F_{v,i}$

A simple rule to check if the jump condition for an equation is correct is adding up term by term the equations for the two phases and imposing that the summation of the terms that should not appear in a mixture equation is zero. In the present case, it is:

$$\begin{aligned} & \frac{\partial}{\partial t} A(\alpha_l \rho_l w_l + \alpha_v \rho_v w_v) + \frac{\partial}{\partial z} A(\alpha_l \rho_l w_l^2 + \alpha_v \rho_v w_v^2) \\ & + A(\underbrace{\alpha_l + \alpha_v}_{=1}) \frac{\partial p}{\partial z} + (p - p_i) \frac{\partial}{\partial z} A(\underbrace{\alpha_l + \alpha_v}_{=1}) \\ & = A(\alpha_l \rho_l + \alpha_v \rho_v) g_z + A(\underbrace{\Gamma_l + \Gamma_v}_{=0}) w_i - A(\underbrace{F'_{l,vm} + F'_{v,vm}}_{=0}) \\ & - A(\underbrace{F_{l,i} + F_{v,i}}_{=0}) - A(\underbrace{F_{v,w} + F_{v,w}}_{\text{overall wall friction}}) + (\underbrace{C_{w,l} + C_{w,v}}_{=1})(p_w - p_i) \frac{\partial A}{\partial z} \end{aligned}$$

And then:

$$\begin{aligned} & \underbrace{\frac{\partial}{\partial t} A(\alpha_l \rho_l w_l + \alpha_v \rho_v w_v)}_{\text{mixture rate of change of momentum per unit length}} + \underbrace{\frac{\partial}{\partial z} A(\alpha_l \rho_l w_l^2 + \alpha_v \rho_v w_v^2)}_{\text{mixture advection of momentum per unit length}} + \underbrace{A \frac{\partial p}{\partial z}}_{\text{Total pressure term}} \\ & = \underbrace{A(\alpha_l \rho_l + \alpha_v \rho_v) g_z}_{\text{mixture body force per unit length}} - \underbrace{A(F_{l,w} + F_{v,w})}_{\text{mixture wall friction}} - \underbrace{(p - p_i) \frac{\partial}{\partial z} A + (p_w - p_i) \frac{\partial A}{\partial z}}_{=0, \text{ if } p_w = p} \end{aligned}$$

ENERGY BALANCE EQUATIONS:

$$\begin{aligned} & \frac{\partial}{\partial t} A\alpha_k \rho_k \left(u_k + \frac{w_k^2}{2} \right) + \frac{\partial}{\partial z} A\alpha_k \rho_k \left(h_k + \frac{w_k^2}{2} \right) w_k \\ &= -p_i \frac{\partial}{\partial t} (A\alpha_k) + A\alpha_k \rho_k g_z w_k + A\Gamma_k \left(h_k + \frac{w_k^2}{2} \right) \quad (k = l, v) \\ &+ AQ_{k,i} + AQ_{k,w} + AF_{k,i} w_i + AF_{k,vm} w_i \\ & \text{(rate of change + advection = interfacial pressure term + body force term} \\ & \text{+ mass transfer term + interfacial heat transfer + wall heat transfer} \\ & \text{+ interfacial friction term + virtual mass term)} \end{aligned}$$

The additional constitutive terms involved in these equations are:

- The phasic heat transfer rate at the interface $Q_{k,i} = \left[\frac{W}{m^3} \right]$: it is generally evaluated on the basis of interfacial heat transfer coefficients, $H_{k,i} = [W/(m^3 K)]$, also accounting for the interfacial area per unit volume, multiplied by the difference between the interfacial and the phasic temperatures, $T_i (= T_{sat}(p))$ in the absence of noncondensable gases) and T_k respectively:

$$Q_{k,i} = H_{k,i} (T_i - T_k)$$

- The phasic heat transfer rate at the wall $Q_{k,w} = \left[\frac{W}{m^3} \right]$: it is generally evaluated on the basis of wall heat transfer coefficients, $H_{k,w} = [W/(m^3 K)]$, also accounting for the phasic heat transfer area with the wall, multiplied by the difference between the wall and the phasic temperatures, T_w and T_k respectively:

$$Q_{k,w} = H_{k,w} (T_w - T_k)$$

In this case, we will find the appropriate jump condition by adding the phasic energy balance equations and discussing the obtained equation in front of the expected form of the mixture energy balance equation. It is:

The relationship can be rewritten as:

$$\Gamma_v = -\frac{Q_{l,i} + Q_{v,i}}{h_v - h_l}$$

Showing that at the interface heat and mass transfer are intimately linked with each other

In particular:

- If the interface releases heat to the phases, i.e., the summation of the convection interfacial heat transfer rates is positive, $Q_{l,i} + Q_{v,i} > 0$, then it is $\Gamma_v < 0$, i.e., condensation takes place; the heat released is equal to the latent heat released by the condensation process, $-\Gamma_v(h_v - h_l)$;

- If the interface receives heat from the phases, i.e., the summation of the convection interfacial heat transfer rates is negative, $Q_{l,i} + Q_{v,i} < 0$, then it is $\Gamma_v > 0$, i.e., boiling or evaporation takes place; the heat received by the interface is equal to the latent heat needed by the vaporization process, $\Gamma_v(h_v - h_l)$.

This view of the simultaneous heat and mass transfer processes can be applied to both “bulk” and “wall” mass transfer processes:

- Bulk mass transfer refers to homogeneous boiling or condensation, where the interface is made of bubble or droplet surfaces or even the liquid surface in stratified or annular flow conditions;

- Wall mass transfer refers to heterogeneous processes due to local non-equilibrium, as subcooled boiling or film wise condensation, where the interface is located close to the wall in a region where steep temperature gradients occur.

Apportioning the mass transfer in bulk and wall contribution is one of the tasks pursued in codes for evaluating heat and mass transfer, as the two conditions refer to different phenomena

CHAPTER III

TEXAS CODE

This chapter consists of five sections. The first section introduces the concept of TEXAS code. Conservation equations for the Eulerian vapor and liquid fields, and only momentum and energy equations for the Lagrangian fuel particle field are described in the next section. The third section discusses the phase change model used in the TEXAS code. The fourth section is Switch Void Fraction (SVF) in Pressure Iteration. And finally, the modification of TEXAS code for simulation of two-phase natural circulation will be presented.

3.1 Brief description of TEXAS code

The TEXAS computer model is one of the major tools used at the Department of Engineering Physics, University of Wisconsin for simulations of fuel-coolant interaction during its mixing, triggering and explosion phases. TEXAS is a model based on a one-dimensional hydrodynamics code originally developed at Los Alamos National Laboratory as part of the SIMMER development, adapted at Sandia National Laboratories and finally modified by the University of Wisconsin for fuel-coolant interactions. The original TEXAS code was a parametric model developed by Young [24] for the design and analysis of fuel-coolant interaction experiments for LMFBR safety related issues. In an attempt to extend the capabilities of TEXAS, Chu and Corradini [25] incorporated a dynamic fragmentation model and a complete set of constitutive correlations for interfacial mass, momentum, and energy transport term; i.e., TEXAS-II. Since then, several improvements to the explosion propagation modeling, in particular, have been introduced by Tang [26]. A chemical reaction model to account the heat generation by oxidation of metallic melt was added by Murphy [27]. These updates, together with the complete model of the fragmentation of the fuel during the mixing phase, warranted a new release of the code, TEXAS-V.

The TEXAS code is a transient, three fluid, one-dimensional models capable of simulating fuel-coolant mixing interactions. The three fields include two Eulerian fields for coolant liquid and vapor, and one Lagrangian field for fuel particles.

The multifield feature of the code allows it to model thermal and mechanical nonequilibrium between coolant liquid and vapor which is very likely the case for fuel-coolant interactions. Fig. 3.1 shows conceptual picture of current TEXAS mixing model. The code has the ability to handle flow regime transitions, which is also important to realistically model the heat transfer process. The “Lagrangian” treatment for the fuel field makes it easier to track the fuel particle movement, and eliminates some numerical difficulties encountered in pure Eulerian codes. The fragmentation model used in the code is based on hydrodynamic instabilities (i.e., Rayleigh-Taylor). The code also provides choices of velocity, pressure, and reflective (or closed) boundary conditions, giving more flexibility to users in different applications. A semi-implicit numerical technique is used in TEXAS which is a modified version of the SIMMER-II method, the actual forerunner of the TEXAS hydrodynamic formulation. With this method, the pressure iteration is done in a loop in which the energy and momentum equations are solved semi-implicitly, whereas the continuity equations are solved implicitly by adjusting the pressure distribution such that the errors of the continuity equations for all cells are reduced to a given tolerance. The Newton-Raphson method is employed in this pressure iteration.

In the following discussion, we briefly review the basic governing conservation equations and the two key constitutive fragmentation models: the fragmentation model for mixing and the explosion and the phase change model. In addition to these two constitutive models, interfacial exchange terms of mass, momentum, and energy are needed to couple the conservation equations among different fields. The complete set of constitutive relations for these interfacial exchange terms have been developed and incorporated into the code. All these exchange terms are modeled in three different flow regimes: bubbly flow, droplet flow, and transition flow. For detailed descriptions of all these terms, readers are referred to Chapter 4 of Chu's PhD thesis [28]

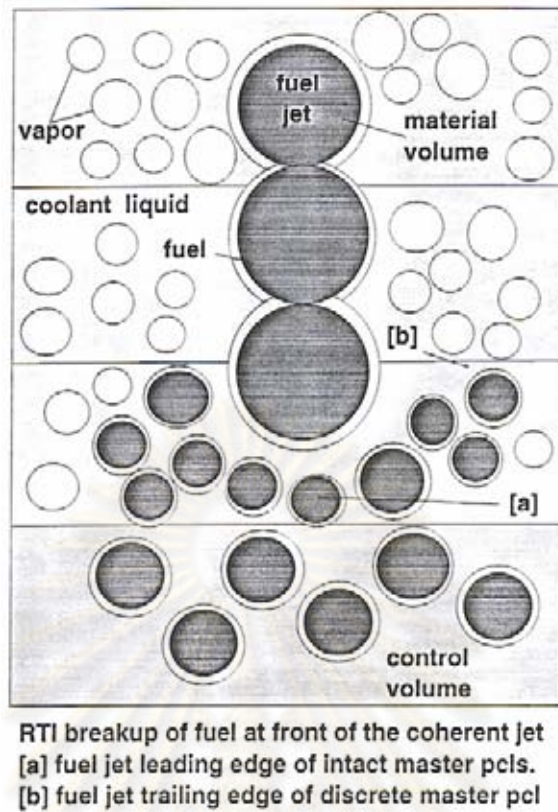


Fig. 3.1 Conceptual picture of current TEXAS mixing model[25]

3.2 Conservation Equations

Conservation equations are the bases of all hydrodynamic computer models. In TEXAS, there are mass, momentum, and energy equations for the Eulerian vapor and liquid fields, and only momentum and energy equations for the Lagrangian fuel panicle field. The macroscopic densities for the vapor and liquid (ρ'_g and ρ'_l) are used in these conservation equations. ρ'_g and ρ'_l are defined as:

$$\rho'_g = \alpha_g \rho_g \quad (3.1)$$

$$\rho'_l = \alpha_l \rho_l \quad (3.2)$$

Where α_g and α_l are the volume fractions of the vapor and liquid with respect to the total volume of coolant in an Eulerian cell. With this definition of the macroscopic densities (Equations (3.1) - (3.2)), the conservation equations are listed below:

3.2.1 Mass Equations

Vapor:

$$\frac{\partial \rho'_g}{\partial t} + \nabla \cdot (\rho'_g \vec{u}_g) = \Gamma_e - \Gamma_c \quad (3.3)$$

Liquid:

$$\frac{\partial \rho'_l}{\partial t} + \nabla \cdot (\rho'_l \vec{u}_l) = \Gamma_c - \Gamma_e \quad (3.4)$$

Where:

\vec{u}_g = velocity of vapor field

\vec{u}_l = velocity of liquid field

Γ_e = evaporation rate

Γ_c = condensation rate

3.2.2 Momentum Equations

Vapor:

$$\begin{aligned} \rho'_g \frac{\partial \vec{u}_g}{\partial t} + \rho'_g \vec{u}_g \frac{\partial \vec{u}_g}{\partial z} = & -\rho'_g g - \alpha_g \frac{\partial P}{\partial z} + K_{gl} (\vec{u}_l - \vec{u}_g) \\ & - K_{wg} \vec{u}_g - V_g + A_m \frac{\partial}{\partial t} (\vec{u}_l - \vec{u}_g) \\ & - \Gamma_e (\vec{u}_g - \vec{u}_l) + M_{gp} \end{aligned} \quad (3.5)$$

Liquid:

$$\begin{aligned} \rho'_l \frac{\partial \vec{u}_l}{\partial t} + \rho'_l \vec{u}_l \frac{\partial \vec{u}_l}{\partial z} = & -\rho'_l g - \alpha_l \frac{\partial P}{\partial x} + K_{gl} (\vec{u}_g - \vec{u}_l) \\ & - K_{wl} \vec{u}_l - V_l + A_m \frac{\partial}{\partial t} (\vec{u}_g - \vec{u}_l) \\ & - \Gamma_c (\vec{u}_l - \vec{u}_g) + M_{lp} \end{aligned} \quad (3.6)$$

Fuel particle:

$$M_{pk} \frac{du_{pk}}{dt} = -M_{pk} g + D_k (u_g - u_{pk}) + E_k (u_l - u_{pk}) \quad (3.7)$$

Where:

g = gravity

P = pressure

K_{gl} = vapor-liquid macroscopic drag coefficient

K_{wg} = wall-liquid friction coefficient

K_{wl} = wall-vapor friction coefficient

V_g = viscous loss term for vapor field

V_l = viscous loss term for liquid field

A_m = transient virtual mass force coefficient

M_{gp} = summation of vapor-Lagrangian particle drags

M_{lp} = summation of liquid-Lagrangian particle drags

D_k = vapor-Lagrangian particle drag term

E_k = liquid-Lagrangian particle drag term

3.2.3 Energy Equations

Vapor:

$$\begin{aligned} \frac{\partial}{\partial t}(\rho_g I_g) + \frac{\partial}{\partial t}(\rho_g I_g \bar{u}_g) = -P \left[\frac{\partial \alpha_g}{\partial t} + \frac{\partial}{\partial t}(\alpha_g \bar{u}_g) \right] \\ + W_g + Q_{gw} + Q_{gp} + Q_{gi} \\ - C_g + S_g + (\Gamma_e - \Gamma_c) h_{gs} \end{aligned} \quad (3.8)$$

Liquid:

$$\begin{aligned} \frac{\partial}{\partial t}(\rho_l I_l) + \frac{\partial}{\partial t}(\rho_l I_l \bar{u}_l) = -P \left[\frac{\partial \alpha_l}{\partial t} + \frac{\partial}{\partial t}(\alpha_l \bar{u}_l) \right] \\ + W_l + Q_{lw} + Q_{lp} + Q_{li} \\ - C_l + S_l + (\Gamma_c - \Gamma_e) h_{ls} \end{aligned} \quad (3.9)$$

Fuel particle:

$$M_{pk} \frac{dI_{pk}}{dt} = R_{lk} (T_l - T_{pk}) + R_{gk} (T_g - T_{pk}) + R_{ik} (T_{sat} - T_{pk}) + R_{wk} (T_w - T_{pk}) + S_{pk} \quad (3.10)$$

Where:

I_g = internal energy of vapor field

I_l = internal energy of liquid field

I_{pk} = internal energy of Lagrangian particle

W_g = viscous work for vapor

W_l = viscous work for liquid

Q_{gw} = wall-vapor heat transfer term

Q_{lw} = wall-liquid heat transfer term

Q_{gp} = vapor-Lagrangian particle heat transfer term

Q_{lp} = liquid-Lagrangian particle heat transfer term

Q_{gi} = vapor-interface heat transfer term

Q_{li} = liquid-interface heat transfer term

C_g = conduction heat transfer term for vapor

C_l = conduction heat transfer term for liquid

h_{gs} = vapor enthalpy at saturation temperature

h_{ls} = liquid enthalpy at saturation temperature

S_g = heat source term for vapor

S_l = heat source term for liquid

S_{pk} = heat source term for Lagrangian particle

T_g = vapor temperature

T_l = liquid temperature

T_{pk} = Lagrangian particle temperature

T_w = wall temperature

T_{sat} = saturation temperature

R_{gk} = macroscopic heat transfer coefficient between vapor and Lagrangian particles of k^{th} group

R_{lk} = macroscopic heat transfer coefficient between liquid and Lagrangian particles of k^{th} group

R_{tk} = macroscopic heat transfer coefficient between vapor-liquid interface and Lagrangian particles of k^{th} group

R_{wk} = macroscopic heat transfer coefficient between wall and Lagrangian particles of k^{th} group

3.3 Phase Change Model

The phase change model is another important constitutive relation in TEXAS-V, which calculates the vaporization or condensation rate, and in turn, determines the local pressure. The technique employed in the model is similar to the simple vaporization-condensation model used in SIMMER-II. But the phase change model in TEXAS-V is fully implicit in the pressure iteration.

The model assumes that the phase change occurs at the interface of the coolant liquid and vapor, and considers all forms of heat transfer between the fuel and coolant under different flow regime conditions. Generally, there are three ways in which the fuel heat is used:

1. to increase the internal energy of the coolant liquid;
2. to increase the internal energy of the coolant vapor;
3. to vaporize the coolant liquid.

Using an energy balance, the model calculates the net heat flow, which becomes the energy associated with the generated vapor, i.e.:

$$\dot{q}_{net,f} = \dot{q}_f - \dot{q}_l - \dot{q}_g \quad (3.11)$$

Where \dot{q}_f is the heat lost by the fuel; and \dot{q}_l and \dot{q}_g are the heat received by the coolant liquid and coolant vapor respectively, which becomes the internal energy of the coolant. The detailed description of these heat transfer terms is given in Chapter 4 of Chu's PhD thesis [28].

Knowing the net heat flow, $\dot{q}_{net,f}$ one can easily calculate the phase change rate per unit volume, i.e.:

$$\dot{m}_g = \frac{\dot{q}_{net,f}}{h_{fg} V_{cell}} \quad (3.12)$$

Where the h_{fg} is the latent heat for the coolant; and V_{cell} is the cell volume.

If the net heat flow, $\dot{q}_{net,f}$ is positive, there is vapor generated, and the vaporization rate is:

$$\Gamma_e = \dot{m}_g, \quad \Gamma_c = 0$$

If the net heat flow, $\dot{q}_{net,f}$ is negative, there is vapor condensed into liquid, and the condensation rate is:

$$\Gamma_c = -\dot{m}_g, \quad \Gamma_e = 0$$

Because this model is based on the assumption that phase changes occur at the interface of the coolant liquid and vapor, it allows the vapor to be produced under subcooled as well as saturated conditions.

3.4 Switch Void Fraction (SVF) in Pressure Iteration

As described in the previous section, TEXAS is a multifluid model, which allows the liquid and vapor to exist at different temperatures. However, the same macroscopic pressure is assumed for both the liquid and vapor within one control volume. The temporal pressure change is found by solving either the liquid or vapor mass equation. The new pressure is then substituted into the other mass equation to find the void fraction. The new pressure is also used to calculate other physical variables. The newly calculated void fraction and other variables are then used in the next pressure iteration until convergence occurs. There is a "switch void fraction (SVF)" given by the user, which determines whether to solve the liquid or vapor mass continuity equation. If the void fraction in a cell is smaller than the SVF, the liquid mass equation is solved otherwise, the vapor equation is solved. In TEXAS-V, the value of 0.5 (or 50%)

was chosen as the switch value (SVF). This value has a significant impact on the convergence efficiency. Because the compressibility of the vapor is much greater than that of the liquid, the local pressure is primarily determined by the vapor density change when a certain amount of vapor is present locally. Therefore, the compressibility difference for the liquid and vapor should be taken into consideration in choosing the appropriate value for SVF. Analysis has been done to select such a value so that at this value, the same change of volume fraction for liquid or vapor will give some pressure change.

The pressure change due to the liquid and vapor density changes are

$$\frac{\Delta P}{\Delta \rho_l} \cong \frac{\partial P}{\partial \rho_l} \quad (3.13)$$

$$\frac{\Delta P}{\Delta \rho_g} \cong \frac{\partial P}{\partial \rho_g} \quad (3.14)$$

For given void fraction change, the corresponding density changes for the liquid and vapor are:

$$\Delta \rho_l = -\rho_l \frac{\Delta \alpha_l}{\alpha_l} \quad (3.15)$$

$$\Delta \rho_g = -\rho_g \frac{\Delta \alpha_g}{\alpha_g} \quad (3.16)$$

and

$$\alpha_l + \alpha_g = 1 \quad (3.17)$$

Combining these equations, one obtains the expression of the appropriate value for SVF, α_g

$$\alpha_g = \frac{\frac{\rho_g}{\frac{\partial \rho_g}{\partial P}}}{-\frac{\rho_l}{\frac{\partial \rho_l}{\partial P}} + \frac{\rho_g}{\frac{\partial \rho_g}{\partial P}}} \quad (3.18)$$

and

$$\frac{\rho_l}{\frac{\partial \rho_l}{\partial P}} \cong \frac{\rho_g}{\frac{\partial \rho_g}{\partial P}} \quad (3.19)$$

Therefore one has:

$$\alpha_g \approx \left| \frac{\rho_g \cdot \frac{\partial \rho_l}{\partial P}}{\rho_l \cdot \frac{\partial \rho_g}{\partial P}} \right| \quad (3.20)$$

At a pressure of 10 MPa, α_g is about 0.004. Using the new switch void fraction, α_g we have greatly improved the calculation efficiency, especially during the propagation phase when the calculation becomes more sensitive due to the large pressure changes.

3.5 Modification of TEXAS code

TEXAS code was modified to simulate the two-phase rectangular natural circulation. Fig. 3.2 and Fig. 3.3 show the TEXAS program and the modification of TEXAS program respectively. The modifications of TEXAS code are as follow:

- The code related to fuel particles was commented in the program.
- The continuous boundary condition (rectangular loop) was added to the computer program as shown in Fig. 3.3.
- The total run time was changed from milliseconds for thermal explosion to seconds for natural circulation.
- The equation of state for liquid was modified to obtain more accurate result.

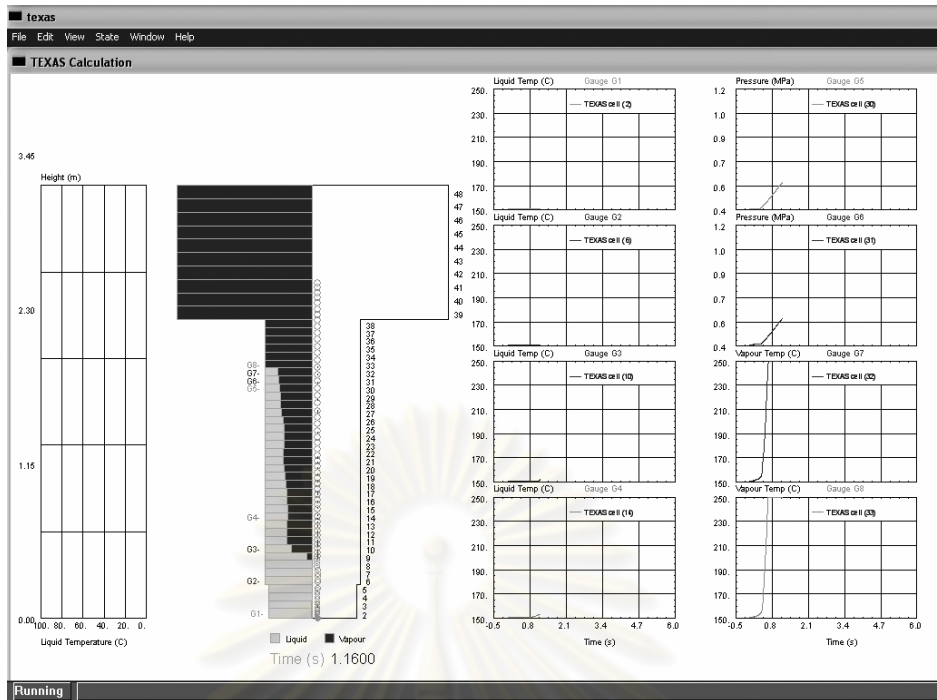


Fig. 3.2 The TEXAS program

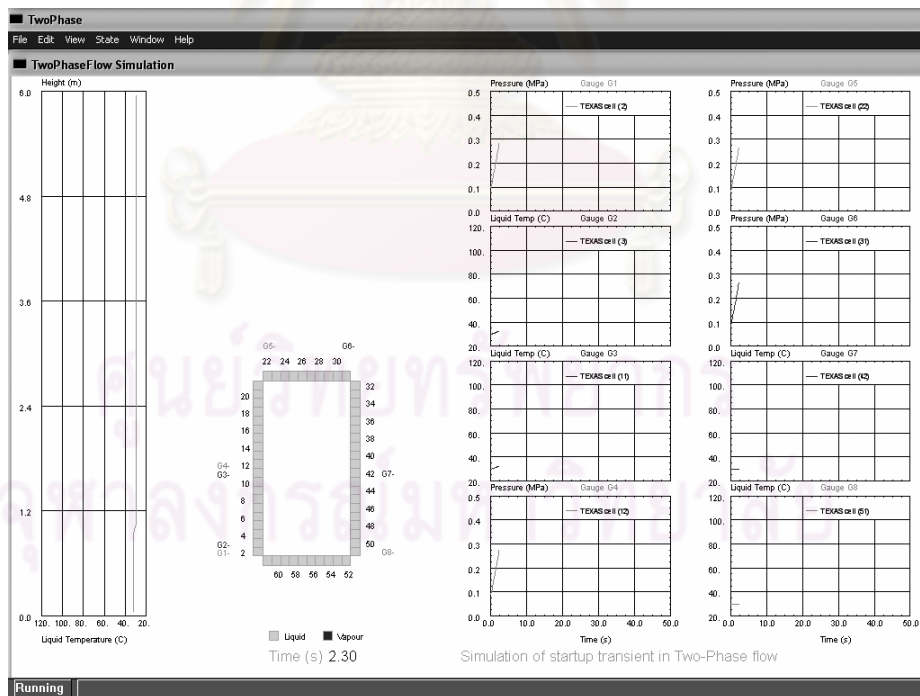


Fig. 3.3 The modification of TEXAS program

CHAPTER IV

EXPERIMENTAL APPARATUS AND PROCEDURE

This chapter describes the experimental equipment and procedures used in this research. Two rectangular natural circulation loops, namely the NCL#1 and the NCL#2, have been designed and constructed for simulation of a two-phase flow under two different configurations. The Fast Fourier Transform (FFT) method is employed to the temperature and the differential pressure oscillation observed.

4.1 Experimental apparatus for the NCL#1

Fig. 4.1 and Fig. 4.2 show respectively the schematic diagram and the actual setup of the NCL#1. The loop consists of the riser, the downcomer, the vertical heating, and the vertical cooling sections. The loop piping has the inner and the outer diameters of 22 and 25 mm respectively. An expansion tank with an atmospheric opening is installed on the top of the loop to allow volumetric expansion of the fluid. The entire loop is made of glass. The heating and the cooling sections are of the same length. The heating section is an annulus; the inner heating rod is made of stainless steel while the outer tube is made of glass. The outer glass tube has an inner diameter of 47 mm, an outer diameter of 50 mm, and a length of 500 mm. The inner U-shape heating rod is 8 mm in diameter and 400 mm in length. The cooler is a tube-in-tube type with the cooling water flowing in the annulus formed between the glass tubes. The hydraulic diameter of the annulus is 22 mm. The entire loop is in thermal contact with the atmosphere and is subjected to heat loss to the ambient.

The loop is equipped with the 1.6 mm diameter type K thermocouples to measure the temperature changes across the heater and across the primary and the secondary sides of the cooler. The thermocouples are positioned to measure the temperature at the tube center. The heating power is obtained from the electric current and voltage measured by analog AC ammeter and voltmeter, respectively. The uncertainty of the temperature measurement is within ± 1 °C. Data are acquired and stored in a computer via the RS-232 interface.

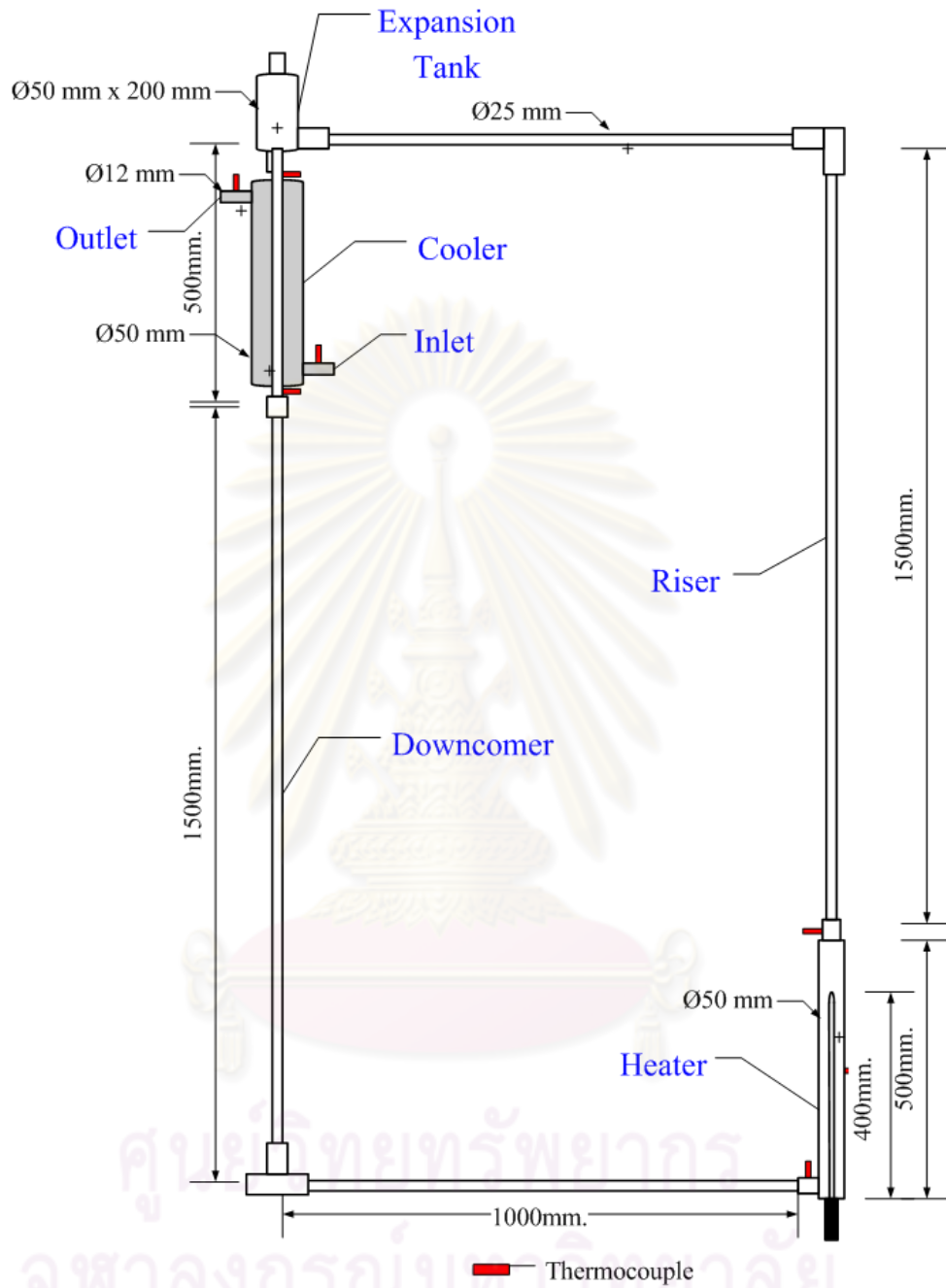


Fig. 4.1 Schematic diagram of the NCL#1

4.2 Experimental procedure for the NCL#1

The primary loop was filled with water. To remove the gases dissolved in the water, the loop was heated to reach the natural circulation condition with a high heating power to boil the water. The experiments were carried out in this loop at several

heating power levels under the on/off condition for the cooling system. The heating power and the coolant water flow rate were maintained at the constant level during the entire duration of an experiment. The cooling water inlet temperature was 24 ± 1 °C. The following procedure was used for each test. At first, start the data acquisition and check of the uniformity of the system temperature and comparison with the ambient temperature. It should be noted that data acquisition from 7 type K thermocouples was performed every 2 s (time needed to record all the signals were 1 s). Next, start the cooling flow and the heating power. Finally, the test was concluded after 8000 s.



Fig. 4.2 The picture of NCL#1

4.3 Experimental apparatus - NCL#2

Fig. 4.3 and Fig. 4.4 show respectively the schematic diagram and the actual setup of the NCL#2. The loop consists of the vertical heating section, the riser, the condenser and the downcomer. The vertical heating section is an annulus; the inner heating rod is made of stainless steel while the outer tube is made of glass. The outer glass tube is measured 22 mm and 25 mm for the inner and the outer diameters respectively, with a length of 800 mm. The inner heating rod is 16 mm in diameter and 800 mm long. The gap width between the heating rod and the glass tube is 3 mm. The riser is a glass tube with the inner and the outer diameters of 22 and 25 mm, respectively. The riser is 1120 mm long. The condenser is a tube-in-tube type with the cooling water flowing in the annulus formed between the copper tube and the polyvinyl chloride (PVC) tube. The hydraulic diameter of the annulus is 21.5 mm. The condenser is 800 mm long. The downcomer is made of copper tube. The copper tube has dimensions of 26 mm for the inner and 28.5 mm for the outer diameters, with length equal to 1950 mm. An expansion tank with an atmosphere opening is installed on the top of the loop to allow volumetric expansion of the fluid. The glass tube is uninsulated to allow the visual observation of the flow. The entire loop is in thermal contact with the atmosphere, and is subjected to heat loss to the ambient.

Type K thermocouples are installed to measure the temperature changes across the condenser, the downcomer middle, across the heater, and the riser outlet. The bare wire butt welded thermocouples with the diameter of 0.5 mm are selected for fast response time. The response time is defined as the time required to reach 63.2% of an instantaneous temperature change. The pressure sensor is installed to measure differential pressure across the heater. Fig. 4.5 shows block diagram of the data recorder. The MAX6674 cold-junction-compensation thermocouple-to-digital converter performs cold-junction compensation and digitizes the signal from a type-K thermocouple. The microcontroller reads data from the MAX6674 via SPI interfacing and then converts to temperature value. The MPX5050DP is a piezoresistive transducer with on-chip signal conditioned, temperature compensated and calibrated. The output signal from MPX5050DP is read and converts by the microcontroller with a built-in 10-bit

analog-to-digital converter (ADC). The resolutions for the measured temperature and differential pressure are $0.125\text{ }^{\circ}\text{C}$ and 0.05 kPa , respectively. The uncertainty of the temperature measurement is within $\pm 1\text{ }^{\circ}\text{C}$. Data are acquired and stored in a computer via RS-232 interfacing.

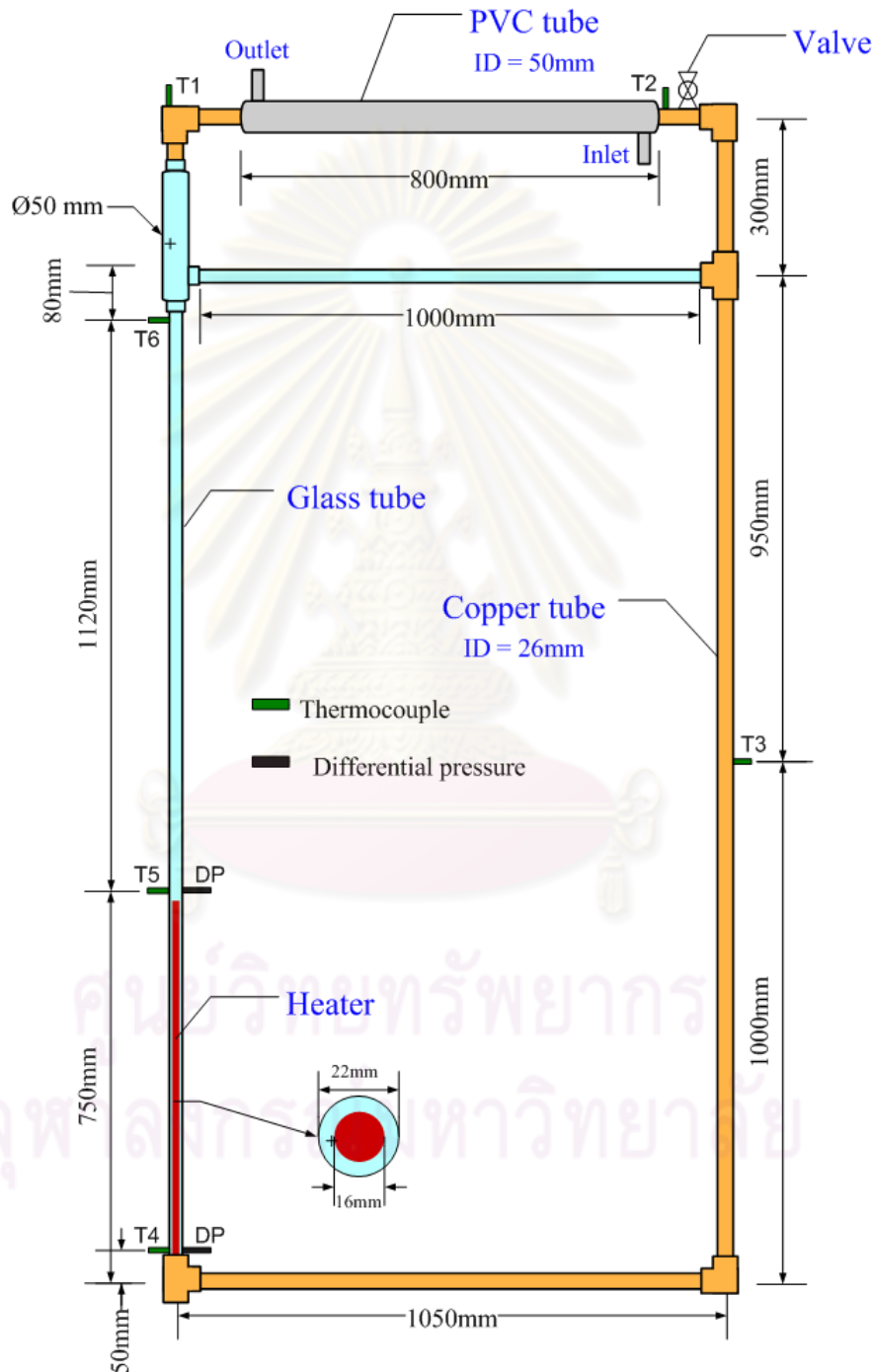


Fig. 4.3 Schematic diagram of the NCL#2

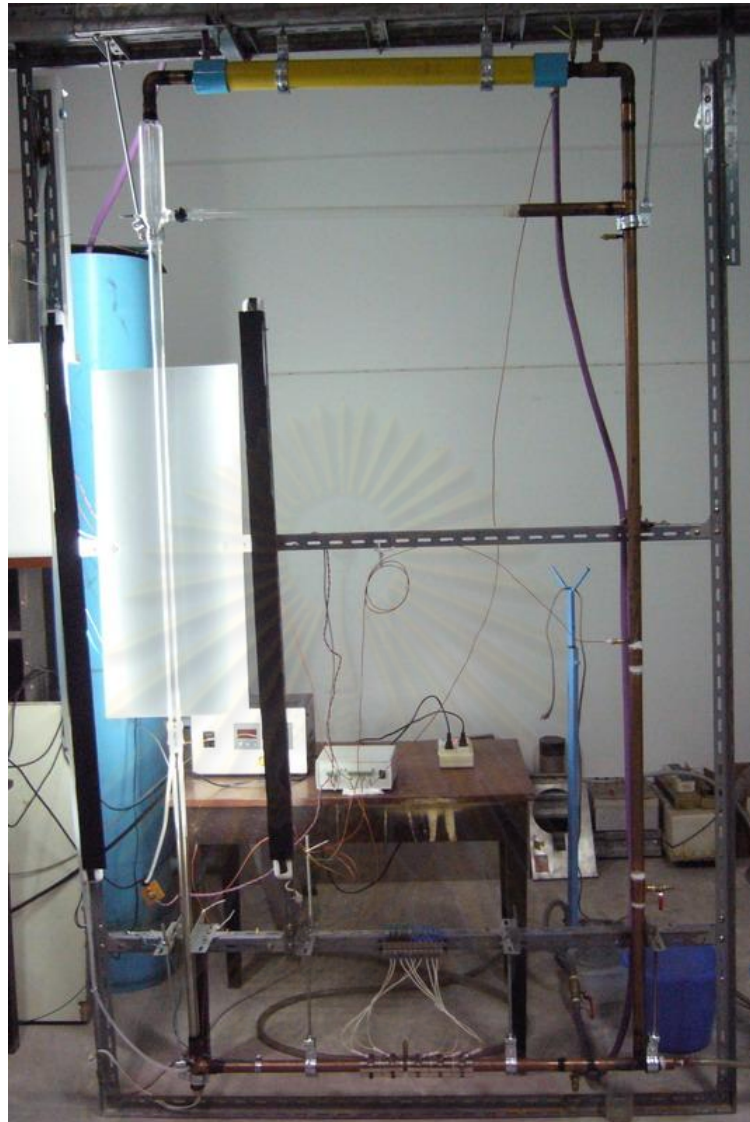


Fig. 4.4 The picture of NCL#2

Fig. 4.6 shows a block diagram of the power controller. The dimmer circuit and the power adjust knob are used to control the heating power. The current transformer, type TADK, is used for reducing the electric current from 15 A to 5 A. The heating power is obtained from the electric current and voltage as measured by digital AC ammeter and voltmeter (Carlo Gavazzi, type DI3-72 AV5), respectively.

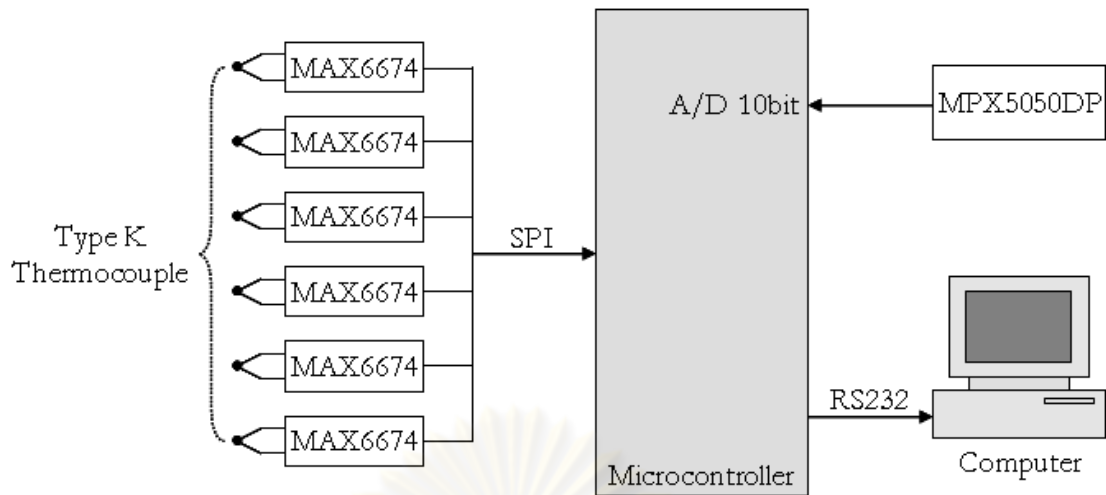


Fig. 4.5 Block diagram of the data recorder

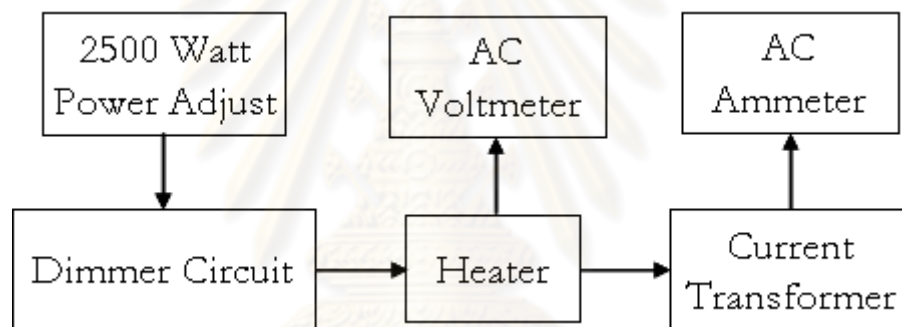


Fig. 4.6 Block diagram of the power controller.

Photographs of bubbles at the riser are taken by a single-lens reflex (SLR) camera (Olympus E510). The camera's shutter speed is 1/1000 second. Two 36 W fluorescent lamps are used as light source.

4.4 Experimental procedure for NCL#2

The loop was filled with water. To remove the gases dissolved in the water, the loop was heated to reach the natural circulation condition with a high heating power to boil the water. Two-phase natural circulation experiments were carried out in this loop at several heating power levels. The heating power was maintained at a constant level during the entire duration of an experiment. At the beginning of each experiment, before switching on the heating power the system temperature was

checked for uniformity, and compared with the ambient temperature. Temperatures were recorded at 1-second interval. After switching on the heating power, temperature data is recorded until stable flow behavior is observed.

4.5 Fast Fourier Transform method

Fast Fourier Transform (FFT) of the temperature oscillation was computed with the Discrete Fourier Transform (DFT) function ($Y = \text{fft}(X)$ in MATLAB program). The function $Y = \text{fft}(X)$ implement the transform pair given for vectors of length N is defined by:

$$X(k) = \sum_{j=1}^N x(j) \omega_N^{(j-1)(k-1)}$$

Where $\omega_N = e^{(2\pi i)/N}$ is an N^{th} root of unity.

Appendix B.1 shows the MATLAB code for computing the FFT.



ศูนย์วิทยทรัพยากร
จุฬาลงกรณ์มหาวิทยาลัย

CHAPTER V

RESULTS AND DISCUSSIONS

This chapter is separated into 4 sections. The first section reports the results of the NCL#1. Effect of cooling system on single-phase natural circulation is presented and temperature oscillation of water is also discussed. The next section reports the results of the NCL#2. The third section of this chapter presents the results from computer simulation. The results from computer program are compared with the experimental data and will be presented in the final section.

5.1 The results of the NCL#1

5.1.1 Effect of cooling system on single-phase natural circulation

The water temperature measured across the heater and the cooler at 473 W heating powers when the cooling system was turned off and turned on are as shown in Fig. 5.1 and Fig. 5.2, respectively. It should be noted that the time required to reach the steady state was decreased with the cooling system turning on.

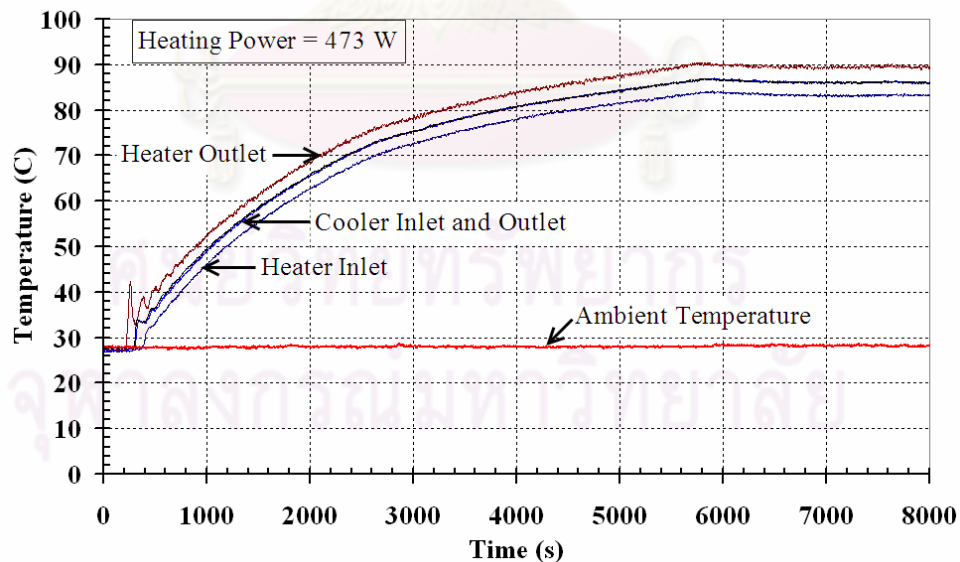


Fig. 5.1 The water temperature at 473 W heating powers when the cooling system was turned off

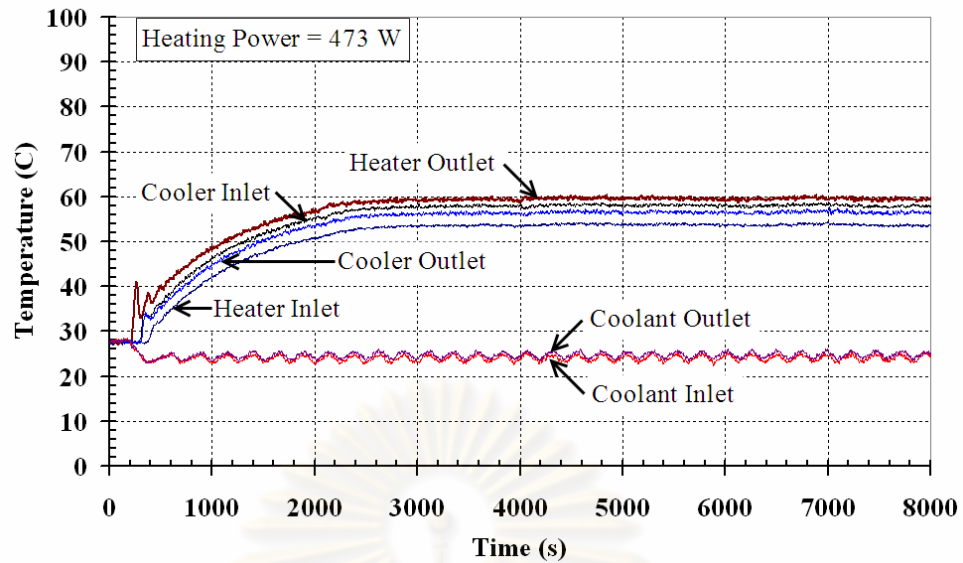


Fig. 5.2 The water temperature at 473 W heating powers when the cooling system was turned on

Maximum temperatures at the heater outlet for different heating power levels are as shown in Fig. 5.3. It was found that the maximum temperature was increased with the increasing heating power. In addition, for the same heating power, the maximum temperature was much higher when the cooling system was turned off compared with that obtained when the cooling system was turned on. It should be noted that the heating power level was limited to 473 W because the maximum temperature in the heating section was already very close to the saturating temperature for the water at atmospheric pressure.

Fig. 5.4 shows the temperature differences across the heater for different heating power levels with the cooling system turning off and turning on. It was found that at any given time the temperature difference only was slightly increased with the increasing heating power. The same behaviors for temperature differences were observed regardless of the turning condition of the cooling system.

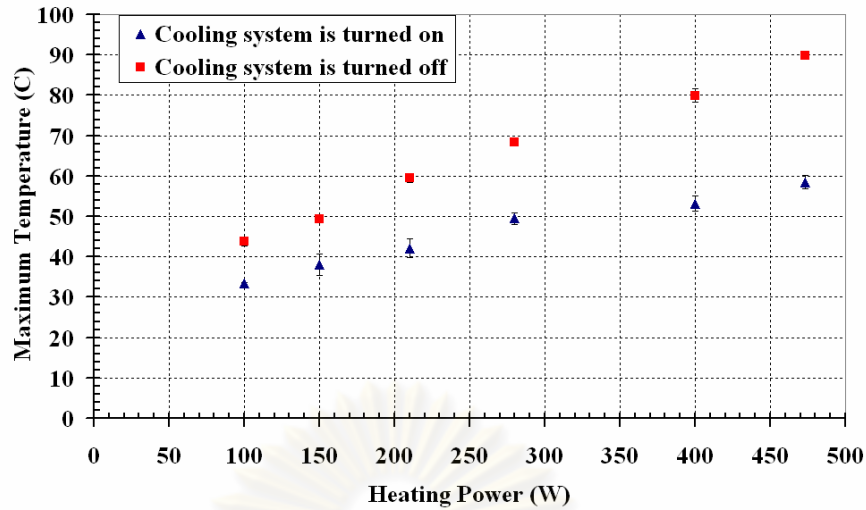


Fig. 5.3 The maximum temperature at the outlet heater for the different heating power levels

The maximum temperature at the heater outlet was found to depend on both the heating power level and the presence of the cooling system. However, the temperature difference across the heater was only affected by the heating power level. This was considered due to the limitation of the heater capacity. In effect the amount of heat received by the water flowing through the heater remained the same regardless of the inlet temperature.

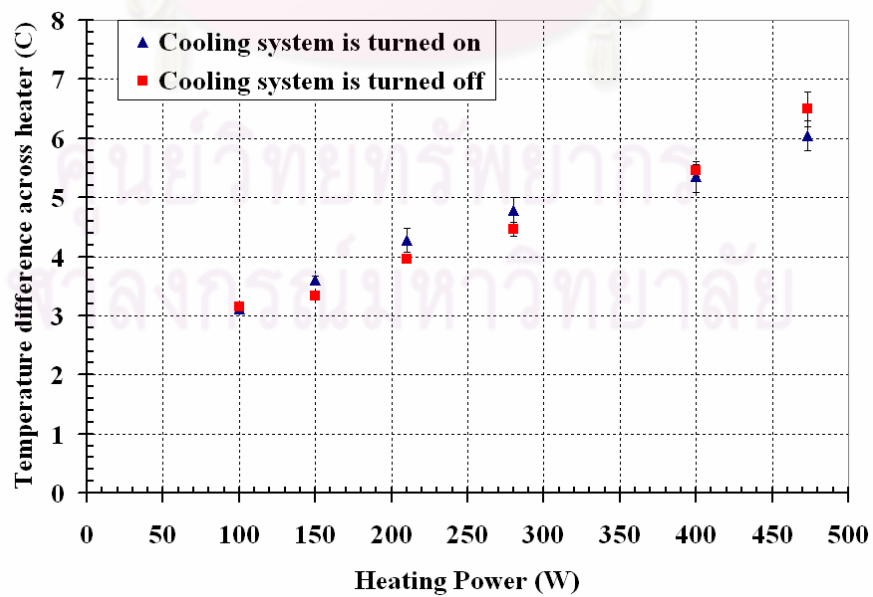


Fig. 5.4 Effect of heating power on the temperature difference across the heater

The mass flow rate due to the density gradient at the steady state was computed from the heating power and the temperature difference across the heater based on the conservation of energy. The macroscopic conservation of energy equation for a steady flow was expressed as

$$Q = \dot{m}C_p(T_o - T_i)$$

where T_i and T_o were respectively the mean fluid temperatures at the inlet and the outlet of the heating section, \dot{m} was the mass flow rate, C_p was the specific heat capacity, and Q was the heating power. The value of C_p is temperature dependent. For this study, the value averaged from that at the inlet and the outlet is used. The values of mass flow rates computed at various heating power levels are as plotted in Fig. 5.5. The result indicated that the mass flow rate was increased with the increasing heating power. Again, the same mass flow rates were acquired regardless of the turning condition of the cooling system.

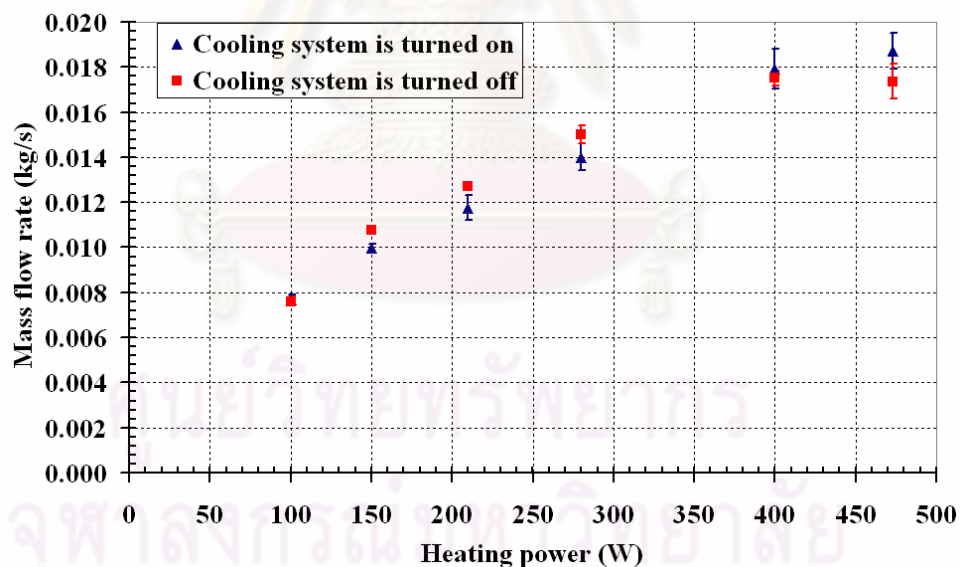


Fig. 5.5 Effect of heating power on the mass flow rates

4.1.2 The temperature oscillation

The water temperatures measured at the heater inlet and outlet at 575 W heating powers are as shown in Fig 5.6. The fluctuation in water temperature due to flow oscillation was observed during the starting of heater and after the water boiling. At the

water heater startup, the heater power was turned on but the water flow rate in the loop was essentially zero. As the water in the heating section absorbed heat from heater and caused the water temperature at the heater outlet to increase, the natural circulation was then initiated since the buoyancy force due to the density gradient had become greater than the overall friction in the loop. As the flow was established in the loop, the water temperature at the heater outlet would be decreased since the heating section was filled with colder water.

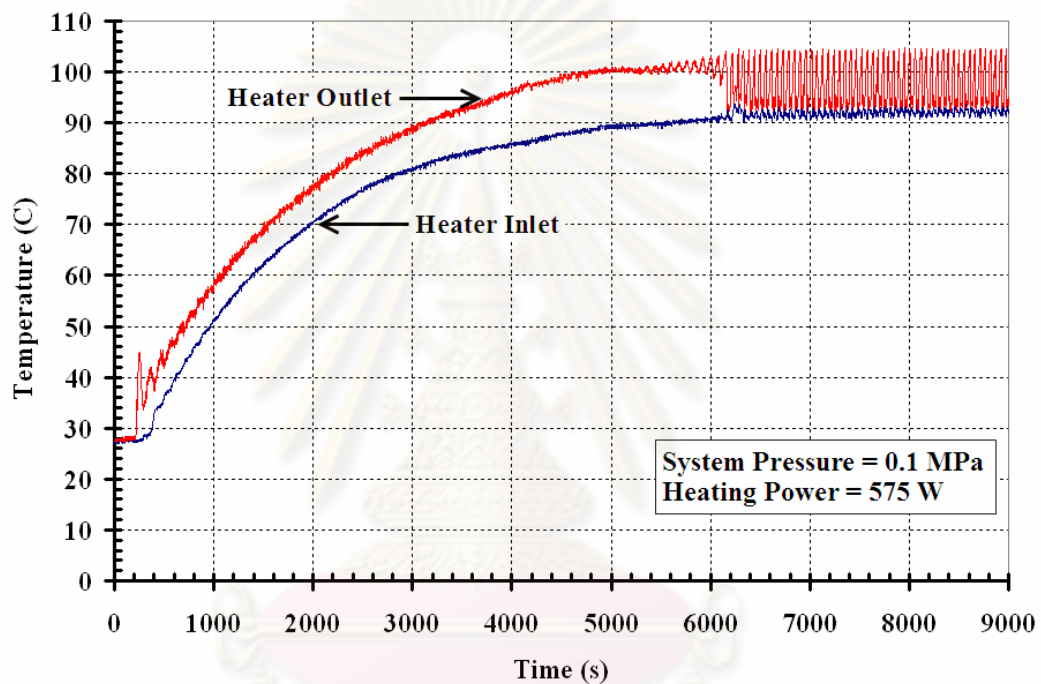


Fig. 5.6 The water temperature at the heater inlet and outlet of 575 W heating powers

As shown in Fig. 5.6, the water temperature at the heater outlet initially fluctuated wildly before it was settled down and began to gradually increase toward the boiling point. The amplitude of the initial fluctuation was found to increase as the heating power level was increased as show in Fig. 5.7. It should be noted that no boiling was observed for the heating power level that was less than or equal to 475 W.

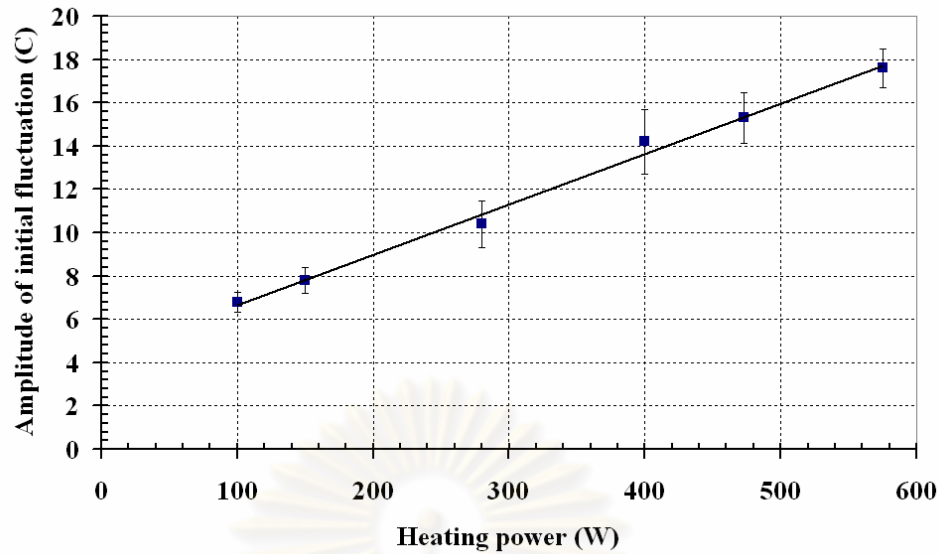


Fig. 5.7 The amplitude of initial fluctuation of the water temperature at the heater outlet

After the water boiling, the water began to boil more steam bubbles were produced and collected at the top horizontal tube. The process of the temperature oscillation at the heater outlet is as presented in Fig. 5.8. It could be described into 3 steps. In step 1, the collected steam was released from the expansion tank. At this point, two phenomena had been observed. First, the subcooled water flowed down the downcomer tube at the very fast speed. The heat was then transferred less effectively to the water because the water only spent a short amount of time in the heating section. This caused the boiling to stop. Second, the water from the expansion tank flowed in reverse direction to replace the void created by the release of the steam. When the two flows met, the net flow rate was decrease. In step 2, the water temperature was increased because the water was absorbed more heat due to stagnant flow and the boiling was re-started. In step 3, the steam bubbles were produced rapidly and rose again to the top without getting trapped in the top horizontal tube. The water temperature at the heater outlet was decreased rapidly due to the subcooled water flow down at high speed. The process then repeated again from step 1.

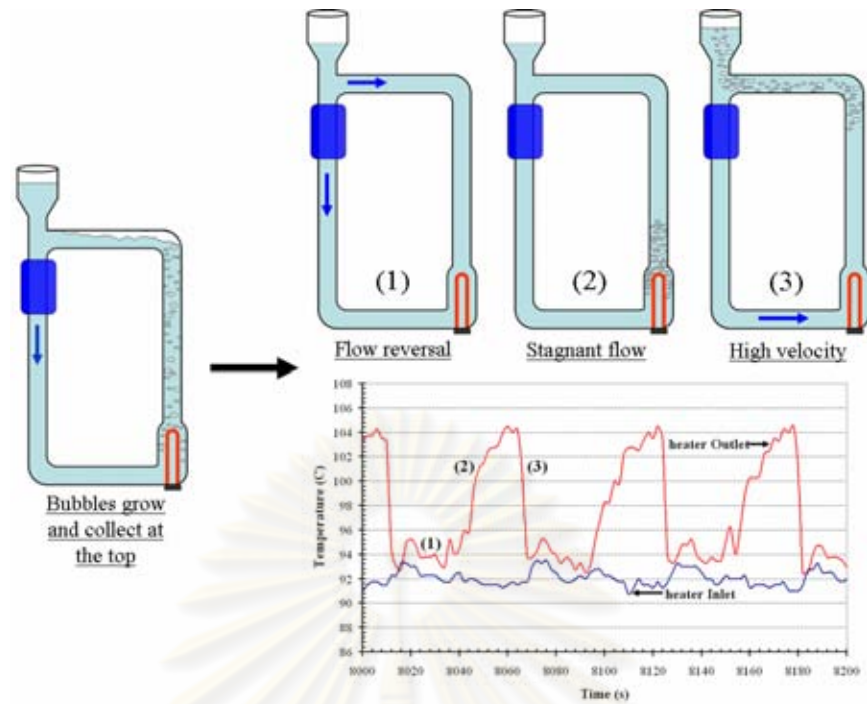


Fig. 5.8 The process of the water temperature oscillation after the water boiling

FFT method was used to analyze the water temperature oscillation at the heater outlet. FFT profiles of the water temperature oscillation at 575 W and 630 W heating powers are as shown in Fig. 5.9 and Fig. 5.10, respectively. The main frequency was found to be 0.02 Hz for 575 W heating powers. At 630 W heating powers, the main frequency was 0.025 Hz. The re-started boiling time in step 2 of the process of the water temperature oscillation was decreased when the heating power levels was increased. It should be noted that some of the hot water spilled during the boiling instability at 630 W heating powers.

ศูนย์วิทยทรัพยากร
จุฬาลงกรณ์มหาวิทยาลัย

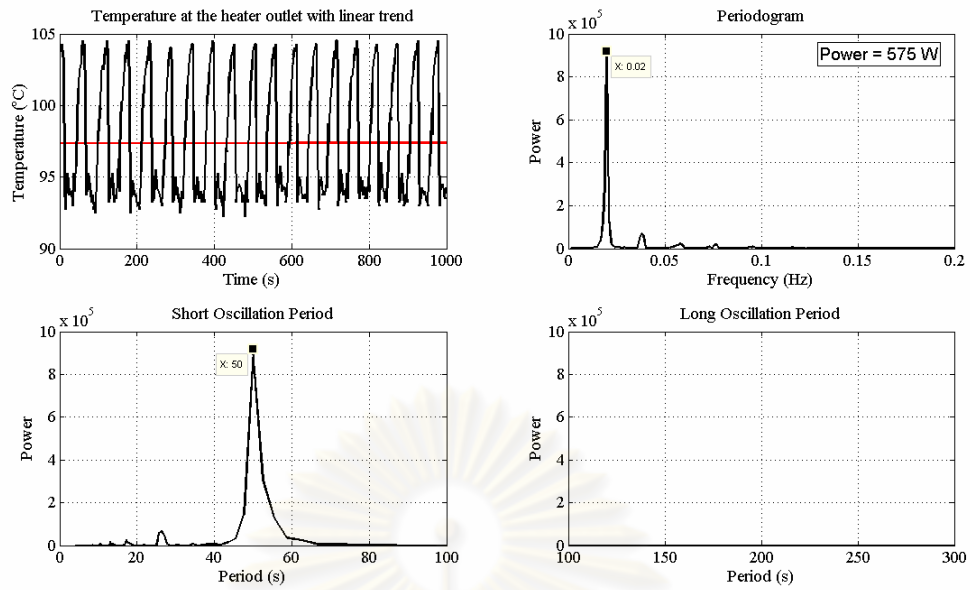


Fig. 5.9 FFT profile of the temperature oscillation at 575 W heating powers

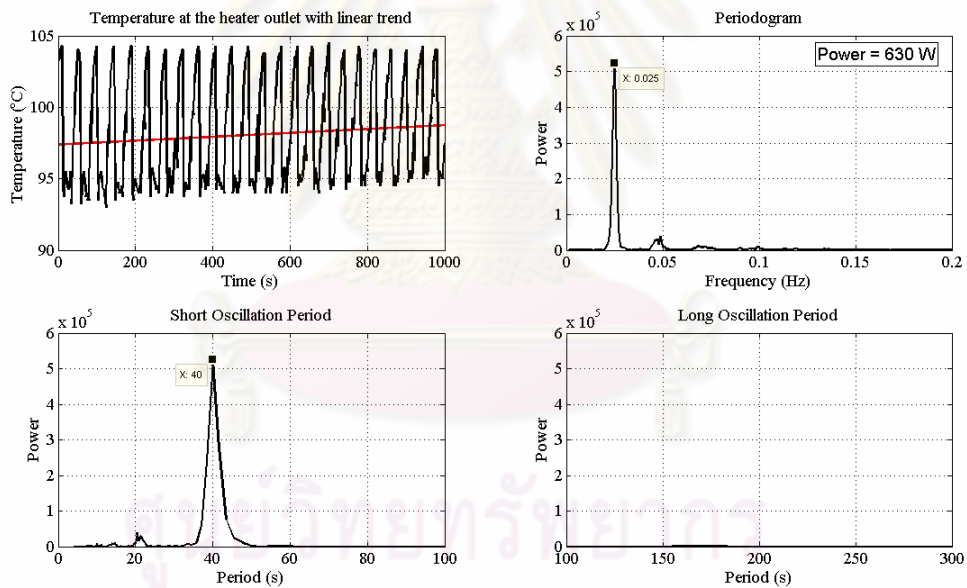


Fig. 5.10 FFT profile of the temperature oscillation at 630 W heating powers

From the result of this work, it was speculated that the temperature oscillation of water in this configuration was due to the presence of the horizontal tube. In order to minimize the oscillation in the two-phase flow caused by this configuration, the horizontal tube should be minimized or eliminated.

5.2 The results of the NCL#2

Fig. 5.11 and 5.12, show respectively the temperature profiles and the differential pressure across the heater at various heat flux levels: 6.0, 8.0, 12.5, and 18.0 kW/m^2 . Each graph in Fig. 5.11 shows the temperatures at the heater inlet and outlet, and at the condenser inlet and outlet. Note that the time scale in each graph is not the same as boiling occurs faster at higher heat flux. As shown in Fig. 5.11(a), the temperature oscillation is not observed at all positions mention above. Fig. 5.11(b)-(d) shows the amplitude of temperature oscillation at the condenser outlet increased with increasing heat flux. The temperature oscillation at the heater outlet is due to the process of flashing-induced density wave oscillation, but the temperature oscillation at the condenser outlet is due to heated water flowing through the condenser. It should be note that flashing-induced density wave oscillation was observed when stable two-phase oscillation was occurred. At subcooled boiling start, geysering was observed at the riser. Process of geysering and flashing-induced density wave oscillation will be presented in the next section.

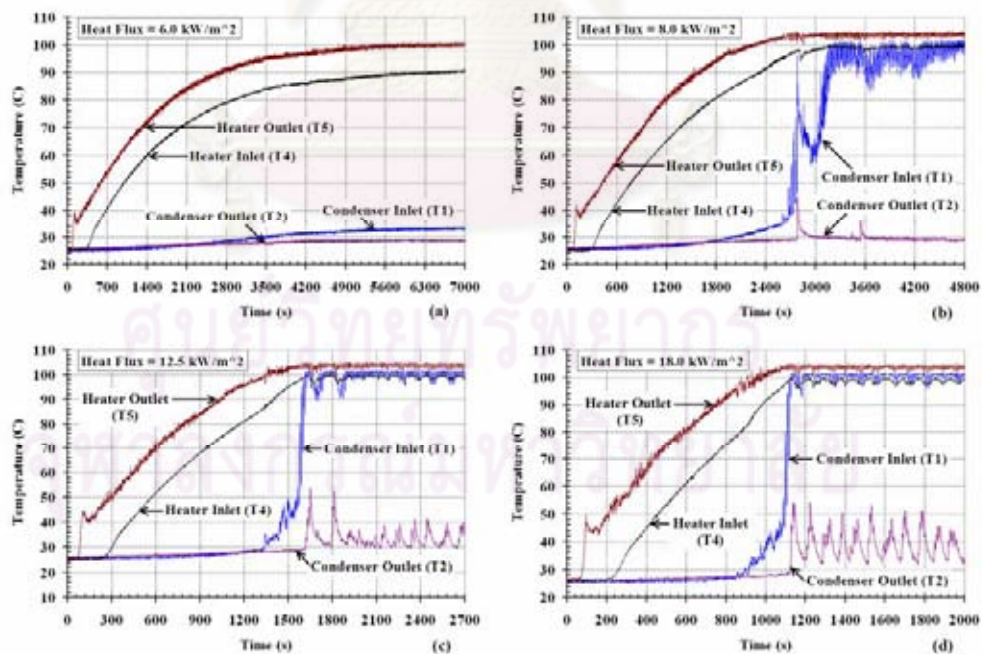


Fig. 5.11 The temperature profiles at various heat flux levels (a) 6.0 kW/m^2 , (b) 8.0 kW/m^2 , (c) 12.5 kW/m^2 , and (d) 18.0 kW/m^2

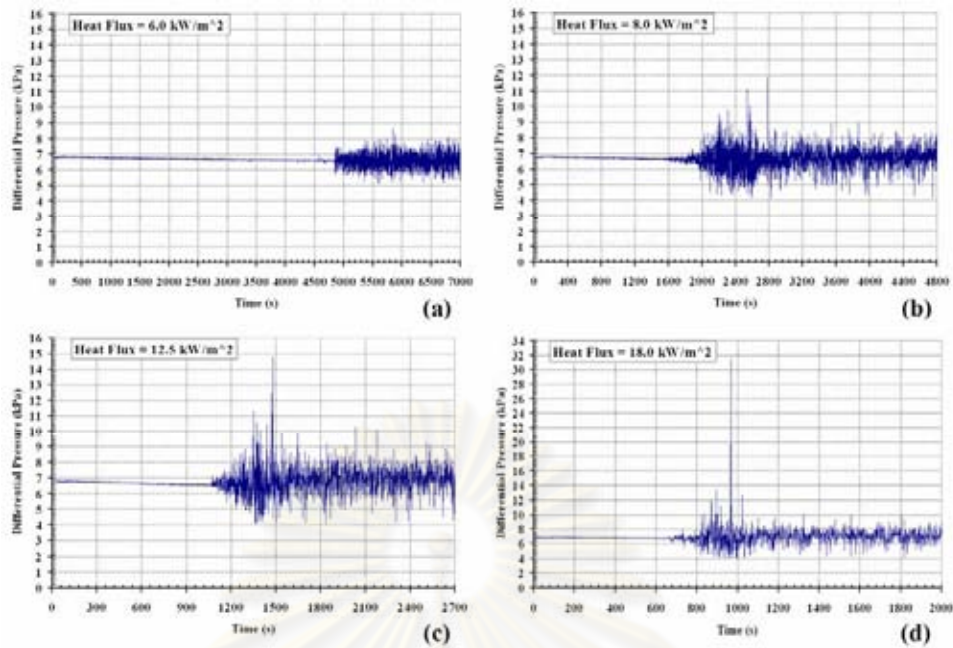


Fig. 5.12 The differential pressure across the heater at various heat flux levels
 (a) 6.0 kW/m², (b) 8.0 kW/m², (c) 12.5 kW/m², and (d) 18.0 kW/m²

5.2.1 Geysering induced by condensation

As subcooled boiling occurs, bubbles departing from heater rod are condensed in subcooled water at the riser. In 1993, Aritomi et al. [8] observed the process of geysering in parallel boiling channels as shown in Fig. 5.13. Their proposed model for the driving mechanism of geysering is as follows:

“A large bubble covering the entire flow cross section is formed and grows towards the outlet plenum due to the decrease in hydrostatic head. As soon as the large bubble reaches the outlet plenum, it is mixed with subcooled water and condensed rapidly therein. Subcooled water reenters rapidly from the inlet plenum as the pressure drop corresponds to that in the other channel. If the condensation rate, that is, the reentering rate is higher than the circulation one, flow reversal is induced in the other channel. Both channels are filled with liquid and non-boiling condition is restored. After a while, a slug bubble is formed in the other channel because temperature of fluid reentering from the outlet plenum is higher than that in the channel. Such a process periodically repeats alternatively in both channels.”[8]

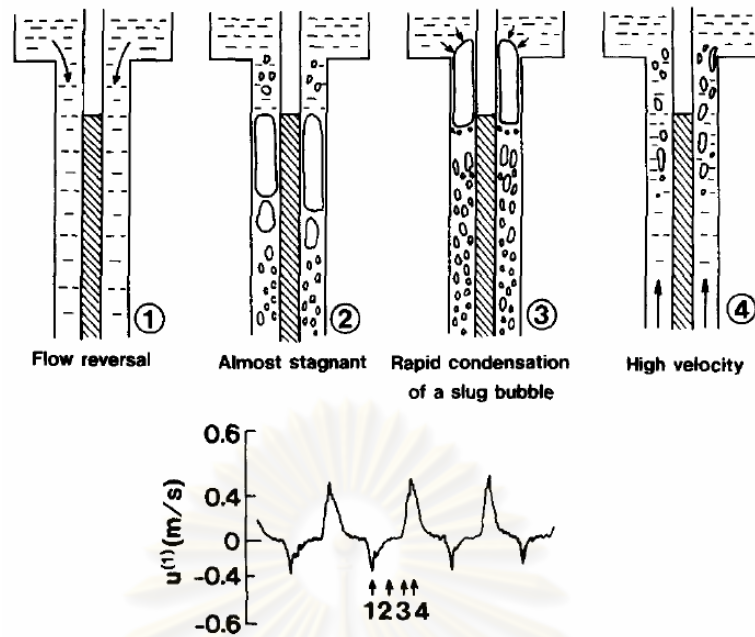


Fig. 5.13 Proposed model of geysering in parallel boiling channels [8]

Geysering was observed at the heater outlet for 8.0 heat flux as shown in Fig. 5.14. When subcooled boiling occurs at the heating section, a slug bubble is formed at the heater outlet. As the slug bubble enters to the riser, it is condensed with subcooled water. This process occurs until the water temperature in the riser reaches saturation point.



Fig. 5.14 Recorded bubble images at the heater outlet

5.2.2 Flashing-induced density wave oscillation

In 2005, Furuya et al. [11] presented process of flashing-induced density wave oscillation as shown in Fig. 5.15. They described it in the following steps:

- “(a) Water heated by the heater (at 110 C for instance) flows into the chimney.
- (b) Boiling initiates where the water temperature exceeds the local saturation temperature.
- (c) Decrease in static head of water immediately promotes further evaporation, which is known as the flashing phenomenon.
- (d) Natural circulation flow rate increases due to enlarged vapor volume resulting in outflow of the steam bubbles. In turn, the temperature at the chimney inlet becomes relatively low because of short dwell time in the heated region.
- (e) After the chimney is filled with cold water, the flow rate decreases and the temperature at the chimney inlet becomes relatively high because of long dwell time in the heated region due to stagnant flow. The process repeats again from process (a).”[11]

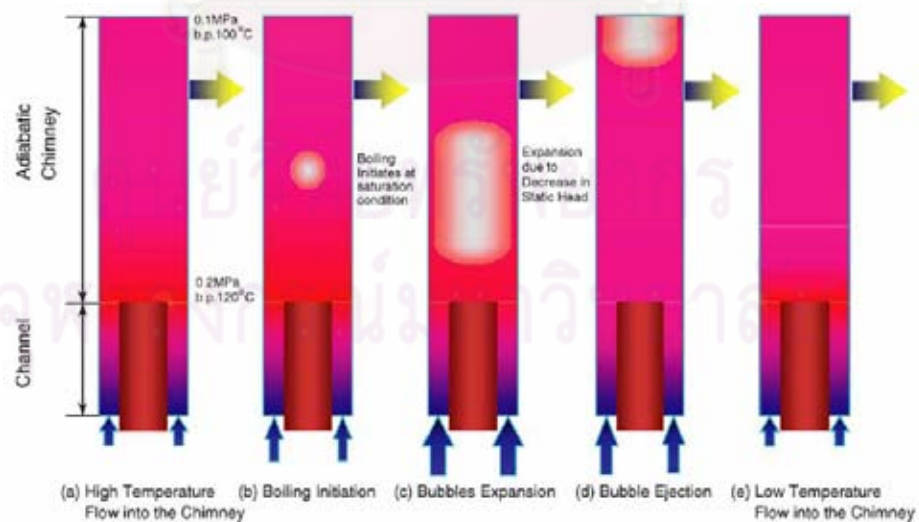


Fig. 5.15 Process of flashing-induced density wave oscillation [11]

Flashing-induced wave density oscillation was observed and bubble images were recorded at the riser middle for 8.0 heat flux as shown in Fig. 5.16. As can be observed, a slug bubble ($t = 0$ s) rises upward to the expansion tank and transfer heat to the water in the riser. When the water temperature exceeds the saturation point, it starts to boil ($t = 1$ s). In $t = 1-4$ s, Bubbles expand due to decrease in static head of water, which is flashing phenomenon.

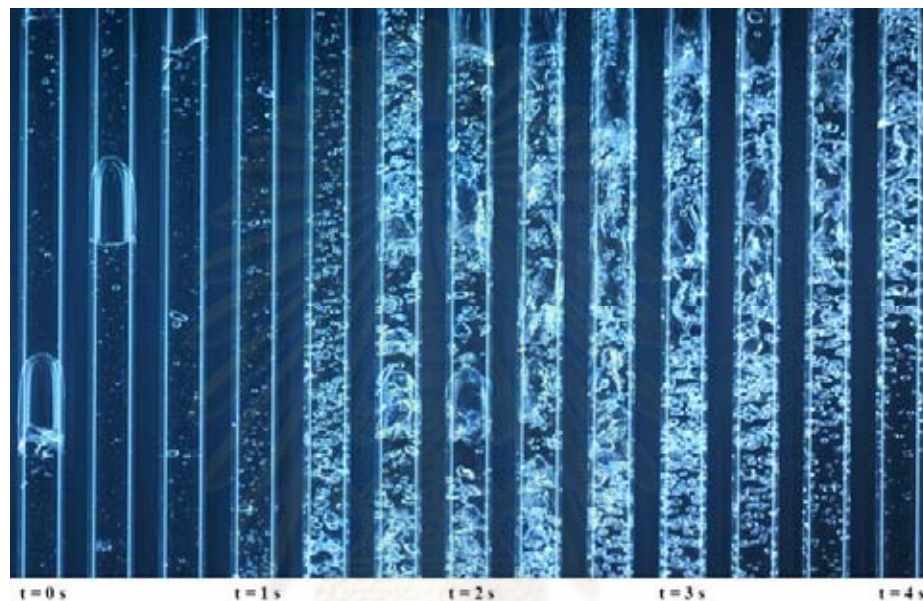


Fig. 5.16 Recorded bubble images at the riser middle

5.2.3 Spectrum analysis with FFT

The FFT was used to analyze the oscillation curve of the temperature and the differential pressure. At first, the frequency spectrum of the temperature oscillation at the heater outlet and the condenser outlet were presented. The frequency spectrum of the temperature oscillation at 8.0 kW/m² heat flux is shown in Fig. 5.17. The main frequency was found to be around 0.051 Hz for the temperature oscillation at the heater outlet, but there was no temperature oscillation observed at the condenser outlet. The frequency spectrum of the temperature oscillation at the heater outlet and at the condenser outlet for 12.5 and 18.0 kW/m² heat fluxes are shown in Fig. 5.18 and 5.19, respectively. At the heater outlet, the frequency of the temperature oscillation was found to be around 0.089 Hz for both heat fluxes. However, the spectrum became broadened with higher heat flux. The frequency of the temperature oscillation at the condenser

outlet increased from 0.01 to 0.014 Hz when heat flux increased from 12.5 to 18.0 kW/m^2 . The frequency at the condenser outlet matched the low frequency component at the heater outlet. Therefore, the temperature oscillation at the heater outlet was a combined effect between the instability due to presence of the condenser and the flashing-induced density wave oscillation.

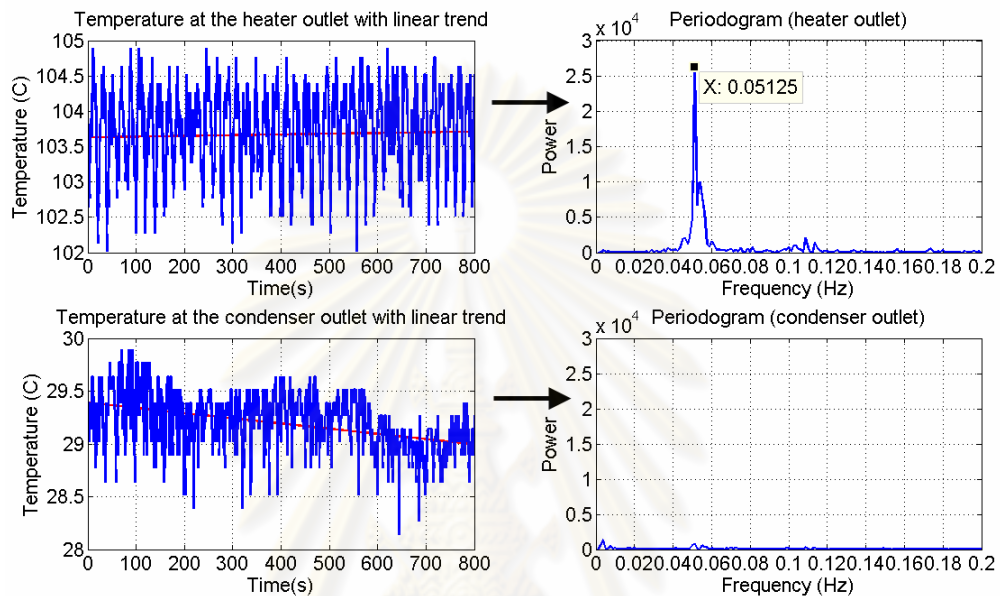


Fig. 5.17 FFT profiles of the temperature oscillation at the heater outlet and the condenser outlet for 8.0 kW/m^2 heat flux

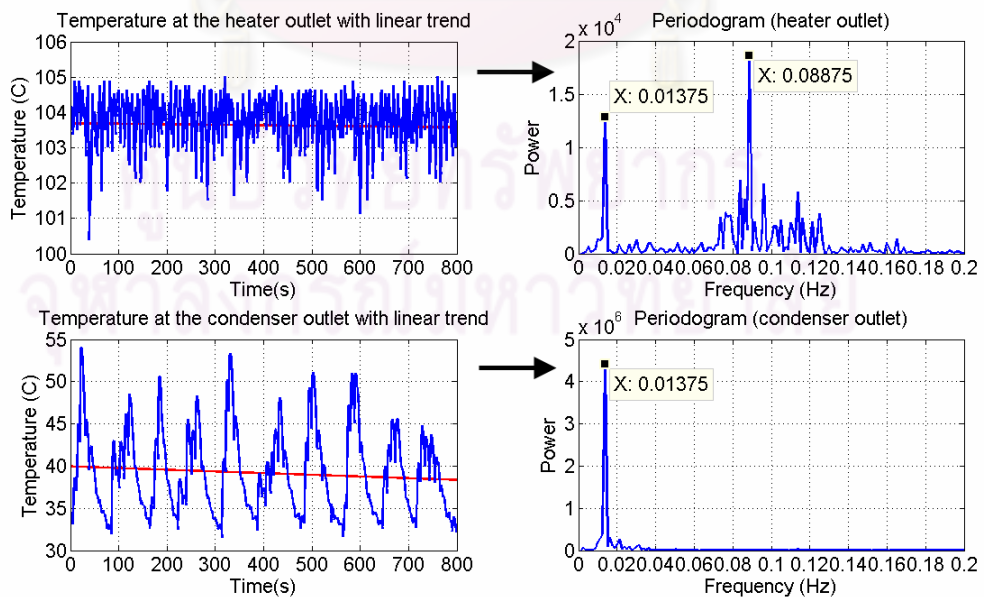


Fig. 5.18 FFT profiles of the temperature oscillation at the heater outlet and the condenser outlet for 12.5 kW/m^2 heat flux

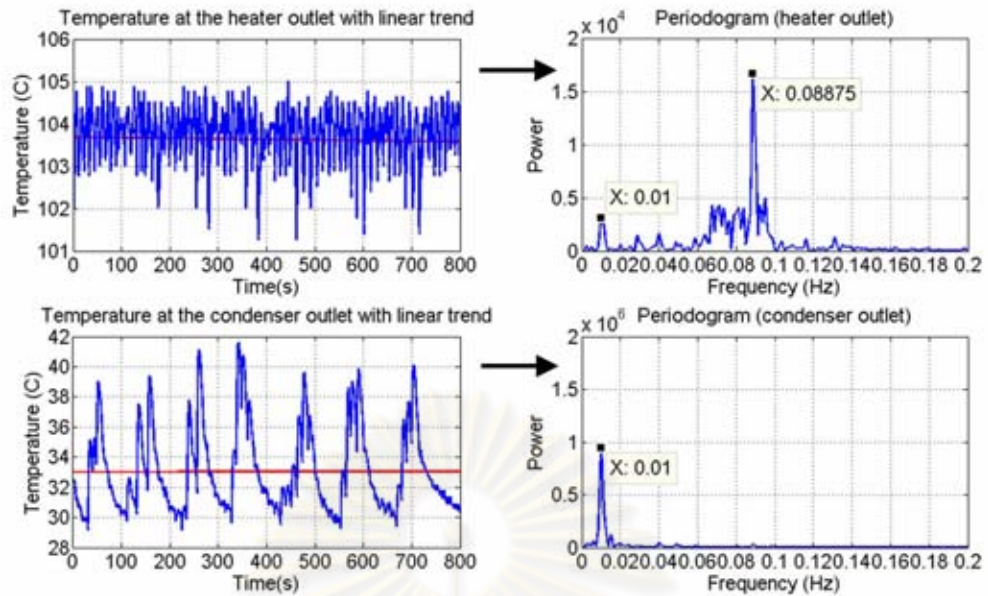


Fig. 5.19 FFT profiles of the temperature oscillation at the heater outlet and the condenser outlet for 18.0 kW/m^2 heat flux

For comparison, the frequency spectrums of the differential pressure oscillation at different heat fluxes were also analyzed. Fig. 5.20, 5.21, and 5.22 show FFT profiles of the differential pressure for 8.0 , 12.5 , and 18.0 kW/m^2 heat fluxes, respectively. It was found that the frequency of the differential pressure oscillation matched the frequency of the temperature oscillation at the heater outlet for each and every value of heat flux used. Therefore, it was concluded that the oscillations of both of differential pressure and the temperature at the heater outlet were driven by the boiling, which in turn was directly affected by the heat flux used in the experiment.

ศูนย์วิทยทรัพยากร
จุฬาลงกรณ์มหาวิทยาลัย

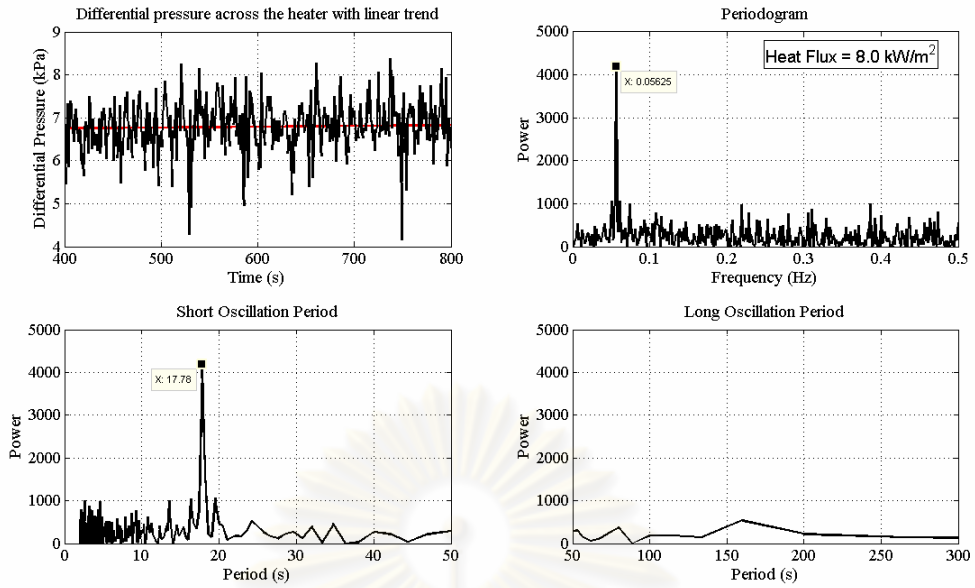


Fig. 5.20 FFT profiles of the differential pressure across the heater at 8.0 kW/m² heat flux

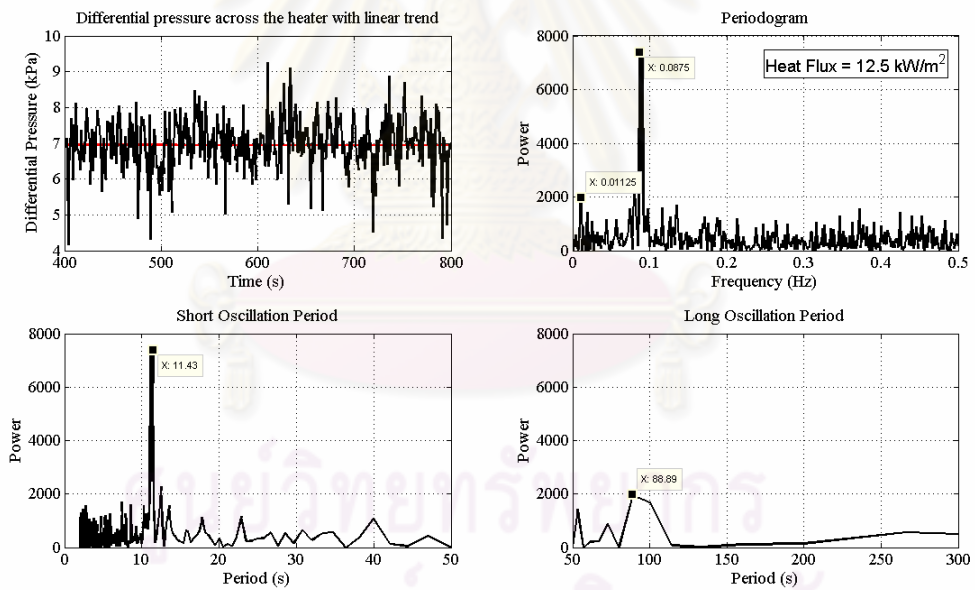


Fig. 5.21 FFT profiles of the differential pressure across the heater at 12.5 kW/m² heat flux

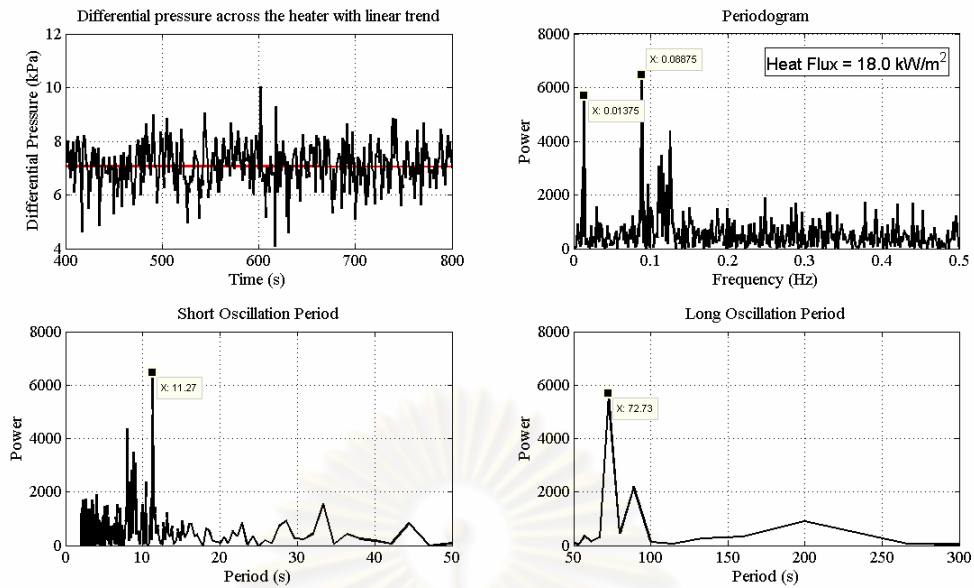


Fig. 5.22 FFT profiles of the differential pressure across the heater at 18.0 kW/m^2 heat flux

From the result of this work, the temperature oscillation of water in this configuration was due to flow instabilities which were known as geysering and flashing-induced density wave oscillation. FFT was a good method to analyze the oscillation curve when it became more complex.

5.3 The results from computer simulation

The TEXAS code was modified for simulation of a two-phase flow in the rectangular natural circulation loop as described in section 3.5. Fig. 5.23 shows a computer model for (a) the NCL#1 and (b) the NCL#2. The loop diameter is 22 mm. The loop height and width are 2000 mm and 1000 mm, respectively. The loop is divided into 60 meshes. Each mesh size is 100 mm long. The time step varies from 1 ns to 0.1 s. The initial conditions are shown in Table 5.1. The constant heat flux at heating section is used for heat input in the computer program.

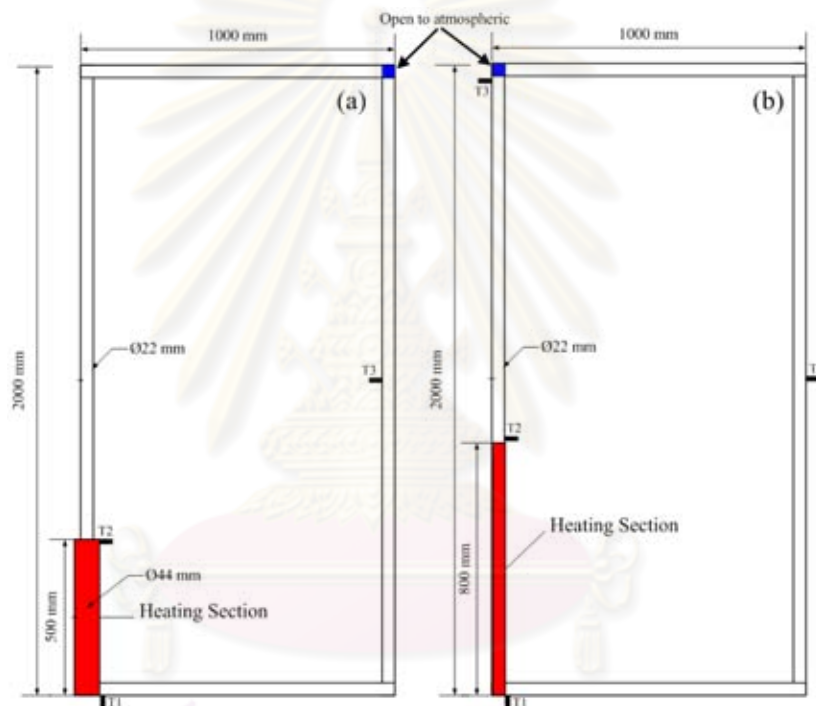


Fig. 5.23 A computer model for (a) the NCL#1 and (b) the NCL#2

Table 5.1 Initial conditions for computer simulation

Parameters	Value
System pressure (MPa)	0.1
Liquid and vapor velocity (m/s)	0
Liquid temperature (K)	303
Vapor temperature (K)	373
Wall temperature (K)	373
Void fraction	0

Fig. 5.24, 5.25, and 5.26 show the water temperature, liquid velocity, and pressure for the NCL#1, respectively. Liquid velocity in the tube diameter of 22 mm was higher than the tube diameter of 44 mm due to large cross section area. The pressure at the heater inlet was higher than the heater outlet due to pressure gradient in the loop. As shown in Fig. 5.26, the pressure initially fluctuated wildly before it was settled down. The fluctuation of pressure was due to build-up of pressure before initiated natural circulation.

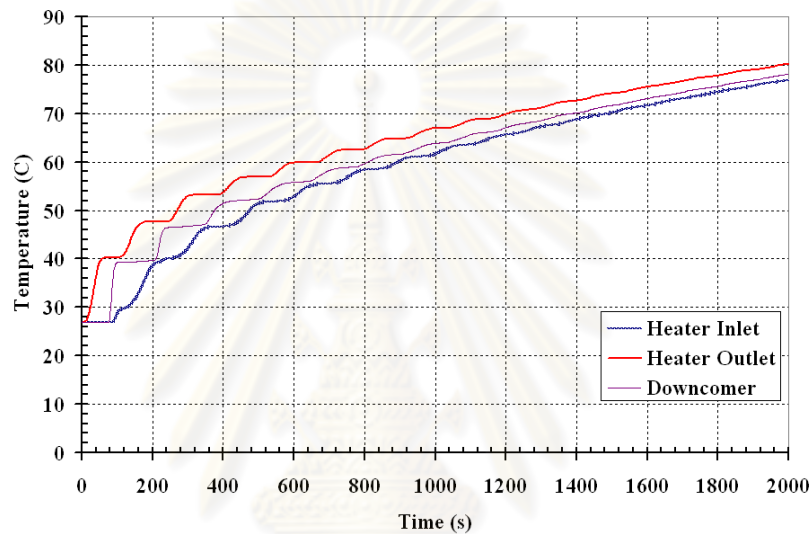


Fig. 5.24 Temperature profiles at 400 W heating powers

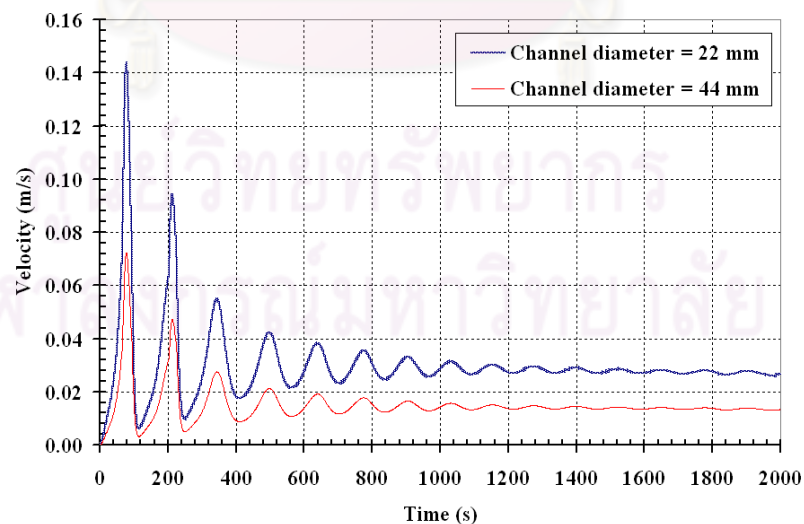


Fig. 5.25 Liquid velocity at 400 W heating powers

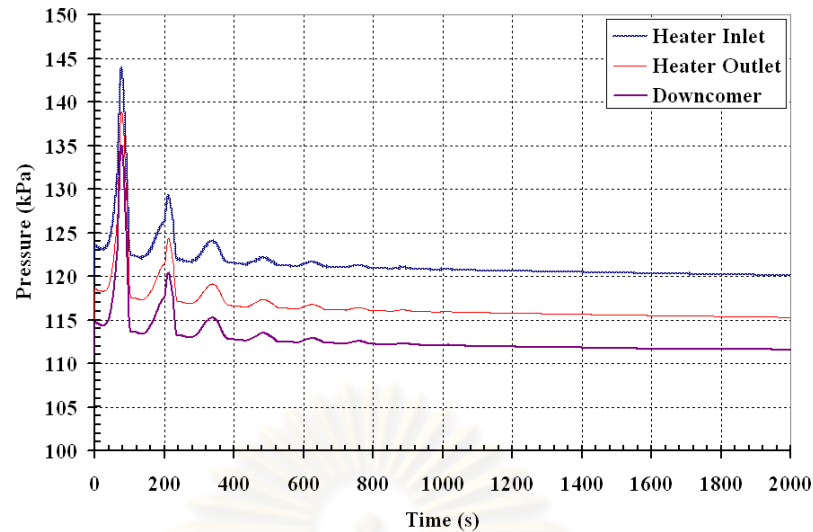


Fig. 5.26 Pressure at 400 W heating powers

Fig. 5.27 shows the water temperature at the heater outlet for the different heating power levels. It was found that at the same time, the water temperature was much higher when the heating power level was increased. The relationship between the water temperature and the water density is shown as Fig. 5.28. The water density was decreased with the increasing water temperature. This was indicated that equation of state for water in the computer program was correct.

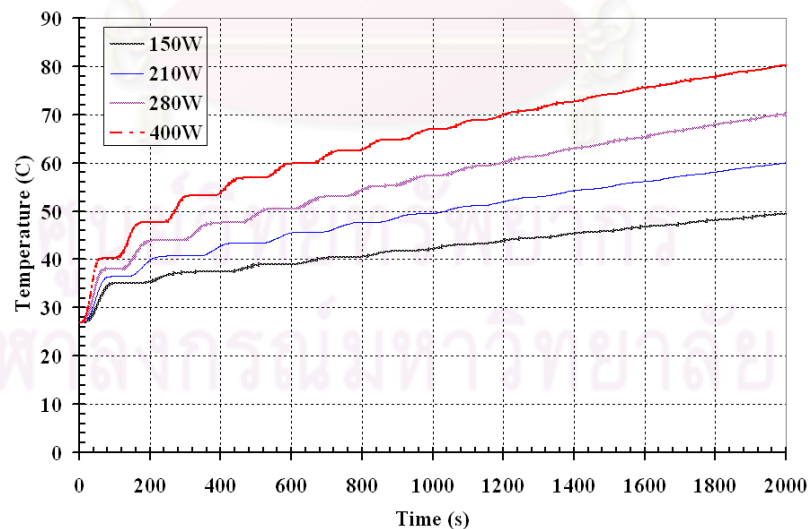


Fig. 5.27 The water temperature at various heating power levels

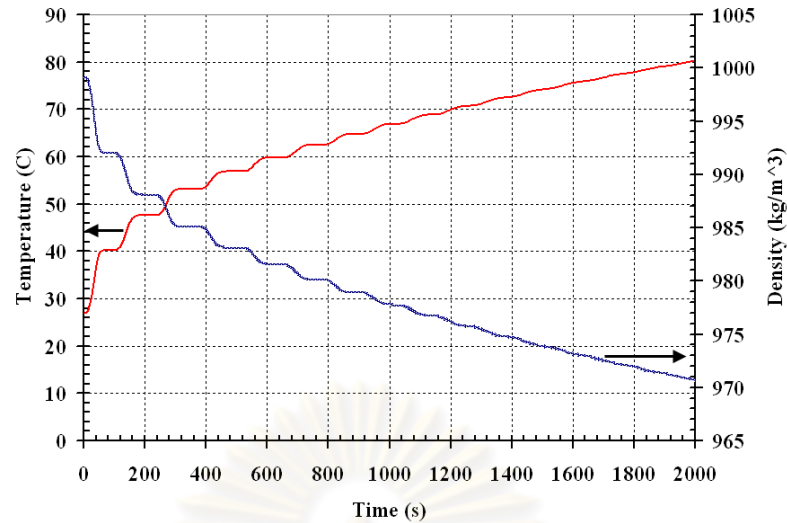


Fig. 5.28 The relationship between the water temperature and the water density

The water temperature oscillation was not observed in the computer simulation for 575 W heating powers as shown in Fig. 5.29. The differential pressure across the heater and the void fraction at the heater outlet for 575 W heating powers are shown in Fig. 5.30 and 5.31, respectively.

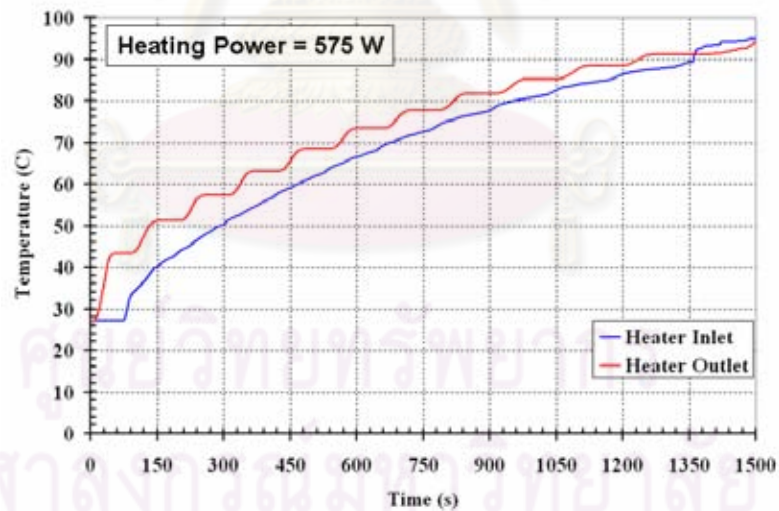


Fig. 5.29 Temperature profiles at 575 W heating powers

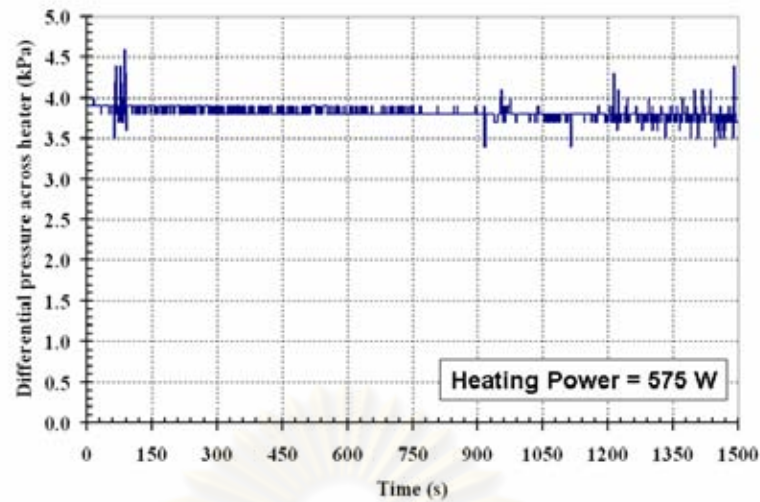


Fig. 5.30 Differential pressure across the heater at 575 W heating powers

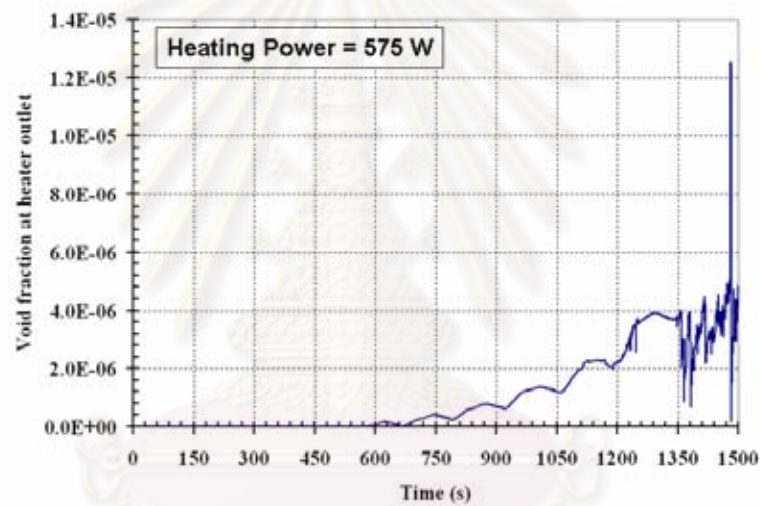


Fig. 5.31 Void fraction at the heater outlet at 575 W heating powers

Fig. 5.32, 5.33, and 5.34 show the water temperature, liquid velocity, and system pressure for the NCL#2. As shown in Fig. 5.33, the velocity initially fluctuated wildly before it was settled down. The fluctuation of velocity was due to large temperature difference along the loop at initiated flow. Again, the water temperature oscillation was not observed in the computer simulation for this loop.

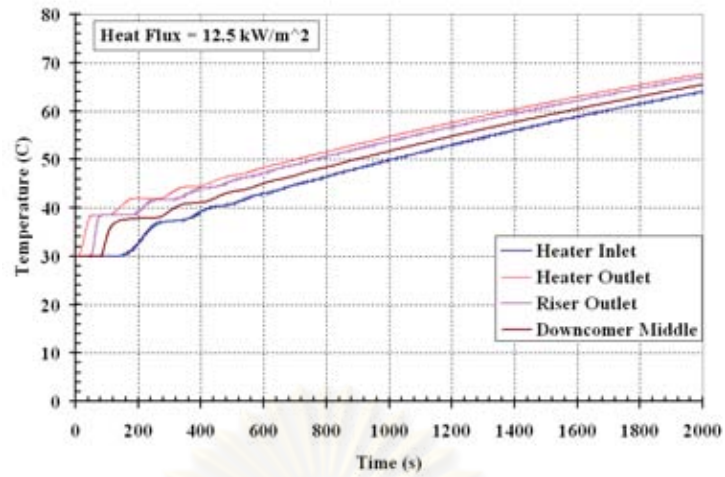


Fig. 5.32 Temperature profiles at 12.5 kW/m^2 heat fluxes

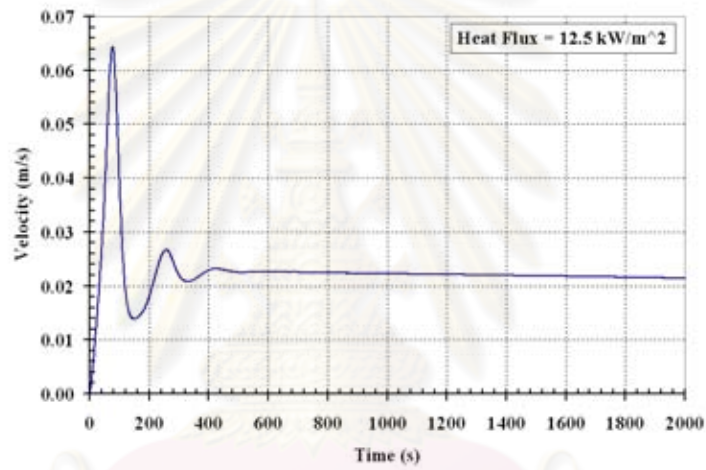


Fig. 5.33 Liquid velocity at 12.5 kW/m^2 heat fluxes

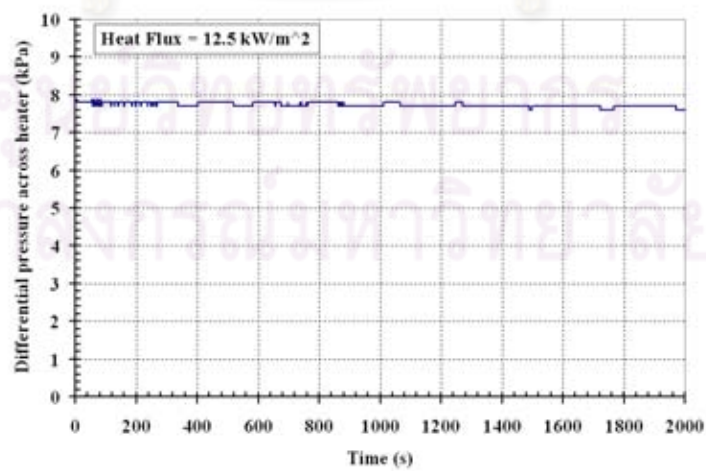


Fig. 5.34 Differential pressure across the heater at 12.5 kW/m^2 heat fluxes

5.4 Comparison of numerical and experimental results

Fig. 5.35-5.37 show the comparison of the numerical and experimental results. For the maximum temperature and the amplitude of initial fluctuation, the numerical results agree with the experimental results. However, the temperature difference across the heater is different from the experimental results. In addition, the water temperature oscillation was not observed in the computer simulation due to limitation of the computer program. Therefore, the computer program still required further modification.

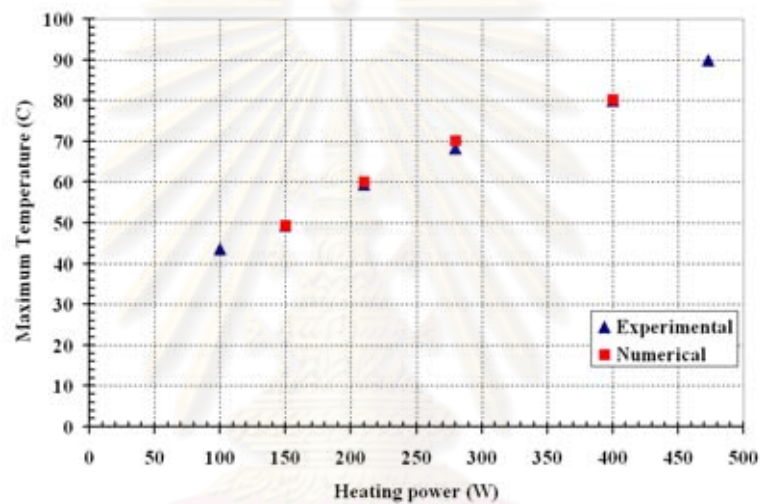


Fig. 5.35 Comparison of numerical and experimental results for the maximum water temperature

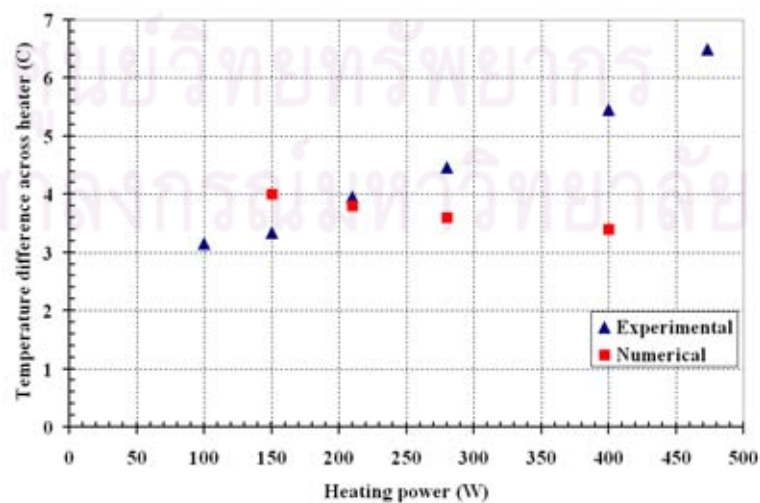


Fig. 5.36 Comparison of numerical and experimental results for the temperature difference across the heater

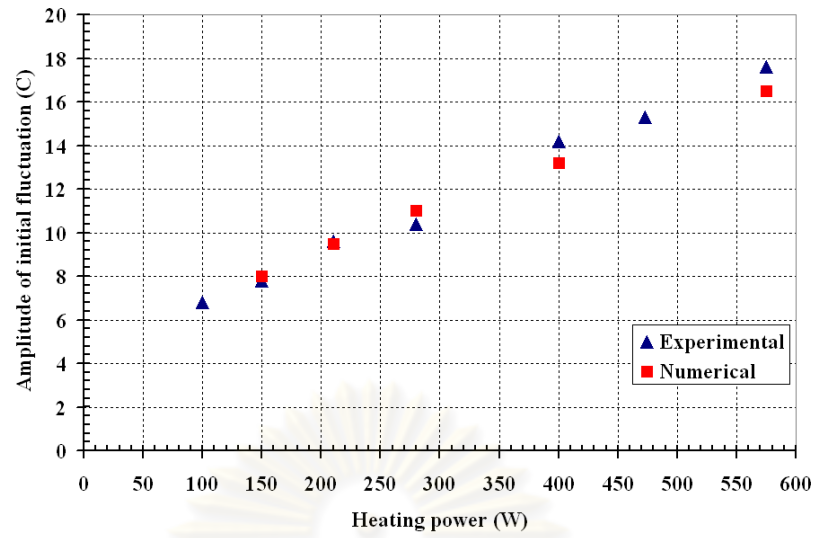


Fig. 5.37 Comparison of numerical and experimental results for the amplitude of initial fluctuation

ศูนย์วิทยทรัพยากร
จุฬาลงกรณ์มหาวิทยาลัย

CHAPTER VI

CONCLUSIONS AND SUGGESTIONS

5.1 Conclusions

The conclusions from this work are as follows:

1. Two rectangular natural circulation loops have been designed and constructed for simulation of a two-phase flow under two different configurations.
2. At the same heating power level, the water temperature was much higher when the cooling system was turned off.
3. Regardless of the turning condition of the cooling system, the same temperature differences across the heater were measured.
4. The mass flow rate due to the density gradient was found to be increased with the increasing heating power level.
5. The amplitude of the initial fluctuation was found to increase as the heating power level was increased.
6. It was speculated that the temperature oscillation of water in the NCL#1 was due to the presence of the horizontal tube. In order to minimize the oscillation in the two-phase flow caused by this configuration, the horizontal tube should be minimized or eliminated.
7. The temperature oscillation of water in the NCL#2 was due to flow instabilities which were known as geysering and flashing-induced density wave oscillation.
8. The Fast Fourier Transform (FFT) was a good method to analyze the oscillation curve when it became more complex.
9. The frequency of the temperature oscillation at the heater outlet was found to be increased with the increasing heating power level for the NCL#1.
10. In the NCL#2, the effect from heat loss in the condenser caused the temperature oscillation frequency at the heater outlet to increase as the heat flux increased. The rate of increase became slower until saturation occurred at high heat flux.

11. The frequency of the temperature oscillation at the condenser outlet was found to increase when the heat flux was increased.

12. The frequency of the differential pressure oscillation matched the frequency of the temperature oscillation at the heater outlet for each and every value of heat flux used. Therefore, the oscillations of both differential pressure and the temperature at the heater outlet were driven by the boiling, which in turn was directly affected by the heat flux used in the experiment.

13. The TEXAS code was modified to simulate the two-phase flow in the rectangular natural circulation loop.

14. The results from the computer simulation agreed with the experimental results. However, the simulation had some limitation, and still required further modification.

5.2 Suggestions

The suggestions from this work are as follows:

1. There is uncertainty in the heating power measurement when a dimmer circuit is used to control the input power supply. To get more accuracy in the heating power measurement, a slide regulator should be used to control the input power supply.

2. As can be observed, the void fraction varied along the riser. Therefore, the void fraction measurement system should be developed to measure the void fraction from the heater outlet to the expansion tank.

3. The high speed video camera should be used to record the phenomenon during the transient startup.

4. A flow meter should be installed to measure flow rate in the loop.

5. The effect of surface roughness of the heater on boiling instability should be investigated in the future.

6. Effect of expansion tank and heat loss should be added to the computer simulation.

7. Constant heat flux value and position of heating section should be moved from heater.f to input.txt. Therefore, user can change any value without rebuild program.

8. Effect of mesh size should be studied in the future.



ศูนย์วิทยทรัพยากร
จุฬาลงกรณ์มหาวิทยาลัย

REFERENCES

- [1] Nayak, A.K., Dubey, P., Chavan, D.N., and Vijayan, P.K. Study on the stability behaviour of two-phase natural circulation systems using a four-equation drift flux model. Nuclear Engineering and Design 237 (2007) : 386-398.
- [2] Kakac, S., and Bon, B., A review of two – phase flow dynamic instabilities in tube boiling systems, International Journal of Heat and Mass Transfer 51 (2008) : 399-433.
- [3] Durga Prasad, G.V., Pandey, M., and Kalra, M.S., Review of research on flow in stabilities in natural circulation boiling systems, Progress in Nuclear Energy 49 (2007) : 429-451.
- [4] Nayak, A.K., and Vijayan, P.K., Flow instabilities in boiling two-phase natural circulation systems: a review, Science and Technology of Nuclear Installations (2008) : 1-15.
- [5] Tadrist, T., Review on two-phase flow instabilities in narrow spaces, International Journal of Heat and Fluid Flow 28 (2007) : 54-62.
- [6] Zvirin, Y., A review of natural circulation loops in pressurized water reactors and other systems, Nuclear Engineering and Design 67 (1981) : 203-225.
- [7] Boure, J.A., Bergles, A.E., and Tong, L.S., Review of two-phase flow instability, Nuclear Engineering and Design 25 (1973) : 165-192.
- [8] Aritomi, M., Chiang, J. H., and Mori, M., Geysering in parallel boiling channels, Nuclear Engineering and Design 141 (1993) : 111-121.
- [9] Chiang, J.H., Aritomi, M., Inoue, R., and Mori, M., Thermo-hydraulics during start-up in natural circulation boiling water reactors, Nuclear Engineering and Design 146 (1994) : 241-251.
- [10] Kuran, S., et al., Startup transient simulation for natural circulation boiling water reactors in PUMA facility, Nuclear Engineering and Design 236 (2006) : 2365-2375.

- [11] Furuya, M., Inada, F., and van der Hagen, T.H.J.J., Flashing-induced density wave oscillations in a natural circulation BWR – mechanism of instability and stability map, Nuclear Engineering and Design 235 (2005) : 1557-1569.
- [12] Paniagua, J., Rohatgi, U.S., and Prasad, V., Modeling of thermal hydraulic instabilities in single heated channel loop during startup transients, Nuclear Engineering and Design 193 (1999) : 207-226.
- [13] Chaiwat Muncharoen, The effect of flow loop conditions on stabilities of two – phase natural circulation caused by boiling, Doctoral dissertation, Department of Nuclear Technology, Faculty of Engineering, Chulalongkorn University, 2002.
- [14] Nayak, A.K., et al., A numerical study of boiling flow instability of a reactor thermosyphon system, Applied Thermal Engineering 26 (2006) 644-653.
- [15] Rao, N.M., Chandra Sekhar, Ch., Maiti, B., and Das, P.K., Steady-state performance of a two-phase natural circulation loop, International Communications in Heat and Mass Transfer 33 (2006) : 1042-1052.
- [16] Wu, C.Y., Wang, S.B., and Pan. C., Chaotic oscillations in a low pressure two-phase natural circulation loop under low power and high inlet subcooling conditions, Nuclear Engineering and Design 162 (1996) : 223-232.
- [17] Situ, R., et al., Flow structure of subcooled boiling flow in an internally heated annulus, International Journal of Heat and Mass Transfer 47 (2004) : 5351-5364.
- [18] Khodabandeh, R., Furberg, R., Instability, heat transfer and flow regime in a two-phase flow thermosyphon loop at different diameter evaporator channel, Applied Thermal Engineering 30 (2010) : 1107-1114.
- [19] Yun, G., Cheng, G., Heyi, Z., The application of Fast Fourier Transform (FFT) method in the twin-channel system instability under ocean conditions, Annals of Nuclear Energy 37 (2010) : 1048-1055.
- [20] Kosar, A., Özdemir, M.R., Keskinöz M., Pressure drop across micro-pin heat sinks under unstable boiling conditions. International Journal of Thermal Sciences 49 (2010) : 1253-1263.
- [21] Thome, J.R., Engineering data book III, Wolverine Tube, 2006.

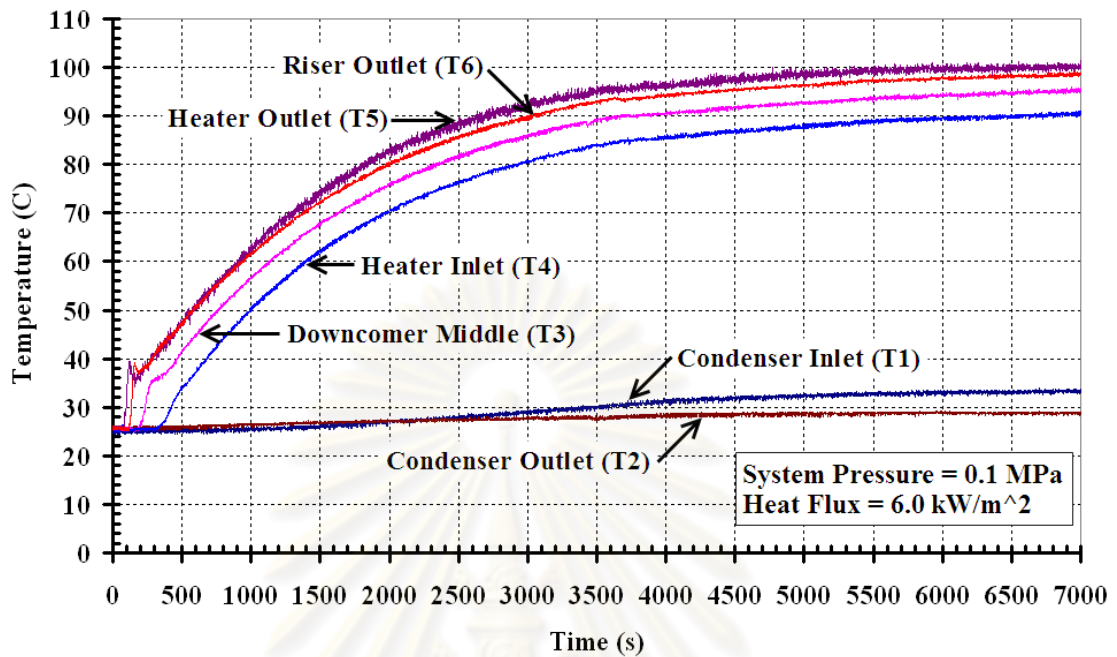
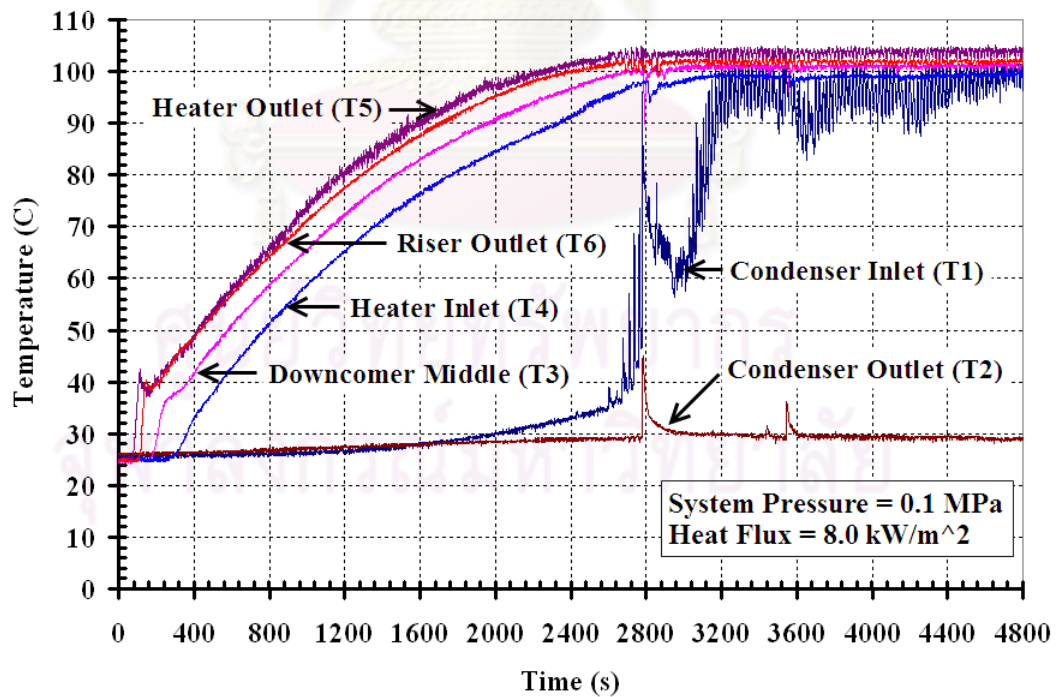
- [22] Baehr, H.D., and Stephan, K., Heat and Mass Transfer, 2nd Berlin : Springer, 2006.
- [23] Ambrosini, W., Lecture notes for the course on single and two-phase thermal-Hydraulics, University of Pisa, Italy.
- [24] Young, M.F., The TEXAS code for fuel-coolant interaction analysis, Proc. ANS/ENS LMFBR Safety Topical Mtg., Lyon-Ecully, France, 1982.
- [25] Chu C.C., et al., A dynamic model for droplet fragmentation, Transaction of American Nuclear Society 47 (1984).
- [26] Tang, J., Modeling of the complete process of one-dimensional vapor explosions, Doctoral dissertation, University of Wisconsin, 1993.
- [27] Murphy, J., A hydrogen generation model for TEXAS, Master's Thesis, University of Wisconsin, 1992.
- [28] Chu, C.C., One-dimensional transient fluid model for fuel-coolant interaction analysis, Doctoral dissertation, University of Wisconsin, 1986.



Appendices

ศูนย์วิทยทรัพยากร
จุฬาลงกรณ์มหาวิทยาลัย

Appendix A.1 Temperature profiles for the NCL#2

Fig. A1.1 Temperature profiles at 6.0 kW/m^2 heat fluxFig. A1.2 Temperature profiles at 8.0 kW/m^2 heat flux

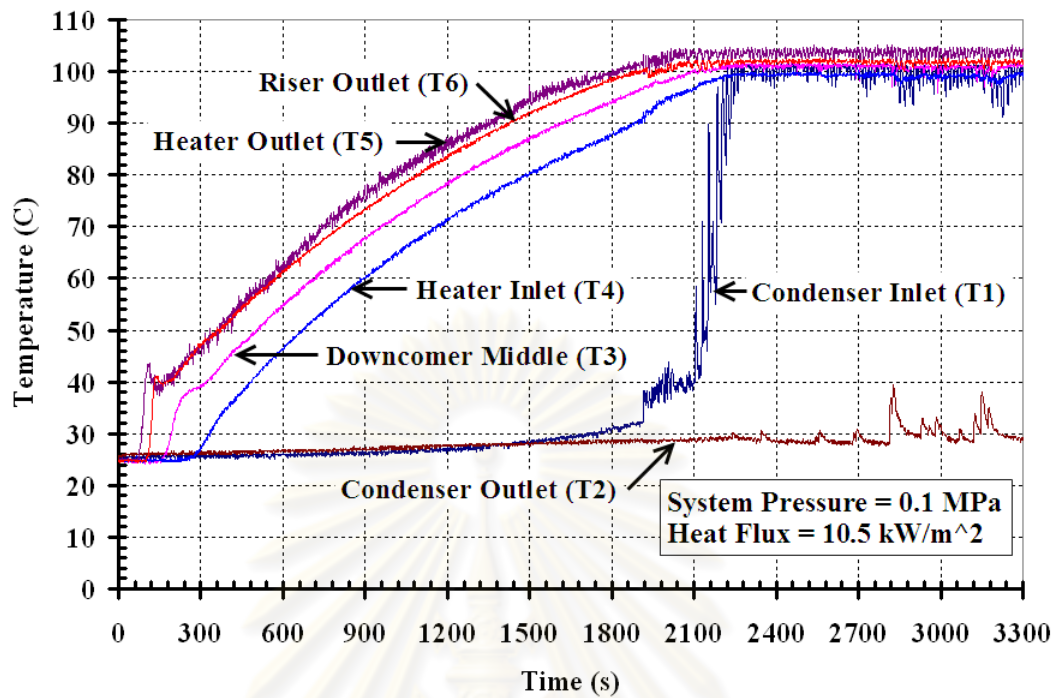


Fig. A1.3 Temperature profiles at 10.5 kW/m^2 heat flux

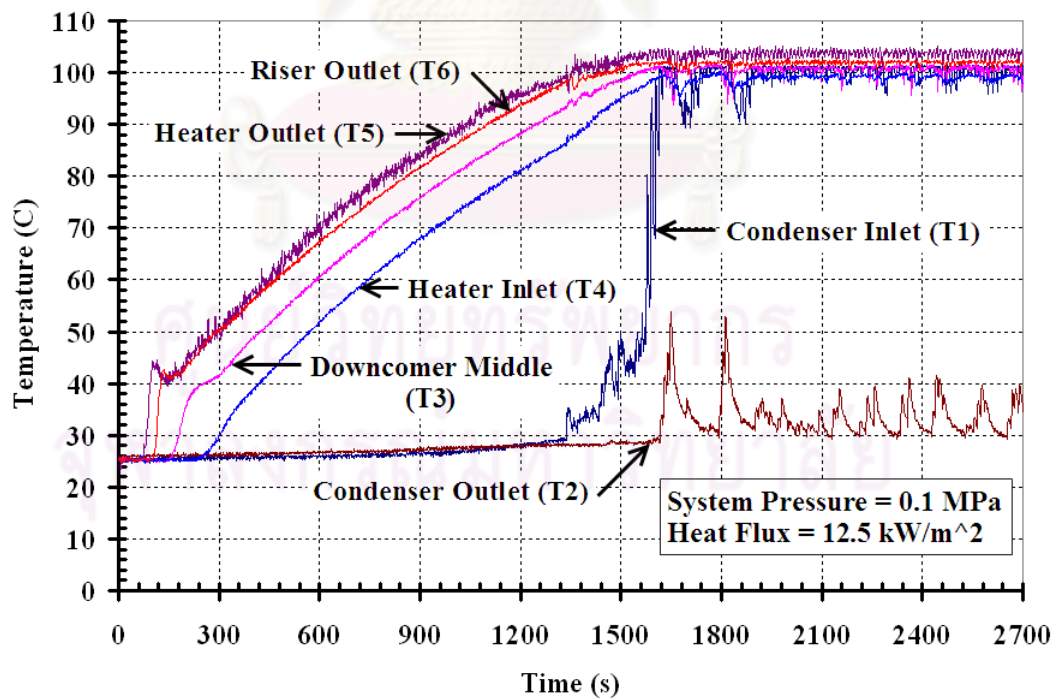


Fig. A1.4 Temperature profiles at 12.5 kW/m^2 heat flux

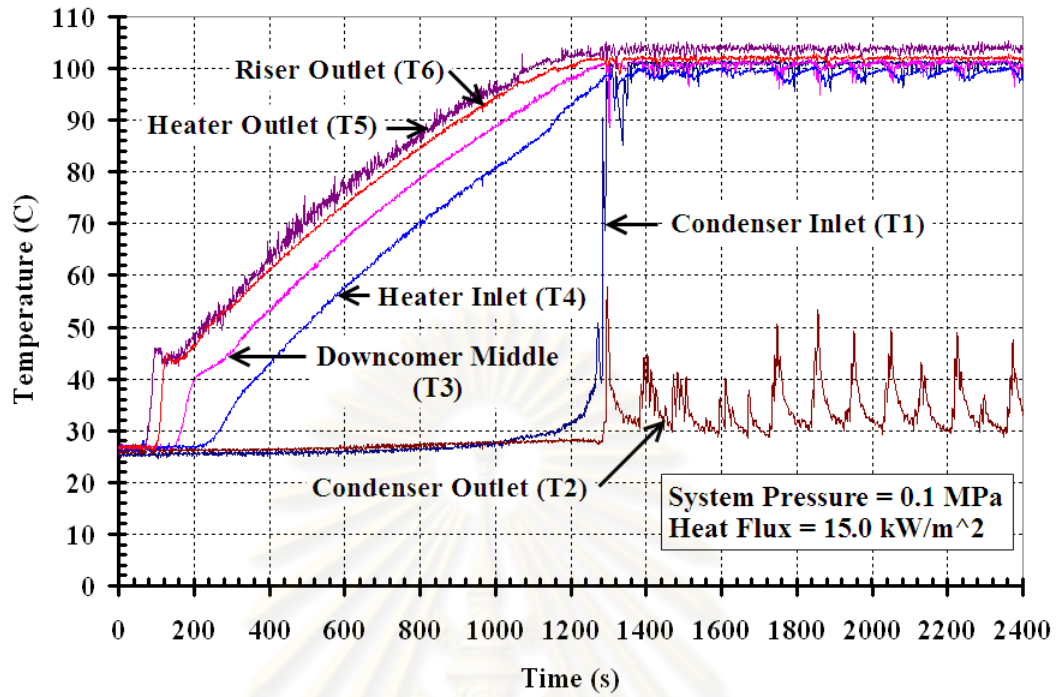


Fig. A1.5 Temperature profiles at 15.0 kW/m² heat flux

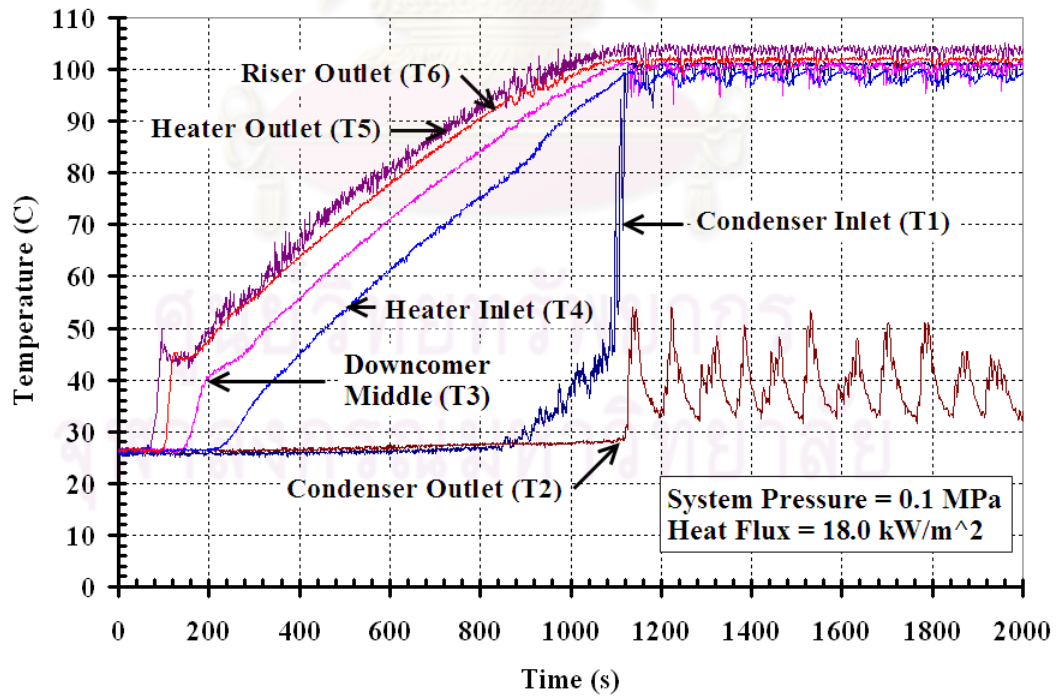
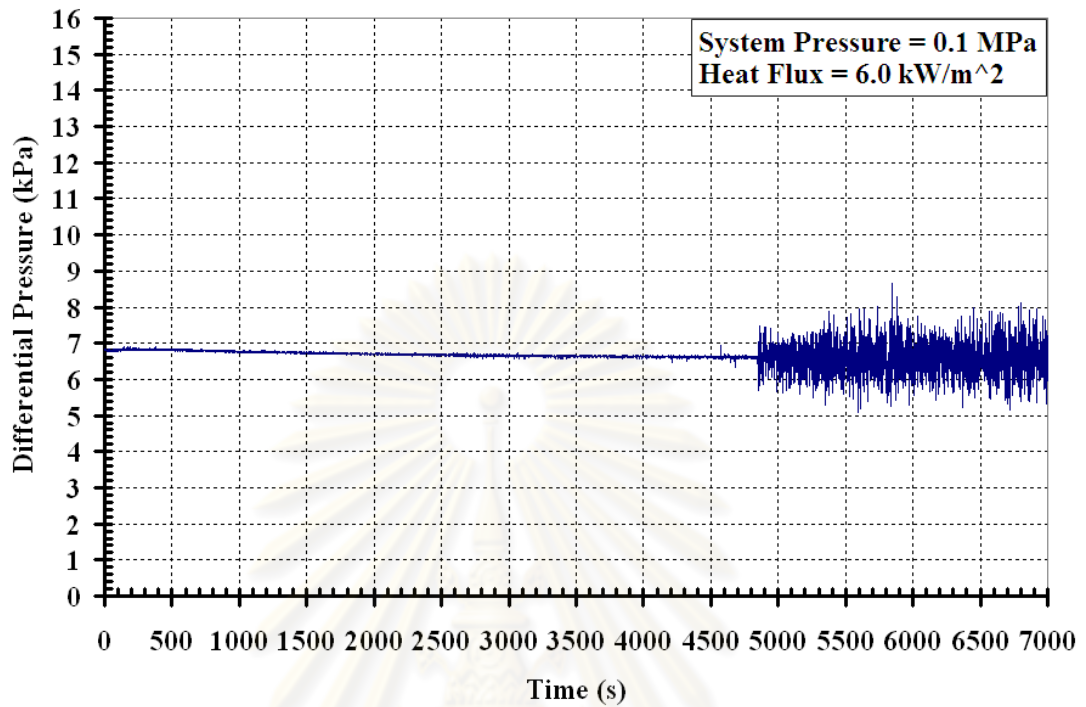
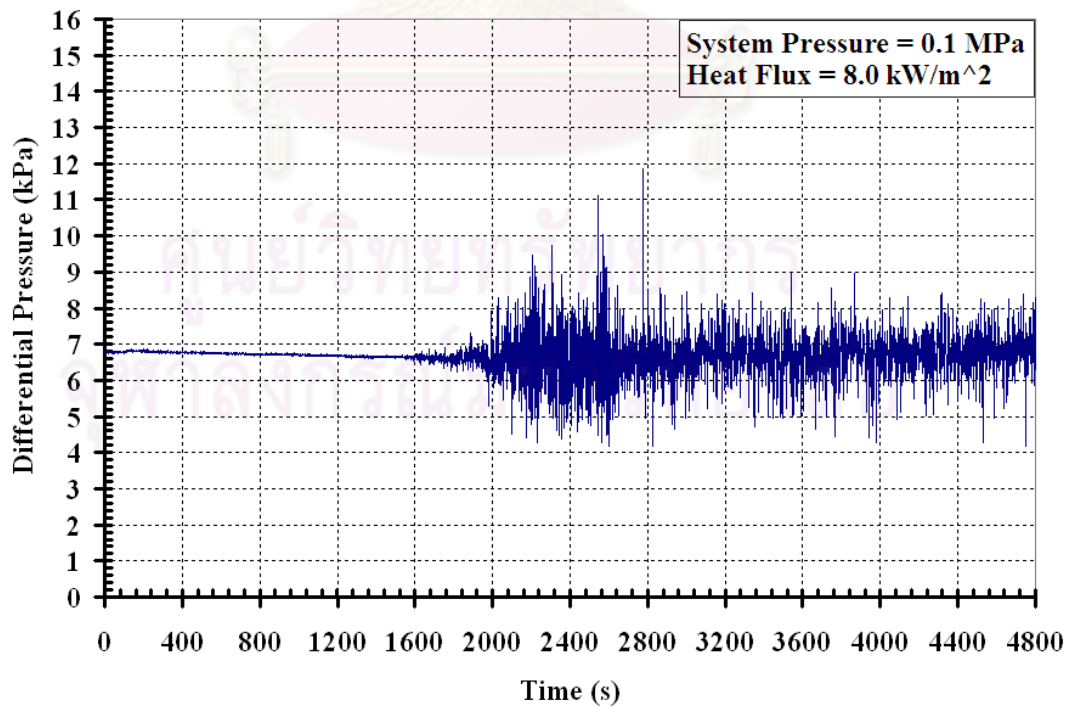


Fig. A1.6 Temperature profiles at 18.0 kW/m² heat flux

Appendix A.2 Differential pressure across the heater for the NCL#2

Fig. A2.1 Differential pressure across the heater at 6.0 kW/m² heat fluxFig. A2.2 Differential pressure across the heater at 8.0 kW/m² heat flux

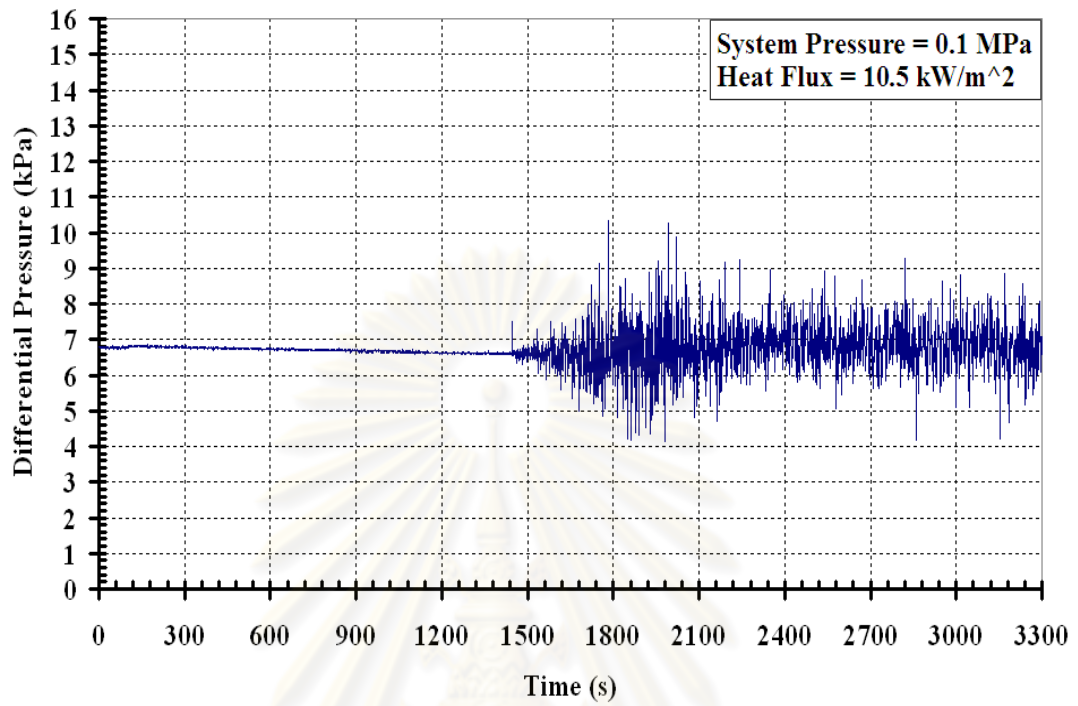


Fig. A2.3 Differential pressure across the heater at 10.5 kW/m² heat flux

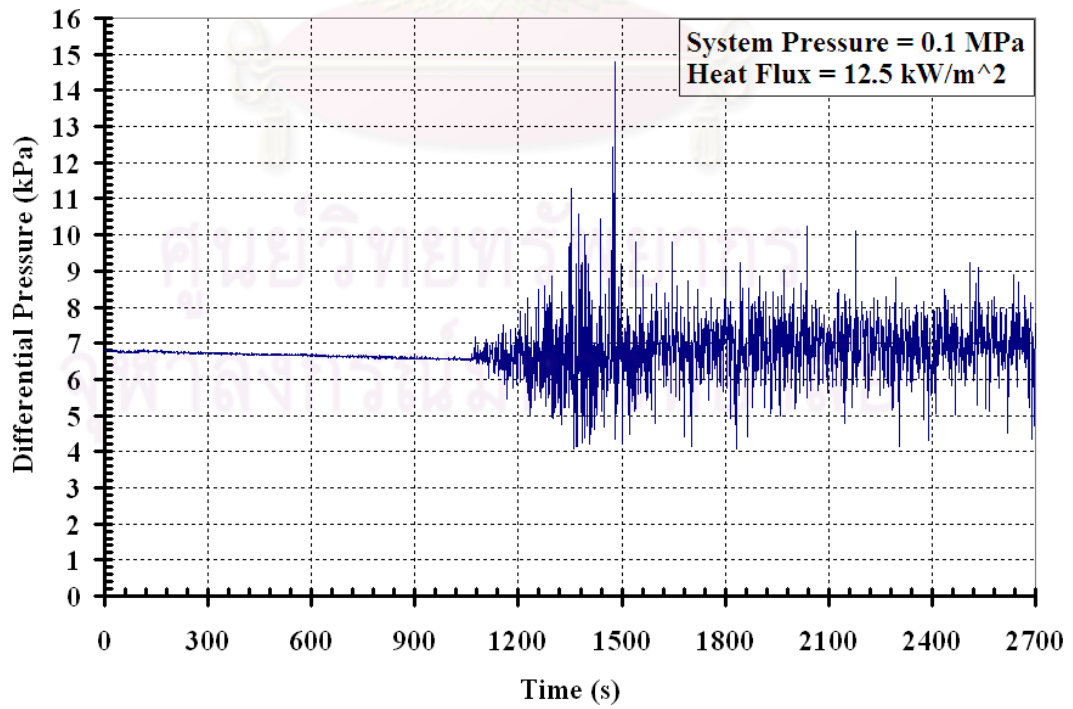


Fig. A2.4 Differential pressure across the heater at 12.5 kW/m² heat flux

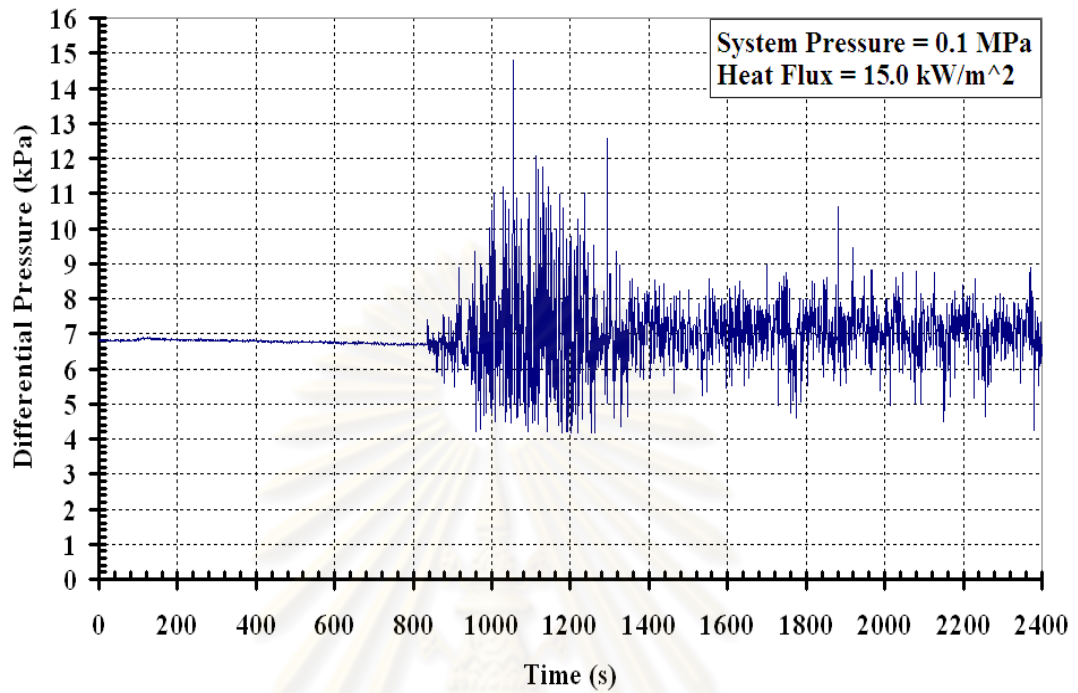


Fig. A2.5 Differential pressure across the heater at 15.0 kW/m² heat flux

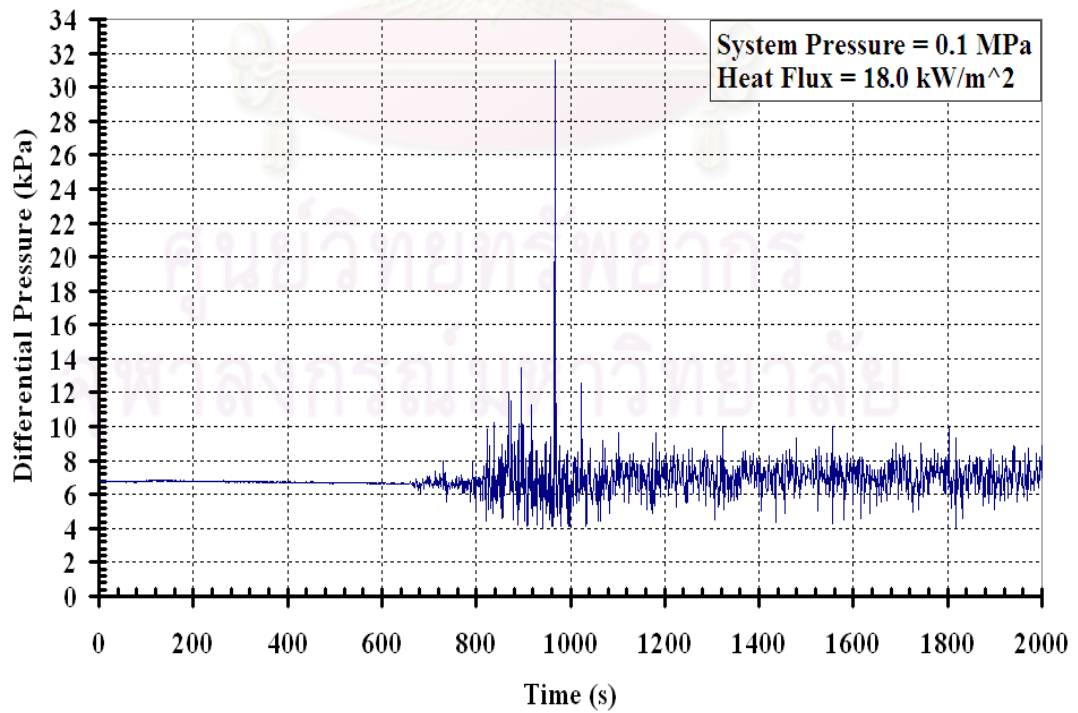


Fig. A2.6 Differential pressure across the heater at 18.0 kW/m² heat flux

Appendix B.1 MATLAB code for FFT

```

load Pressure.txt

t = Pressure(:,1)';      % Time (s)
temp = Pressure(:,2)'; % Heat flux = 8.0 kW/m2
%temp = Pressure(:,3)'; % Heat flux = 10.5 kW/m2
%temp = Pressure(:,4)'; % Heat flux = 12.5 kW/m2
%temp = Pressure(:,5)'; % Heat flux = 15.0 kW/m2
%temp = Pressure(:,6)'; % Heat flux = 18.0 kW/m2
n = length(temp);      %Number of samples
c = polyfit(t,temp,1);
trend = polyval(c,t);
subplot(2,2,1);
plot(t,[temp;trend],'r-',t,temp,'k-', 'linewidth',2)
grid on;               %Turn on grid lines for this plot
set(gca,'XLim',[400 800]);
set(gca,'XTickLabel',{400:100:800},...
    'FontName','times',...
    'FontSize',14);
set(get(gca,'XLabel'),'String','Time (s)',...
    'FontName','times',...
    'FontSize',14);
set(get(gca,'YLabel'),'String','Differential Pressure (kPa)',...
    'FontName','times',...
    'FontSize',14);
set(get(gca,'Title'),'String','Differential pressure across the heater with linear trend',...
    'FontName','times',...
    'FontSize',14);
y = temp - trend;
Y = fft(y);           %Finite Fourier Transform
Fs = 1;              %Sample rate

```



```

f = (1:n/2)*Fs/n;    %Nyquist frequency (n/2)*(Fs/n) = Fs/2
power = abs(Y(1:floor(n/2))).^2;
subplot(2,2,2);
plot(f,power,'k-', 'linewidth',2)
grid on;
set(gca,'XLim',[0 0.5]);
set(gca,'XTickLabel',{0:0.1:0.5},...
    'FontName','times',...
    'FontSize',14);
set(get(gca,'XLabel'),'String','Frequency (Hz)',...
    'FontName','times',...
    'FontSize',14);
set(get(gca,'YLabel'),'String','Power',...
    'FontName','times',...
    'FontSize',14);
set(get(gca,'Title'),'String','Periodogram',...
    'FontName','times',...
    'FontSize',14);
text(0.25,4.2e3,'{Heat Flux = 8.0 kW/m}^2',...
    'VerticalAlignment','bottom',...
    'HorizontalAlignment','left',...
    'FontSize',14,...
    'EdgeColor','black',...
    'BackgroundColor',[1 1 1]);
period=1./f;
subplot(2,2,3);
plot(period,power,'k-', 'linewidth',2)
%axis([0 50 0 5e3]);
grid on;
set(gca,'XLim',[0 50]);
set(gca,'XTickLabel',{0:10:50},...

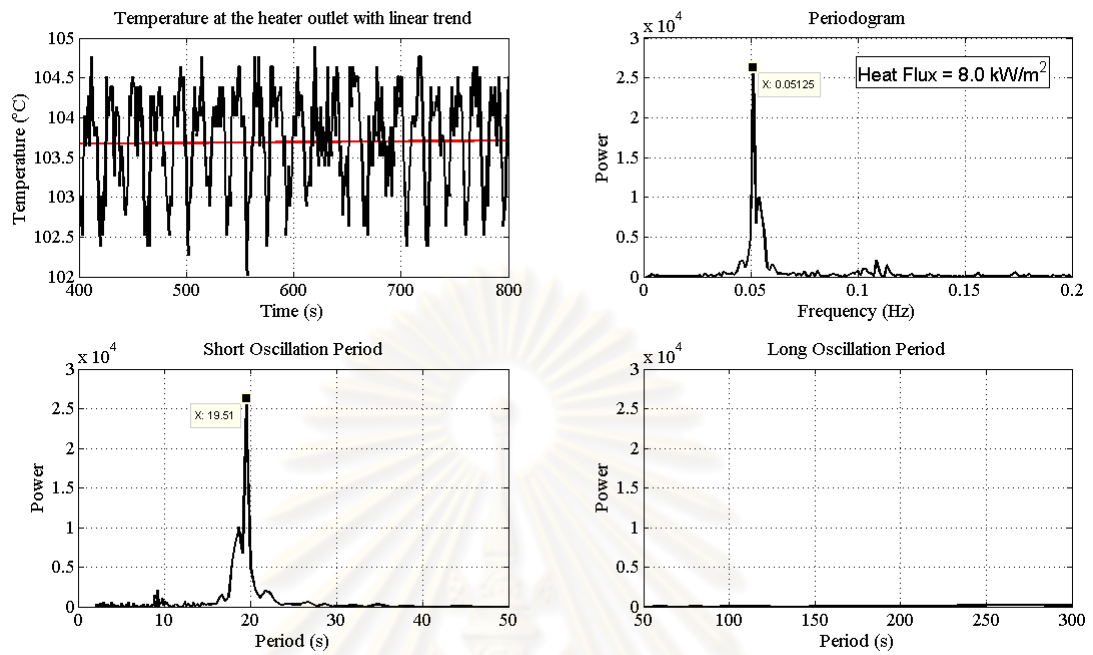
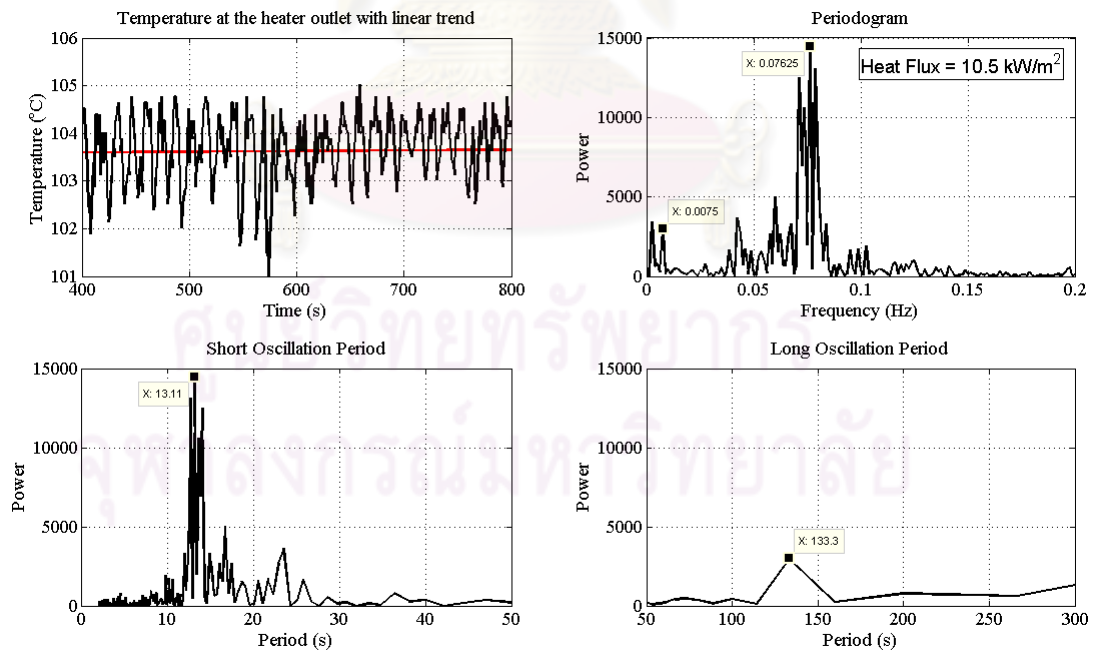
```

```

        'FontName','times',...
        'FontSize',14);
set(get(gca,'XLabel'),'String','Period (s)',...
    'FontName','times',...
    'FontSize',14);
set(get(gca,'YLabel'),'String','Power',...
    'FontName','times',...
    'FontSize',14);
set(get(gca,'Title'),'String','Short Oscillation Period',...
    'FontName','times',...
    'FontSize',14);
subplot(2,2,4);
plot(period,power,'k-', 'linewidth',2)
axis([50 300 0 5e3]);
grid on;
set(gca,'XLim',[50 300]);
set(gca,'XTickLabel',{50:50:300},...
    'FontName','times',...
    'FontSize',14);
set(get(gca,'XLabel'),'String','Period (s)',...
    'FontName','times',...
    'FontSize',14);
set(get(gca,'YLabel'),'String','Power',...
    'FontName','times',...
    'FontSize',14);
set(get(gca,'Title'),'String','Long Oscillation Period',...
    'FontName','times',...
    'FontSize',14);

```

Appendix B.2 FFT profiles of temperature at the heater outlet for the NCL#2

Fig. B2.1 FFT profile of temperature at the heater outlet at 8.0 kW/m^2 heat fluxFig. B2.2 FFT profile of temperature at the heater outlet at 10.5 kW/m^2 heat flux

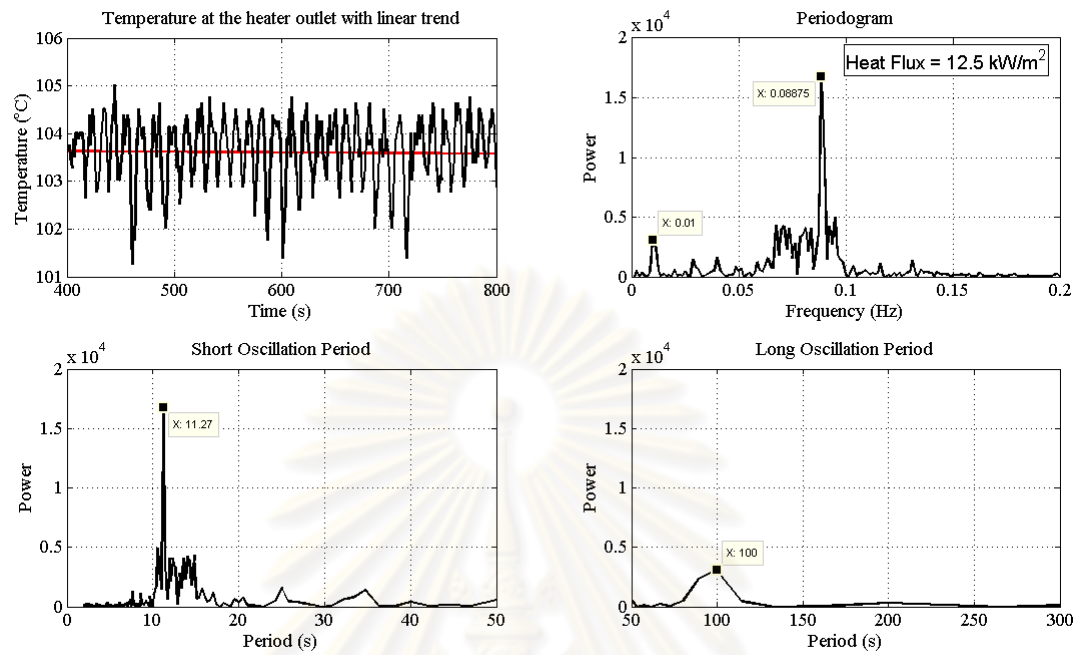


Fig. B2.3 FFT profile of temperature at the heater outlet at 12.5 kW/m^2 heat flux

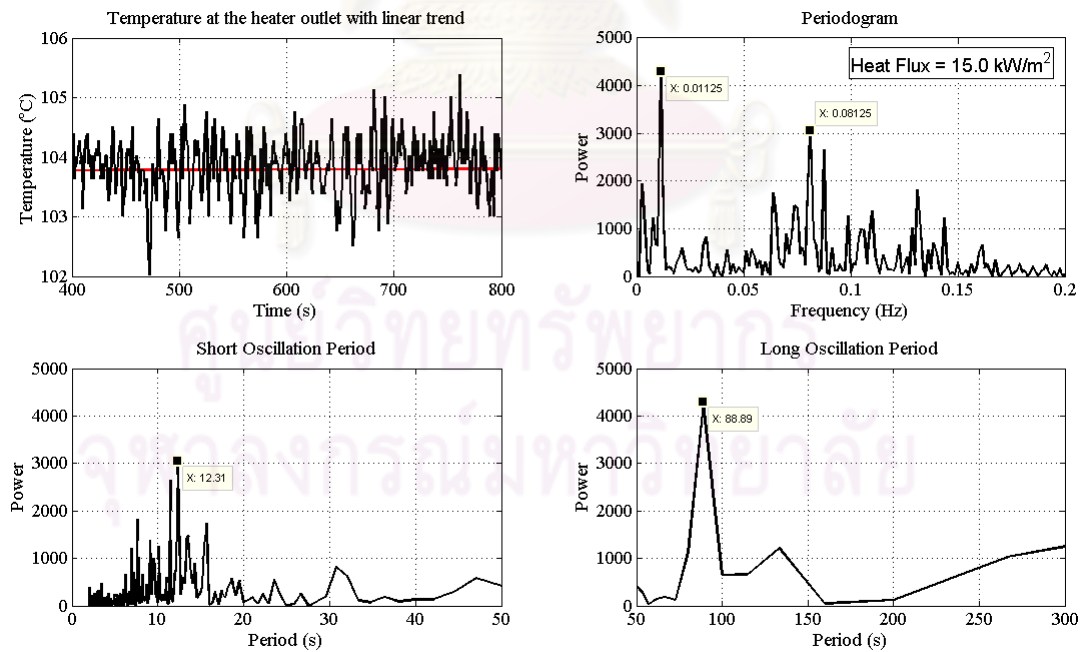


Fig. B2.4 FFT profile of temperature at the heater outlet at 15.0 kW/m^2 heat flux

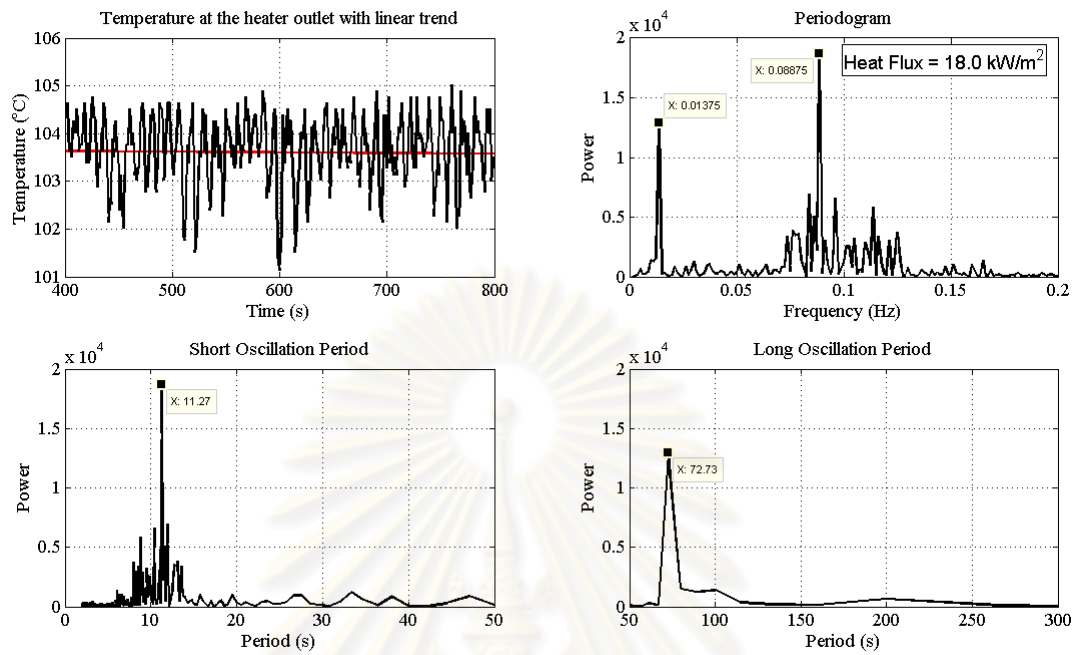


Fig. B2.5 FFT profile of temperature at the heater outlet at 18.0 kW/m² heat flux

Appendix B.3 FFT profiles of temperature at the condenser outlet for the NCL#2

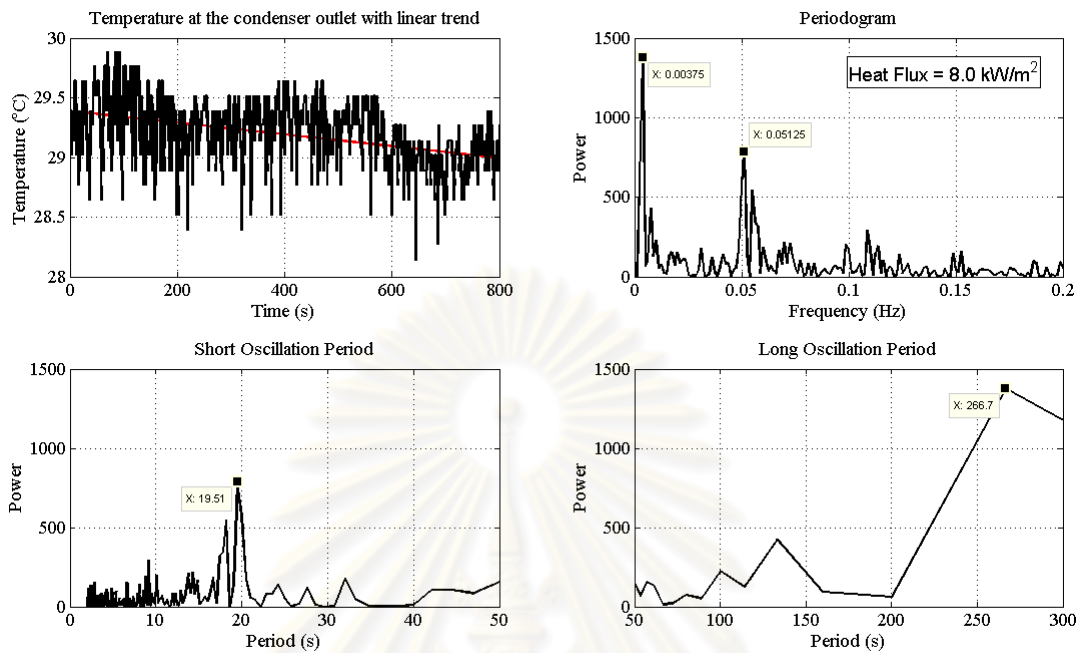


Fig. B3.1 FFT profile of temperature at the condenser outlet at 8.0 kW/m^2 heat flux

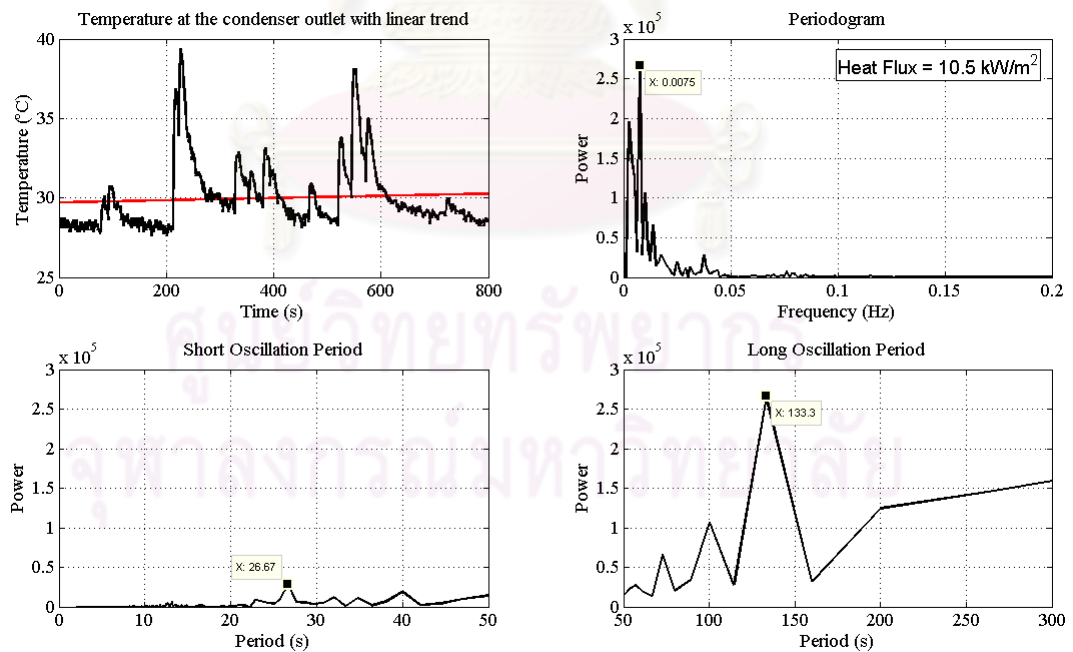


Fig. B3.2 FFT profile of temperature at the condenser outlet at 10.5 kW/m^2 heat flux

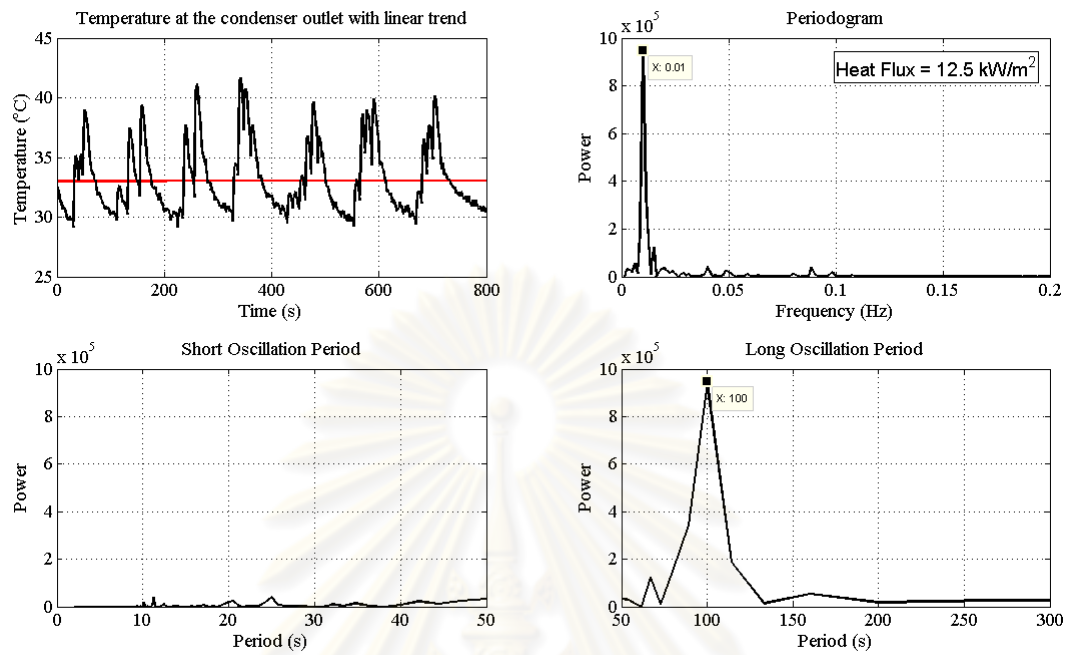


Fig. B3.3 FFT profile of temperature at the condenser outlet at 12.5 kW/m^2 heat flux

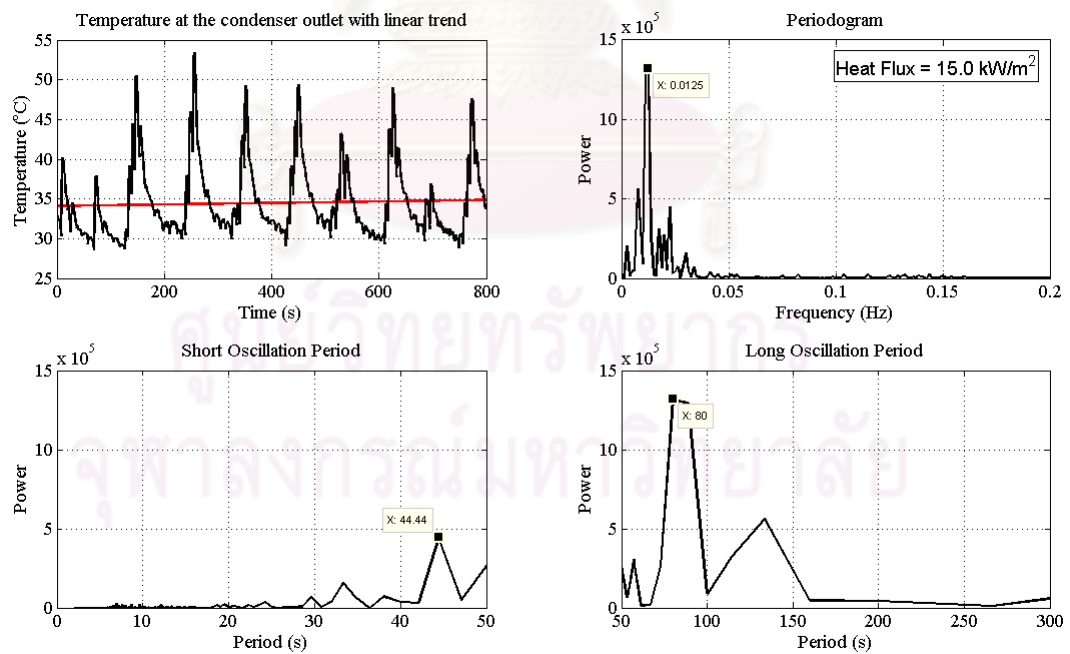


Fig. B3.4 FFT profile of temperature at the condenser outlet at 15.0 kW/m^2 heat flux

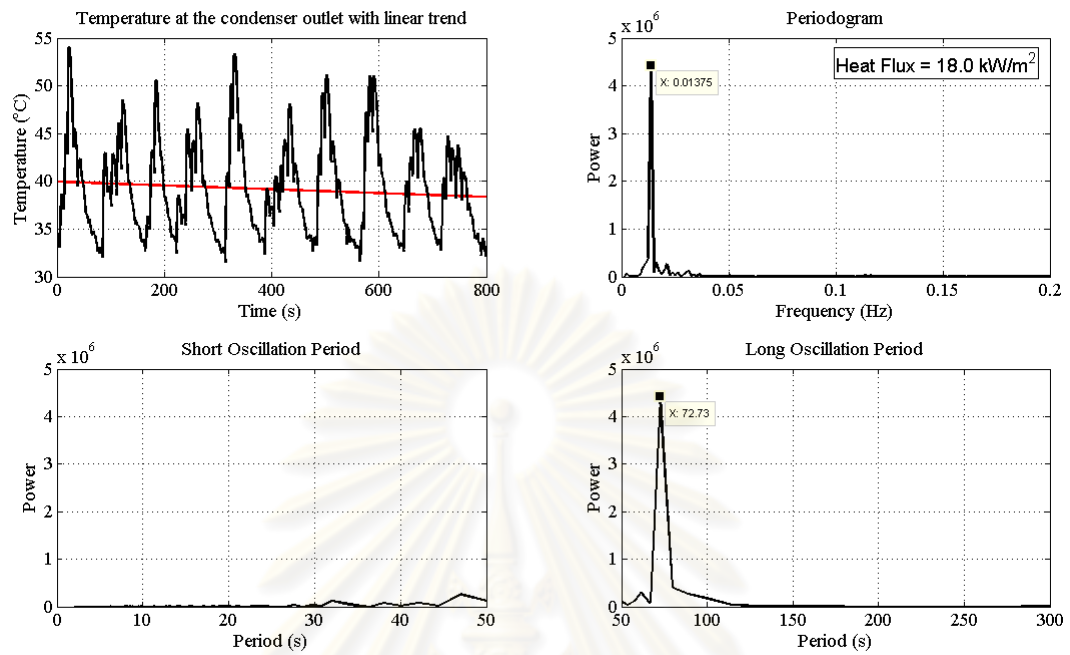


Fig. B3.4 FFT profile of temperature at the condenser outlet at 18.0 kW/m^2 heat flux

ศูนย์วิทยทรัพยากร
จุฬาลงกรณ์มหาวิทยาลัย

Appendix B.4 FFT profiles of differential pressure across the heater for the NCL#2

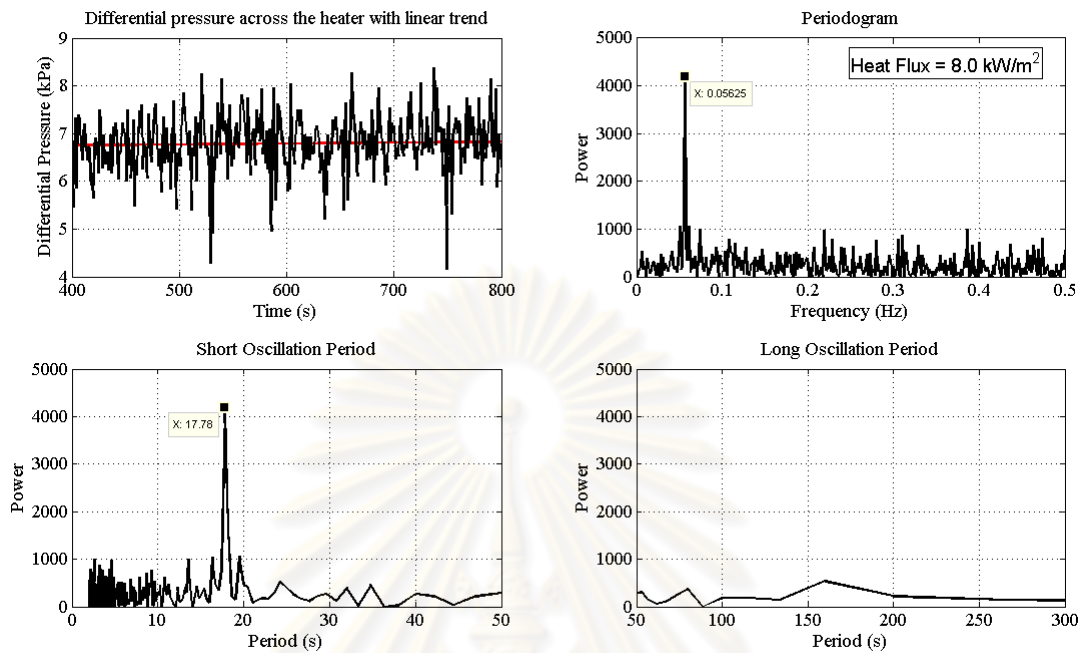


Fig. B4.1 FFT profile of differential pressure across the heater at 8.0 kW/m^2 heat flux

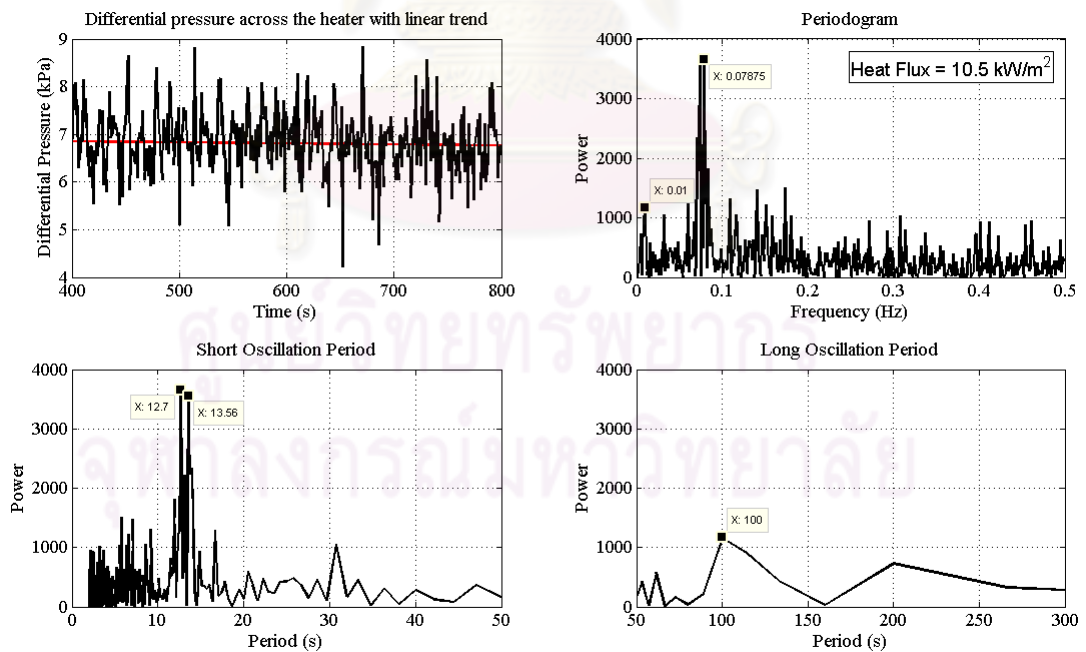


Fig. B4.2 FFT profile of differential pressure across the heater at 10.5 kW/m^2 heat flux

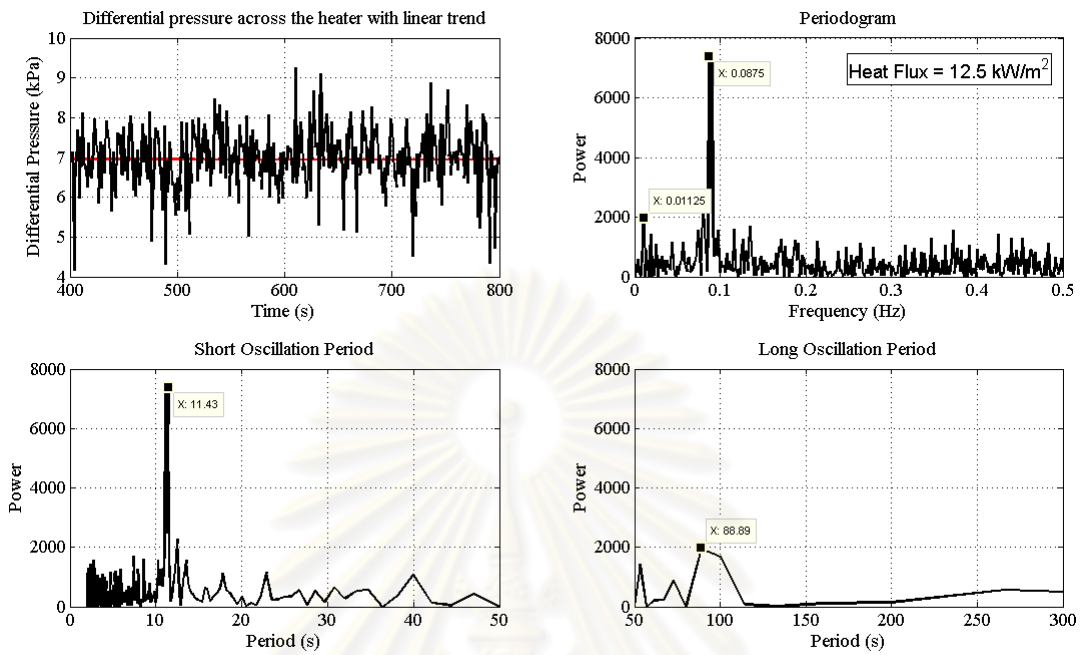


Fig. B4.3 FFT profile of differential pressure across the heater at 12.5 kW/m^2 heat flux

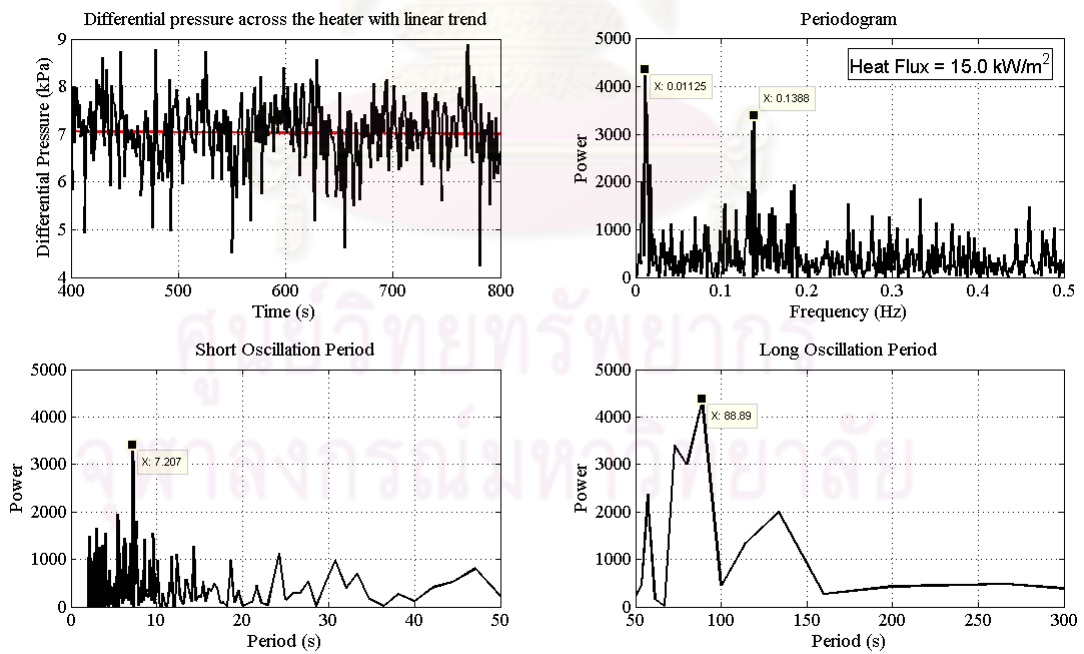


Fig. B4.4 FFT profile of differential pressure across the heater at 15.0 kW/m^2 heat flux

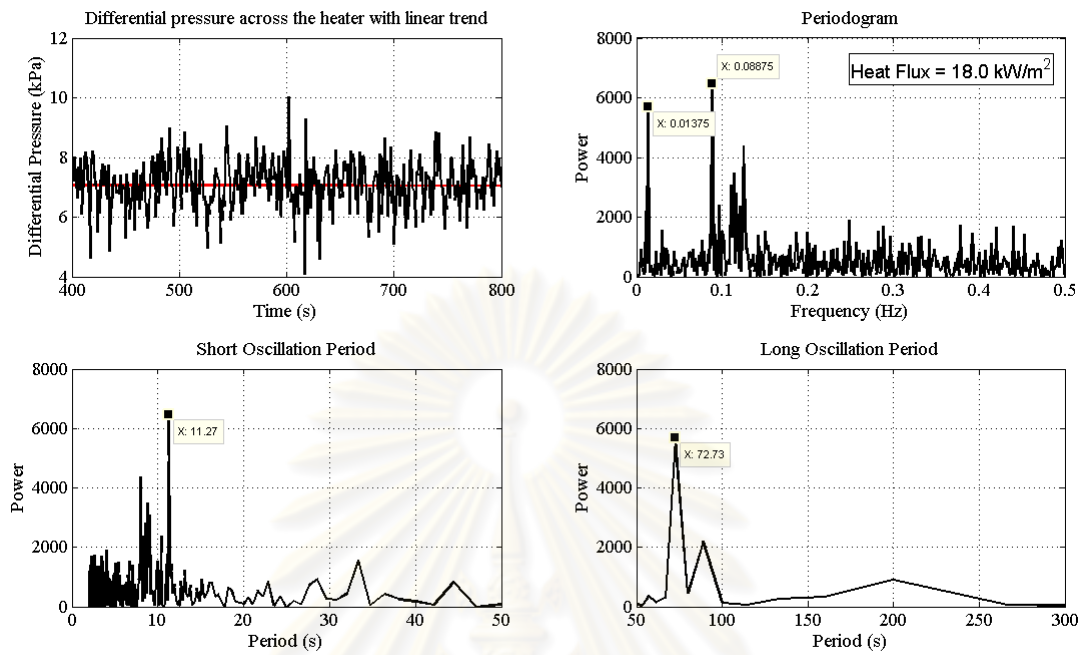


Fig. B4.5 FFT profile of differential pressure across the heater at 18.0 kW/m^2 heat flux

ศูนย์วิทยทรัพยากร
จุฬาลงกรณ์มหาวิทยาลัย

Appendix C Input file for the computer simulation

Detail of input file (Input.txt) used for computer simulation

```

Simulation of startup transient in Two-Phase flow      ! Text (indicated as (1) in Fig. C.1)
&ISET          ! Information about initial setup
IB=60,          ! Number of mesh cell
FLB=1, FLT=1,  ! Bottom and top boundary condition
                ! 1 = continuous boundary (rectangular loop)
                ! 2 = reflective boundary
                ! 3 = gradient free flow boundary
                ! 4 = constant pressure boundary
ITMAX=200,     ! Maximum iteration
THSTAR=0.5,    ! Void fraction for separate flow pattern
EPSL=1E-5, EPSG=3E-3, EPSD=0.5, EPSI=0.5, EPSP=0.5, ! Convergent criteria
THFLAG=.01, ETH=.1 &
&GRID          ! Information about mesh cell (indicated as (2) in Fig. C.1)
DXI(1)=0.1,    NDX(1)=60,      ! Delta X (m)
ARIY(1)=0.0004, NARIY(1)=60,   ! Area (m2) in Y axis
ARIX(1)=0.0004, NARIX(1)=60,   ! Area (m2) in X axis
ARJ(1)=0.0004, NARJ(1)=60 &   ! Area (m2) at junction
&INIT          ! Information about initial conditions
UGO(1)=0.00,   NUG(1)=60,      ! Vapor velocity (m/s)
ULO(1)=0.00,   NUL(1)=60,      ! Liquid velocity (m/s)
PO(1)=1.2e5,   NPO(1)=60,      ! Pressure (Pa)
THO(1)=0.0,    NTH(1)=60,      ! Void fraction
TLO(1)=303.,   NTL(1)=60,      ! Liquid temperature (K)
TGO(1)=373.,   NTG(1)=60,      ! Vapor temperature (K)
GRAVO(1)=9.8,  NGRAV(1)=20,     ! Gravity for vertical tube (upward flow)
GRAVO(2)=0.0,  NGRAV(2)=10,     ! Gravity (m/s2) for horizontal tube
GRAVO(3)=-9.8, NGRAV(3)=20,     ! Gravity for vertical tube (downward flow)

```



```

GRAVO(4)=0.0,      NGRAV(4)=10,      ! Gravity (m/s2) for horizontal tube
TWO(1)=323.,      NTW(1)=60 &      ! Wall temperature (K)
&BOUND           ! Information for constant pressure boundary
PIN=1e5,          ! Pressure (Pa) at inlet
THOUT=0.0,       ! Void fraction at outlet
POUT=1e5 &       ! Pressure (Pa) at outlet
&RUNTIM          ! Information about run time
TMAX=2000.0,     ! Maximum of run time
DT=1D-4,         ! Normal time step (s)
DTMAX=1D-1, DTMIN=1D-9 & ! Maximum and minimum time step (s)
&OUTPUT         ! Position of each gauge that used to display value on each graph
(indicated as (2) and (3) in Fig. C.1)
IPR(1)=61,IPR(2)=61,IPR(3)=10,IPR(4)=10,
IPR(5)=21,IPR(6)=32,IPR(7)=42, IPR(8)=31 &
&CONST          ! Constant value used in computer program
c(18)=0.79, c(20)=0.5, c(21)=1., C(29)=3., C(30)=1., C(31)=20., C(32)=0.45,
C(33)=0., C(34)=0., C(35)=1., C(36)=1., C(37)=0., C(38)=1., C(39)=1., C(40)=1.,
C(41)=0.1,C(42)=1D-4,C(43)=1.,C(44)=1.,C(45)=0.1,C(46)=0.,C(47)=1D-3,
C(48)=1., C(49)=0.1093, C(50)=-0.0785, C(51)=1.0, C(52)=0.246, C(53)=0., C(54)=1.,
C(55)=0., C(56)=1.0, C(57)=0., C(58)=0.,C(59)=0., C(60)=0.,
C(61)=1.0,      ! Time for display value in screen
C(62)=0.0, C(63)=2000.0, ! Minimum and maximum time for each graph
C(64)=0.0, C(65)=6.0,   ! Min and max height (indicated as (4) in Fig. C.1)
C(66)=2, C(67)=0, C(68)=0.10, C(69)=0.15, ! 1 = void fraction
C(70)=4, C(71)=0, C(72)=20.0, C(73)=120.0, ! 2 = pressure (MPa)
C(74)=4, C(75)=0, C(76)=20.0, C(77)=120.0, ! 3 = vapor temperature (C)
C(78)=2, C(79)=0, C(80)=0.1, C(81)=0.15, ! 4 = liquid temperature (C)
C(82)=4, C(83)=0, C(84)=20.0, C(85)=120.0,
C(86)=4, C(87)=0, C(88)=20.0, C(89)=120.0,
C(90)=4, C(91)=0, C(92)=20.0, C(93)=120.0,
C(94)=1, C(95)=0, C(96)=0.0, C(97)=0.1,

```

$C(98)=0.$, $C(100) = 0.0$, $C(101) = 0.0$, $C(102) = 0.05$, $C(103) = 3.083E8$,
 $C(104) = 151.0$, $C(105) = 91.22$, $C(106) = 2.0$, $C(107) = 1$, $C(119) = 1000.3D6$,
 $C(120) = 1000.3D6$, $C(131) = 0.0000134$, $C(132) = 0.285$, $C(133) = 14600.$,
 $C(134) = 5710000.$, $C(135) = 400.0$, $C(136) = 0.0$, $C(141) = 0.01$, $C(142) = 0.3$,
 $C(143) = 1.0e6$, $c(145)=39.848$ &

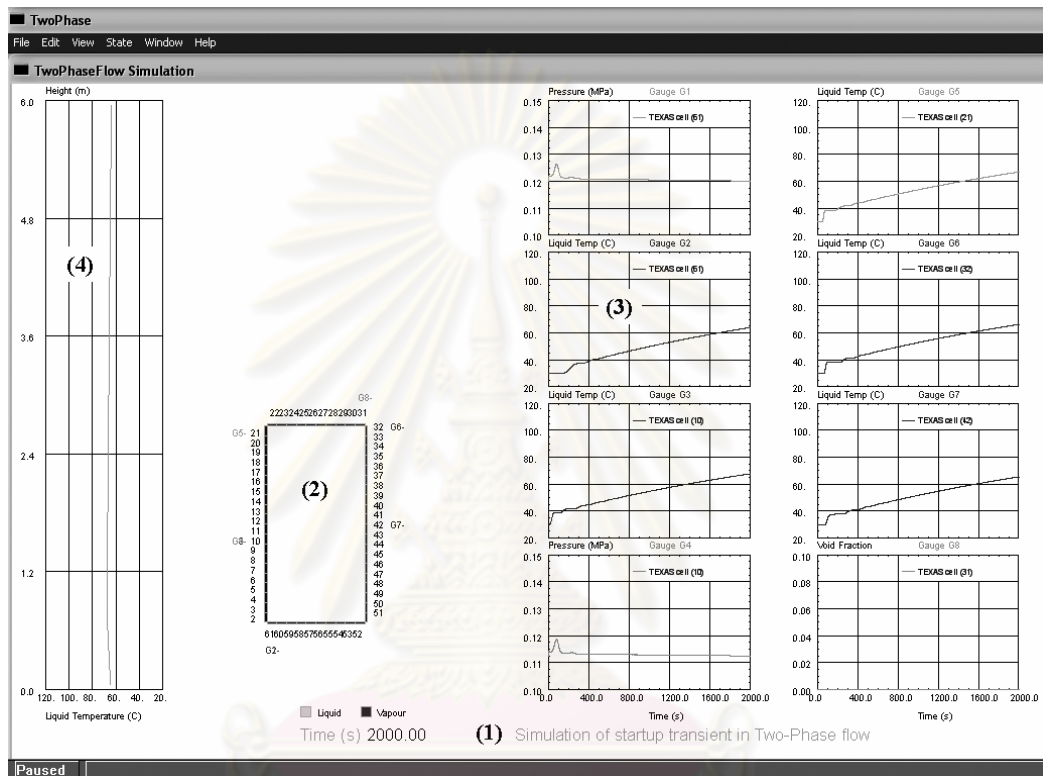


Fig. C.1 Computer program

ศูนย์วิทยทรัพยากร
 จุฬาลงกรณ์มหาวิทยาลัย

Biography

Mr. Somchai Baotong was born on August 15, 1977 at Sisaket province, Thailand. He got Bachelor degree with second class honors from the department of physics, faculty of science, Ubon Ratchathani University in 2000. After graduated he worked as assistance researcher at nuclear engineering material laboratory, department of nuclear technology, faculty of engineering, Chulalongkorn University for 1 year. He got Master degree from department of nuclear technology, faculty of engineering, Chulalongkorn University in 2003. He worked as engineer in hard disk drive industry for 3 years before he began to study the Doctoral degree at the department of nuclear technology, faculty of engineering, Chulalongkorn University in June 2006.



ศูนย์วิทยทรัพยากร
จุฬาลงกรณ์มหาวิทยาลัย